Time course and pathologies of *in vitro* maturation and fertilization of bovine oocytes

von Erica De Monte

Inaugural-Dissertation zur Erlangung der Doktorwürde
der Tierärztlichen Fakultät der Ludwig-Maximilians-Universität
München

Time course and pathologies of *in vitro* maturation and fertilization of bovine oocytes

von Erica De Monte

aus Triest

München 2017

Aus dem Veterinärwissenschaftlichen Department der Tierärztlichen Fakultät
der Ludwig-Maximilians-Universität München

Lehrstuhl für Molekulare Tierzucht und Biotechnologie

Arbeit angefertigt unter der Leitung von Univ.-Prof. Dr. Eckhard Wolf

Mitbetreuung durch Dr. Felix Andreas Habermann

Gedruckt mit Genehmigung der Tierärztlichen Fakultät
der Ludwig-Maximilians-Universität München

Dekan:	Univ.-Prof. Dr. Reinhard K. Straubinger, PhD
Berichterstatter:	Univ.-Prof. Dr. Eckhard Wolf
Korreferent:	Univ.-Prof. Dr. Gabriela Knubben-Schweizer

Tag der Promotion: 29.Juli 2017

TABLE OF CONTENTS

LIST OF ABBREVIATIONS

3D	Three-dimensional
A/T II	Anaphase II – telophase II
ACE	Angiotensin-converting enzyme
ADAM	A disintegrin and metalloproteinases
AI	Anaphase I or ana-/telophase I
AII	Anaphase II
AMP	Adenosine 3', 5' - monophosphate
ART	Assisted reproductive tecniques
BME	Basal medium Eagle's amino acids solution
BSA	Bovine Serum Albumin
CAMKII	Calmodulin-dependent protein kinase II
cAMP	Cyclic adenosine 3', 5' - monophosphate
CG	Cortical granules
CLSM	Confocal Laser Scanning Microscope
COC	Cumulus Oocyte Complex
DAPI	4′,6-Diamidin-2-phenylindol
DNA	Deoxyribonucleic acid
EDTA	Ethylenediaminetetraacetic acid
EGA	Embryonic genome activation
EGTA	Ethylene glycol-bis(β-aminoethyl ether) - N, N, N', N'-tetraacetic acid tetrasodium salt
ESchG	Embryonenschutzgesetz
FSH	Follicle Stimulating Hormone
GV	Germinal vesicle
GVBD	Germinal vesicle breakdown
h	Hours
H3S10p	Phosphorylation of the histone 3 at serine 10
hpi	Hours post insemination
ICSI	intracytoplasmic sperm injection
IP_3	Inositol 1, 4, 5 triphosphate
IVF	*In vitro* fertilization
IVM	*In vitro* maturation
LH	Luteinizing Hormone
LMU	Ludwig-Maximilians-University Munich
MEM	Minimum essential medium
MFs	Microfilaments
MI	Metaphase I
MII	Metaphase II
MI-II	Meiosis I - II transition
MIP	Maximum intensity projection
MPF	M-phase promoting Factor
mPN	Maternal pronucleus
mRNA	Messenger ribonucleic acid

MT	Microtubules
MTOC	Microtubule organizing centers
n	Number of analyzed cells
NA	Numerical aperture
n.d.	Non detectable
NSN	Non-surrounded nucleolus
OCS	Oestrus Cow Serum
OHSS	Ovarian hyperstimulation syndrome
PB	Polar body
PBS	Phosphate-buffered saline
PCOS	Polycystic ovarian syndrome
PLCζ	Phospholipase C
PMC	Pre-maturation procedures
POI	Primary ovarian insufficiency
pPN	Paternal pronulceus
ProMI	Prometaphase I
ProMII	Prometaphase II
PVA	Polyvinyl alcohol
RNA	Ribonucleic acid
SA	Sperm aster
SAC	Spindle assembly checkpoint
SN	Sperm nucleus / surrounded nucleoulus in GV
SNE	Surrounded nucleolus envelope
SOF	Synthetic Oviductal Fluid
TI	Telophase I
TII	Telophase II
UTJ	Uterotubal junction
ZP	Zona pellucida

1 INTRODUCTION

Since the first baby conceived by *in vitro* fertilization was born in 1978, the use of Assisted Reproductive Techniques (ART) has begun spreading both in human and veterinary medicine. Nevertheless, due to its low efficiency in terms of live births, studies have to be undertaken to overcome this limitation (BUCKETT et al., 2008). Due to restrictive embryo protection laws in many European countries, including Germany and Italy, and low numbers of human oocytes and embryos available for fundamental research, only few investigations have been performed. It is thus necessary to switch to suitable animal models. Although embryogenesis in the mouse model is well known, it is not a good representation of early human development. Therefore, more akin species are required. Due to its similarity to human reproductive biology, including oocyte size, monovulatory cycles, and duration of gestation, cattle have been recognized as suitable animal model for human, especially female, reproductive biology and biotechnology research. However, there are still gaps in the knowledge of molecular mechanisms and of dynamic structural changes underlying bovine oocyte maturation and fertilization. Furthermore, little is known about the origins of aneuploidy recorded in a high proportion of human (and bovine) oocytes and embryos, leading to failures in early embryo development, implantation failure, or postimplantation embryonic or fetal death (HASSOLD & HUNT, 2001).

In veterinary medicine, ART are mainly applied in farm animal breeding programs. Cloning (somatic cell nuclear transfer) is discussed (VAJTA & GJERRIS, 2006), and occasionally used as a strategy to rescue endangered species. More importantly, cloning is now part of the routine procedure for generating genetically modified farm animals, as models for human diseases, tissue and organ donors for xenotransplantation and “bioreactors” for the production of pharmaceutical proteins (CAMPBELL et al., 2007).

In this study three-dimensional multicolor fluorescence microscopy was chosen as key approach to investigate dynamic changes in meiotic spindle apparatus, chromosome congression and segregation as well as kinetics of meiosis progression in bovine oocyte maturation. This thesis provides a reference image collection and microscopic atlas of normal and abnormal bovine oocyte

maturation and early stages of fertilization, including the incidence of specific abnormalities and their putative consequences for embryo development.

2 REVIEW OF LITERATURE

2.1 Oocyte Maturation

2.1.1 The oocyte as prerequisite of embryo formation

Although the oocyte contributes only for one half of the genome to the future embryo, normal oocyte maturation is considered a prerequisite for successful fertilization, early embryo formation and further development (SIRARD et al., 2006). As the male gamete is known not to have ability to fertilize the oocyte soon after ejaculation and achieves it by undergoing a process called “sperm capacitation” followed by acrosome reaction, also the female gamete does not have the capability to permit a proper fertilization, to support the subsequent stages of development and to drive the first embryo division still the activation of the embryonic genome (EGA) without undergoing two essential processes. As for the male counterpart the term of choice resulted to be “capacitation”. The sperm capacitation involves changes on sperm surface membrane and it is normally followed by the fusion of the plasma membrane with the outer acrosome membrane. This leads to exocytosis of a numerous lytic enzymes and zona-binding proteins named acrosome reaction. The intrinsic competence of the oocyte was observed to be partially determined in early fetal development (CHOHAN & HUNTER, 2003; CHOHAN & HUNTER, 2004) and during growth (HYTTEL et al., 1997), but it is fully acquired through undergoing a long process called “maturation”. This process involves changes in chromatin organization, structural variations of the cytoskeleton as well as accumulation of proteins and ribonucleic acids (RNAs) necessary to sustain embryo development till EGA (BACHVAROVA et al., 1985; SIRARD et al., 1992; SIRARD, 2001). This process is most critical in early embryogenesis and failures occurring in this delicate phase could prevent the formation of the embryo itself or severely impair the further embryo development.

2.1.2 The Germinal Vesicle stage

Prepuberal development

During fetal life in the ovary, primordial germ cells proliferate by mitotic

divisions and the oogonia are transformed to primary oocytes. These cells proceed into the first meiotic prophase, which occurs between days 75 and 80 post conception in cattle (ERICKSON, 1966). The prophase involves several transitory stages: preleptotene, leptotene, zygotene, pachytene, and diplotene, in which bovine oocytes halts. At the pachytene stage (170 days after conception in the bovine), the oocyte becomes surrounded by a single layer of several pre-granulosa cells and an intact basal lamina, composing the primordial follicles. This kind of follicle-enclosed oocytes form a determined store of thousand oocytes, which remain arrested at pachytene stage. The oocytes contained in primordial follicles are organized in clusters called nests. Primordial follicle activation involves the transformation of the surrounding granulosa cells from a flattened to a cuboidal shape and subsequent breakdown of the nests. These resulting oocytes are primary oocytes. At puberty, the cumulus-enclosed oocytes (COCs) are stimulated to undergo the maturation process by follicle stimulating hormone (FSH) released after activation of the hypothalamus-pituitary axis. Tertiary follicles present a diameter of at least 1 mm.

Germinal vesicle oocytes after puberty

Oocyte maturation is achieved through the correct orchestration of complex and tightly linked events of nuclear, cytoplasmic and molecular maturation (SIRARD, 2001). Nuclear maturation implies chromosomal condensation, individualization, congression and segregation, whereas organelles reorganization is characteristic of cytoplasmic maturation. The storage of mRNAs, proteins and transcription factors that are essential for sustaining and driving the first embryo cleavages is indispensable for molecular maturation (DE LA FUENTE & EPPIG, 2001). Several authors investigated the cytoplasmic changes through the observation of the modification in positions of mitochondria, ribosomes, endoplasmic reticulum, cortical granules and Golgi complex during maturation (FERREIRA et al., 2009) and oocyte growth. The organelles appeared to more homogeneously distributed in the cytoplasm in primordial oocytes whereas in tertiary oocytes the organelles were recorded in the periphery of the oocyte (reviewed (HYTTEL et al., 1997). Essential part of oocyte maturation is the increase in diameter that is tightly related to the achievement of the competence to resume meiosis and reach metaphase II stage. The oocytes increase in diameter from 30 μm (primordial stage) to at least 110 μm (late tertiary oocyte stage) (HYTTEL et al., 1997). In the

bovine species, activation of follicular growth is indicated by the acquisition of a complete layer of 11-20 cuboidal granulosa cells surrounding the oocyte, forming the primary follicle. In cows, oocytes and follicles grow simultaneously until the follicle reaches a diameter of 3 mm. At this diameter the oocyte has reached the size of 120-130 μm indicating that the full developmental capacity has been achieved (ARLOTTO et al., 1996).

At this time point, the follicles appear to become responsive to gonadotropins. Development of the secondary follicles is also associated with the first detectable signs of oocyte RNA synthesis. Early tertiary follicles stage oocytes are transcriptionally active and display at least one active nucleolus (FAIR et al., 1995; FAIR et al., 1996; FAIR et al., 1997).

Follicular growth induced by gonadotropins is associated with a change in oocyte chromatin configuration at GV stage, which occurs only if the oocytes are enclosed by cumulus cells (LODDE et al., 2008). During maturation, the cumulus cells and the oocyte communicate via gap junctions. The connections to the oocyte allow the reciprocal communication between these cell types, guaranteeing the proper arrest at Germinal Vesicle stage (GV) or driving the resumption of meiosis. At GV stage, the gap junction appear to be fully open (DIECI et al., 2013; LUCIANO et al., 2014). These authors demonstrated that the capacity to resume meiosis depends on many factors, including nuclear stage, energy balance, and interaction between the cumulus cells and the oocyte. In (DE LA FUENTE & EPPIG, 2001) they showed that oocyte-enclosing granulosa cells are essential for regulating the transcription levels and also influence the chromatin configuration of growing oocytes.

Several studies were undertaken to investigate the chromatin configuration changes in germinal vesicle stage. Although most of these studies were performed in the mouse model (MATTSON & ALBERTINI, 1990; WICKRAMASINGHE et al., 1991; DE LA FUENTE & EPPIG, 2001), many experiments have also been undertaken in the bovine species, (LONERGAN et al., 1994; LIU et al., 2006; LODDE et al., 2007), , as well as in other farm animals. For example ovine germ cells were scrutinized by (RUSSO et al., 2007) whereas goat germinal vesicle oocytes were investigated by (SUI et al., 2005) as well as equine eggs (HINRICHS et al., 2005) and swine oocytes (SUN et al., 2004). Comparative studies were also reported in humans (COMBELLES et al., 2002; MIYARA et al.,

2003) and in monkeys (LEFÈVRE et al., 1989).

In the bovine model, (LUCIANO et al., 2014) reviewed the relationship between dynamic changes in chromatin configuration during GV stage and both functional and structural modifications occurring in the oocyte nuclear and cytoplasmic compartments. These authors observed that oocytes collected from early and middle antral follicles displayed four chromatin configurations, differing amongst each other by condensation degree, transcriptional activity, global DNA-methylation and histone H4 acetylation. The first stage (GV0) was defined by a diffuse filamentous pattern of chromatin spanning throughout the whole nuclear area and presented fully opened gap junction communication. This chromatin configuration appeared to be typical of oocytes recovered from 0.5-2 mm follicles and exhibit very limited capacity to resume meiosis I and reach meiosis II.

The second and the third stages (GV1 and GV2) represented early and intermediate GV stages where the first foci of chromatin condensation were detectable (GV1) or where chromatin was organized in several separate clumps (GV2). GV1 and GV2 were mainly collected from 2-6 mm follicles. At these stages the connections between cumulus cells and oocyte were detected as partially opened. The third chromatin configuration (GV3) exhibited the highest level of chromatin condensation organized in a single chromatin aggregate. GV2 and GV3 oocytes had a significantly higher developmental potential. Soon after the GV3 stage the Germinal Vesicle breaks down (GVBD).

Similar dynamic of molecular and structural changes have been described in (RUSSO et al., 2007) for ovine oocyte maturation. These authors identified 3 stages of chromatin configuration:

1. diffuse chromatin in the whole nuclear area representing absence of full meiotic competence (NSN - non surrounding nucleolus);
2. condensed chromatin surrounding the nucleolus representing the intermediate stage still not presenting the full meiotic competence (SN – surrounding nucleolus)
3. condensed chromatin partially around the nucleolus and partially near to the nuclear envelop representing the achievement of full meiotic competence. (SNE – surrounding nucleolus and envelop)

Similar findings were also reported by (LIU et al., 2006) in the bovine model. In contrast to the observation of (RUSSO et al., 2007), in (LIU et al., 2006) they identified two intermediate stages not surrounding the nucleoli between NSN and SN configuration. The first intermediate pattern was defined by a condensed netlike chromatin (N) whereas the so-called C configuration was associated to clumped chromatin detection. The SNE pattern does not represent the final chromatin pattern before GVBD. Instead, another chromatin condensation degree was observed shorter before resumption of meiosis. This stage was characterized by floccular chromatin near the nuclei and near the nuclear envelope (F). The NSN was mainly observed in small follicles and concomitantly to follicular growth the detections of stage N, C, SN gradually increased in number. The fully grown germ cell presented mainly F configuration. The authors also hypothesized that the proceeding through a less condensed stage might be related both to atresia and to onset of resumption of meiosis and the same question was also suggested by the findings of (SUI et al., 2005). These authors reported analogous findings in goat oocytes named GVn and GVc that could be correlated to configuration N and C. A progressive transcriptional inactivation towards acquisition of meiotic competence was observed. In contrast to all other species investigated, goat oocytes did not show a perinucleolar ring even shortly before GVBD (SUI et al., 2005). This study also demonstrated that serum starvation accelerates chromatin condensation toward resumption of meiosis and prevents the shift from GVn towards GVc. These authors as well suggested that the GVc configuration might incline toward atresia. GV classifications in different animal species were reviewed by (DE LA FUENTE, 2006).

Electron microscopic studies suggested that in human oocytes the compaction of the chromatin around the nucleolus represents the normal chromatin configuration shortly before ovulation (PARFENOV et al., 1989). This is found to be associated with complete cessation of RNA synthesis of the oocytes.

(KASTROP et al., 1990) investigated changes in protein synthesis patterns and protein phosphorylation during oocyte maturation in the bovine. The rate of protein synthesis remained high until 3 h after onset of *in vitro* maturation (IVM), then decreased towards the time of resumption of meiosis corresponding to GVBD (8 to 10 h after onset of IVM), and finally increased again after 12 h IVM. Interestingly, the rate of protein synthesis in oocytes arrested at GV stage

remained high. Oocytes undergoing degeneration displayed an anomalous protein synthesis pattern.

2.1.3 Resumption of meiosis

Once the cumulus cell-oocyte complexes are removed from the follicles, the lack of factors inhibiting the meiosis resumption activates a series of biochemical changes leading to GVBD (PINCUS & ENZMANN, 1935). Resumption of meiosis implies many tightly linked processes which involve chromatin configuration changes and cytoskeletal reorganization and appears to be dependent on the decreasing concentration of cyclic adenosine 3´,5´-monophosphate (cAMP) both in culture conditions and in the oocyte. This is due to a gradual reduction of intercommunications between cumulus cells and oocyte. These intercommunications are mediated by gap junctions (LUCIANO et al., 2011). The cAMP acts also on cumulus cells expansion started after gonadotropic stimulation but the concentration required for stimulating GVBD is higher than for inducing cumulus expansion (LUCIANO et al., 2004). Meiotic maturation of bovine oocytes in culture involves remarkable cytoskeletal reorganization in both oocyte and cumulus cells, as shown by confocal laser scanning microscopy. Resumption of meiosis appeared to be related to a shift in the structure of transzonal gap junctions. Whereas microfilaments dominate initially, microtubules are more prevalent at later stages (ALLWORTH & ALBERTINI, 1993). This substitution appeared to be dependent on the presence of gonadotropic hormones.

Microtubules (MT) and microfilaments (MF) are responsible for arranging chromosomes congression into the metaphase plate and for proper segregation of the chromosomes. (LI et al., 2005) investigated the dynamic evolution of the cytoskeleton in bovine oocytes and tried to correlate the dynamic changes in the nucleus to the cytoplasmic maturation by confocal laser scanning microscopy. Soon after GVBD few microtubular asters nucleated near the chromatin cluster and spread during the later meiotic stages. The MT structures form the so-called spindle and are responsible for the correct alignment of the homologous chromosomes or sister chromatids in the metaphase I (MI) or metaphase II (MII) plate. In contrast to mouse oocytes, the MTs in bovine oocytes seemed not to form a typical bipolar spindle, rather to cover the surface of the aligned chromosomes which form a kind of flat cap. With the reduction of the chromosomes number, the

MII spindle is much smaller than the MI spindle and appears barrel-shaped with longer fibers connected to poles. The shape of the spindle changes from barrel-shaped in both MI and MII stages to a cylinder-shaped in early anaphase I (AI) and anaphase II (AII) stages, and then it develops into a thin cone-shaped structure in telophase I (TI) and telophase II (TII). MTs forming the spindle gradually move towards the first polar body (PB1) and the second polar body (PB2). Almost all the microtubules and the microfilaments are expelled during polar body emission into PB1 and PB2.

2.2 Fertilization

2.2.1 Definition

Fertilization starts with the interaction and subsequent fusion of a spermatozoon and a secondary oocyte and ends in the association of two groups of chromosomes, one of maternal and the other from paternal pronuclear origin (MINHAS et al., 1984).

2.2.2 Insights into the mechanisms of fertilization: gamete interaction

Gamete interaction can occur *in vivo* when the spermatozoa deposited in the female genital tract migrate towards the uterotubal junction (UTJ) and into the oviduct where the fertilization normally takes place. Many genes seem to be responsible for the capability of sperm to reach the fertilization site. The specific roles of individual genes were mainly investigated through the use of knock out mice. The most important findings were reviewed in (MURO & OKABE, 2011; OKABE, 2013). In particular, calmegin-A appeared to play an essential role regarding sperm migration into the UTJ. Sperm A disintegrin and metalloproteinases (ADAMs) apparently play similar roles. This family of regulatory factors is composed by fertilin α (ADAM1), fertilin β (ADAM2) and cyritestin (ADAM3). This important group of molecules includes also the angiotensin-converting enzyme (ACE). In this family, the main influence on sperm migration ability is exerted by ADAM3. Failure of ADAM3 expression leads to a sub- or infertility.

At the time of fertilization, the oocyte is surrounded by cumulus cells. In (JIN et al., 2011) they demonstrated, using retrospective review of video recorded images of single sperm penetration in the mouse, that the spermatozoon fertilizing the

oocyte was already activated through acrosome reaction by contact with the cumulus cells layer instead of by contact with zona pellucida. This explains the short time required by successful fertilizing spermatozoa from attachment to penetration. As proved in (TESAŘIK et al., 1988), compounds secreted by cumulus cells such as progesterone are shown to enhance the capacitation of bovine and human sperm and the acrosome reaction (THÉRIEN & MANJUNATH, 2003)

The interaction between oocyte and spermatozoon is comprised of many steps: (1) sperm-zona binding, (2) penetration of the zona pellucida, (3) sperm adhesion to the oocyte surface, (4) fusion of the oocyte and sperm membranes and sperm nucleus penetration, and (5) syngamy (ANIFANDIS et al., 2014).

2.2.2.1 Sperm-zona pellucida binding

After passing the cumulus cells, the spermatozoon binds to the zona pellucida (ZP). There it binds to one of the three glycoprotein constituting the ZP and specifically the interaction takes place between the sperm combining site and the epitope ZP3 i.e. the ZP3 O-linked oligosaccharides (FLORMAN et al., 1984).

2.2.2.2 Sperm protein Izumo1, its oocyte receptor Juno and CD9

In mammals, the interaction between the male and the female gametes involves three membrane proteins that guarantee the correct binding, fusion and delivery of sperm nucleus into the egg (reviewed by (KLINOVSKA et al., 2014)). The sperm surface protein Izumo1 (INOUE et al., 2005) confers adhesion to the oocyte via its specific receptor Juno oocyte (BIANCHI et al., 2014). Tetraspanin CD9 displayed on the surface by the oocyte plays an essential role both in sperm-egg adhesion and in gametes fusion (KAJI et al., 2000; LE NAOUR et al., 2000; MIYADO et al., 2000; INOUE et al., 2005; RUBINSTEIN et al., 2006). Izumo1 is a testis immunoglobulin superfamily type 1 protein that is exhibited in the equatorial segment on the plasma membrane of sperm that have already undergone the acrosome reaction (OKABE et al., 1987; INOUE et al., 2005; SATOUH et al., 2012). Male mice lacking for Izumo1 and female mice deficient in CD9 or Juno are sterile due to failure of sperm-egg fusion (INOUE et al., 2005; BIANCHI et al., 2014). The binding of the sperm receptor Izumo1 with its receptor Juno on the germ cell drives the concomitantly CD9 accumulation in the area of the contact between the two gametes before fertilization and it is described

in (CHALBI et al., 2014). The authors demonstrated that structures of these receptors are conserved across species; they showed that Izumo1 and Juno are functionally equivalent between human and mouse, and between human and Syrian golden hamster by (BIANCHI & WRIGHT, 2015). The authors suggested that the identification of the receptors essential for the species-specific recognition between sperm and egg can be of great value for the development of diagnostic tests to evaluate the fertility of human gametes before their use in *in vitro* fertilization (IVF) for couples with an unfulfilled wish to have children.

2.2.2.3 The block to polyspermy

As a consequence of sperm nucleus penetration, the so called "sperm factor", the phospholipase C zeta (PLCζ) spreads throughout the cytosplam and activates the phosphoinositol signaling system. This system triggers the calcium (Ca^{2+}) release in the oocyte that is induced by the cleavage of phosphatidylinositol 4,5-bisphosphate into inositol-phosphatase (IP_3) and diacylglycerol. The IP_3 binds to its receptor on the Ca^{2+} channel in the smooth endoplasmic reticulum and opens it. In response to calcium release, the mature oocyte expels cortical granules (CG) into the perivitelline space (WANG et al., 1997) giving rise to the cortical reaction and triggering the block to polyspermy. (RAZ et al., 1998) confirmed this finding and proved that the resumption of meiosis is Ca^{2+}-dependent but protein kinase C-independent. The sperm-oocyte fusion and the subsequent cortical reaction leading to exocytosis of cortical granules activate functional changes of the zona pellucida, the perivitelline space and eventually the oolemma that avoid the fertilization by two or more sperm nuclei. These changes are called "block to polyspermy". In particular, the exocytosis of the cortical granules and the enzymes proteinases, ovoperoxidase, and N-acetylglucosaminidase are thought to be responsible for changes in the zona pellucida (ZP) such as the phosphorylation of the sperm receptors in particular ZP2 and ZP3 (SUN, 2003). In (WASSARMAN, 1994) was shown that proteinases initiate the proteolysis of ZP2 (secundary receptor for spermatozoa) that results in a reduction in solubility of the ZP that is called zona hardening (MOLLER & WASSARMAN, 1989). The authors (WANG et al., 1997; ABBOTT et al., 2001; BIANCHI et al., 2014; SANDERS & SWANN, 2016) also reported that calcium-stimulated CG exocytosis appeared to be related to oocyte competence. In the bovine oocytes as well as in the caprine and in ovine ones, the zona hardening seems to play a key

role to ensure monospermic fertilization. A proteinase displaying a trypsin-like structure is also cooperating in modifying the ZP to prevent polyspermy (BARROS & YANAGIMACHI, 1971). Ovoperoxidase seems to play a role in ZP hardening in the mouse. In (BIANCHI et al., 2014) they reported that the egg receptor Juno is expulsed in vesicles immediately after sperm penetration. Since these events occur at the same time as the zona hardening, the authors suggested a new possible mechanism involved into the block of polyspermy. Further studies are needed to disclose the mechanisms underlying the cortical granule exocytosis and also in relation to Juno binding and block of polyspermy. The Sperm factor triggering the calcium cascade in the oocyte plays also an important role in the resumption of meiosis through the calmodulin-dependent protein kinase II (CAMKII) stimulation. This mechanism is reviewed in (SANDERS & SWANN, 2016).

2.2.2.4 Decondensation and recondensation of the maternal and paternal DNA

Due to the high lipid content of bovine oocytes, visualization of pronuclear formation is hampered and represents a limitation in investigations of fertilization mechanisms. Therefore, the normal procedure for visualization of the pronuclei involves fixation of the oocytes followed by whole-mount staining procedures (MINHAS et al., 1984). This method appeares to be limited due to the impossibility to follow the development of the embryo and this leads to a remarkable loss of important information on the involved mechanisms. In order to overcome these obstacles, many experiments were undertaken performing microinjection of RNAs encoding for proteins combined with fluorescent proteins into the zygotes like in (YAMAGATA et al., 2005), or embryos like in (ZERNICKA-GOETZ & PINES, 2001; LOUVET-VALLÉE et al., 2005), and following the development by live cell video-microscopy.

2.2.2.5 Role of the sperm aster

As described by (SATHANANTHAN et al., 1991; SCHATTEN, 1994; SATHANANTHAN et al., 1996), in most animals, the centrioles, attached at the spermatozoon neck, are transferred by the sperm into the oocyte (PINTO-CORREIA et al., 1994). These organelles, in addition to pericentrosomal material,

give rise to the centrosome. This aggregate of organelles appears to be able to *de novo* nucleate maternal microtubules, forming a so called “sperm aster” (NAVARA et al., 1995b). The inheritance of centrioles appears to be different in species. In mouse (SCHATTEN et al., 1985) and hamster (HEWITSON et al., 1998), the first steps of embryo formation occur without paternal contribution to microtubule organization, even though the centrioles are provided by spermatozoa. In domestic animal species and human, correct bipolar spindle formation during mitosis is strictly dependent to the paternal microtubule organizing center (MTOC). In rabbit oocytes, both maternal and paternal components participate in microtubular organization after fertilization (TERADA et al., 2000). The authors hypothesized that the sperm aster is controlled by the perinuclear distribution of maternal centrosome constituent. The exact role of this radially arrayed microtubule structure is not clearly defined yet but many authors consider it as essential for uniting the maternal and paternal pronuclei, a prerequisite for syngamy. Further, as described by (SCHATTEN et al., 1985) in the mouse model, the centrioles appear to divide into two distinct MTOCs mainly in two groups of MTOCs that are responsible for pole formation during mitosis. In (PALERMO et al., 1994) for humans and in (NAVARA et al., 1994) for bovine they investigated the organization of mitotic spindle during polyspermic fertilization as well as in parthenogenetic activated oocytes. In polyspermic zygotes each paternal pronucleus gave rise to an independent sperm aster and in mitosis often led to supernumerary bipolar mitotic spindles. The authors reported the capability of parthenogenetically activated oocytes to form an anastral bipolar spindle, but a notable rate of misaligned chromosomes was observed. The same authors tried to classify by confocal laser scanning microscopy (CLSM) the spreading of the sperm aster based on diameter and organization type (single or several MTOC). The quality of sperm aster formation was shown to be bull-specific and related to fertility (NAVARA et al., 1996). These findings are in line with observations in humans (SIMERLY et al., 1995). The possible role of the sperm aster in fertility is discussed in (NAVARA et al., 1995a; NAVARA et al., 1996; HEWITSON et al., 1997; PALERMO et al., 1997; TERADA, 2004). In particular, the most important meaning of the sperm aster in clinics for infertility treatment concerns the incapacity of the zygote to reach syngamy due to centrosomal failure. This kind of errors appeared not to be surmountable by ICSI (intracytoplasmic sperm injection) and could lead to a diagnosis of infertility

(HEWITSON et al., 1997; SATHANANTHAN, 1998; RAWE et al., 2002).

3 MATERIALS AND METHODS

3.1 Animals

Ovaries were collected from Fleckvieh cows and heifers at the local slaughterhouses (Munich and Augsburg). Semen from Fleckvieh bull "Mindel" was used for *in vitro* fertilization (IVF).

3.2 Materials

The experiments took place in the laboratories for *in vitro* production of bovine embryos at the Chair for Molecular Animal Breeding and Biotechnology of the Ludwig-Maximilians-University (LMU) Munich. Image acquisition was performed using the Confocal Laser Scanning Microscopy (CLSM) (Zeiss LSM 510 Meta) at the Chair for Anatomy, Histology and Embryology of the Veterinary Faculty, LMU Munich, done by Dr. Felix Andreas Habermann, and using the CLSM Zeiss LSM 710 at the Gene Center of the LMU Munich.

3.2.1 Apparatuses

CLSM LSM 510 Meta	Zeiss, Germany
CLSM LSM 710	Zeiss, Germany
Axio Lab Light Microscope	Zeiss, Germany
MS 5 Stereomicroscope	Leica Germany
Wild Heerbrugg M8 Stereomicroscope	Wild Heerbrugg, Switzerland
Follicle Aspiration Unit 4014	Labotect, Germany
CO_2-O_2 Incubator	Binder GmbH, Germany
CO_2 Incubator	Medcenter Einrichtungen GmbH, Germany
Megafuge 1.0 R Centrifuge	Heraeus Sepatech GmbH, Germany
Stripper	Origio Inc., VA
Neubauer-improved chamber	Superior Marienfeld, Germany
Primo Vision Microscope EVO	Vitrolife, Sweden

3.2.2 Consumables

4-well dishes	Nunc, Germany
Petri dishes (35 mm diameter)	Corning Incorporated, NY, CA
Petri dishes (92 mm diameter)	Nunc, Germany
16-WOW culture dish	Vitrolife, Germany
Coverslips (76x26 mm, 0.17±0.001mm)	Hecht Assistent, Germany
Coverslips (26x26 mm, 0.17±0.001mm)	Hecht Assistent, Germany
Centrifuge tubes (10 ml)	Nunc, Germany
Pipette tips (2.5-1000 µl)	Eppendorf, Germany
Stripper tips 200, 175 and 275µm	Origio, Denmark

3.2.3 Chemicals

Albumin, from bovine serum	Sigma, Germany
Aprotinin, from bovine lung	Sigma, Germany
BME Essential Amino Acids Solution	Sigma, Germany
Deuteriumoxid	Sigma, Germany
EGTA (Ethylene glycol-bis(β-aminoethyl ether)	
- N, N, N’, N’-tetraacetic acid tetrasodium salt	Sigma, Germany
Heparin	Sigma, Germany
Hyaluronidase type I-S	Sigma, Germany
MEM Non-essential Amino acids Solution	Sigma, Germany
$MgCl_2$	Sigma, Germany
NaCl 0.9%	Sigma, Germany
Paraformaldehyde	Sigma, Germany
Phalloidin-TRITC	Sigma, Germany
Pipes	Sigma, Germany
Polyvinylalcohol	Sigma, Germany

Pyruvic Acid	Sigma, Germany
Taxol	Sigma, Germany
Triton X-100	Sigma, Germany
Mineral oil for cell culture	Sigma, Germany
Vectashield with DAPI	Vector Laboratories, USA

3.2.4 Antibodies

In Table 1 the antibodies used in this study are illustrated:

Antibody	**Industry**	**Order-code**
Monoclonal mouse anti-α-tubulin (clone DM1A)	Sigma, Germany	T6199
Polyclonal rabbit anti-H3S10p	Abcam Cambridge, UK	ab5176
Goat-anti-mouse IgG (H+L) Alexa Fluor 488	Dianova, Germany	115-545-166
Goat anti rabbit IgG (H+L) Cy5	Dianova, Germany	111-175-144
Phalloidin-TRITC	Sigma, Germany	P1951
Monoclonal mouse anti γ-H2A.X	Millipore, MA, USA	#05-636

Table 1: List of the antibodies used in this study.

3.2.5 Hormones

Follicle Stimulating Hormone (FSH) from bovine pituitary 50 Units	Sioux Biochemical Inc., USA
Luteinizing Hormon (LH) from bovine pituitary 25 Units	Sioux Biochemical Inc., USA

3.2.6 Software

LSM Image Browser 4.2	Zeiss, Germany
ZEN 2012 (Blue Version)	Zeiss, Germany
ZEN 2012 (Black Version)	Zeiss, Germany

Primo Vision Time-Lapse Embryo Monitoring System:

Primo Vision Capture Software; Primo Vision Analyzer Software Version 4.4.1.01.010	Vitrolife, Sweden
Microsoft Power Point 2010	Microsoft Corporation, USA
Adobe Photoshop CS5	Adobe Systems Inc., USA

3.2.7 Buffer and media for *in vitro* embryo production

All chemicals were used from Sigma, Germany except indicated otherwise.

3.2.7.1 Phosphate-bufferded saline (PBS) solution (Dulbecco and Vogt)

PBS (4 l):

4 l Aqua bidest (Millipore, Germany)

32 g NaCl

0.8 g KCl

4.6 g $Na_2HPO_4*2H_2O$

0.8 g KH_2PO_4

0.4 g $CaCl_2$

0.4 g $MgCl_2*6H_2O$

The solution presented an osmolarity between 275 and 285 and a pH of 7.3-7.4. After gently mixing, the solution was sterile filtered, stored at room temperature and used within two months.

3.2.7.2 Modified Parker´s Medium for *in vitro* oocyte maturation (IVM medium)

The medium chosen for *in vitro* maturation was the Modified Parker´s Medium.

Solution 1 (500 ml):

300 mg Lactic acid

50 ml Aqua bidest. (Millipore, Germany)

Solution 2 (500 ml):

500 ml TCM 199 (Life Technologies, Germany)

1.5 g $NaHCO_3$

7 g HEPES

125 mg Pyruvic acid

550 µl Gentamycin stock solution

Solution 3 (550 ml):

Solution 1 (50.0 ml) + Solution 2 (500.0 ml)

The solution presented an osmolarity between 280-300 mOsmol. It was sterile filtered, stored at 4 °C and used within two months.

Supplementation fresh at the same day of IVM (10 ml):

5.0 % Oestrus Cow Serum (OCS)

50.0 µL FSH (=0.025 U/ml maturation medium)

50.0 µL LH (=0.0125 U/ml maturation medium)

Before use, the medium was supplemented with OCS, FSH and LH and was equilibrated at 39 °C at 5% CO_2 for at least 1 hour.

3.2.7.3 Sperm TALP as swim-up medium for sperm capacitation

Sperm TALP (500 ml):

500 ml Cell Culture Water

2.9 g NaCl

1.045 g $NaHCO_3$

20.0 mg NaH_2PO_4

1.19 g HEPES

5.0 mg Phenol red

1825 µl Na lactate sirup (60%)

155 mg $MgCl_2*6H_2O$

192 mg $CaCl*2H_2O$

The solution presented an osmolarity between 280-300 mOsmol and a pH of 7.4. It was sterile filtered, stored at 4 °C and used within two months.

Supplementation fresh at the same day of IVF (10 ml):

60.0 mg Bovine Serum Albumin (BSA)

500.0 µl Pyruvate stock

Before use, the medium was supplemented with BSA and pyruvate and was equilibrated at 39 °C at 5% CO_2 for at least 1 hour.

3.2.7.4 Fert TALP medium for *in vitro* fertilization

Fert TALP (500 ml):

500 ml Cell Culture Water

3.33 g NaCl

117.5 mg KCl

1.0515 g $NaHCO_3$

23.5 mg NaH_2PO_4

32.5 mg Penicillin

5.0 mg Phenol red

930.0 µl Na lactate sirup (60%)

50.0 mg $MgCl_2*6H_2O$

198.5 mg $CaCl*2H_2O$

The solution presented an osmolarity between 280-300 mOsmol. It was sterile filtered, stored at 4 °C and used within two months.

Supplementation fresh at the same day of IVF (10 ml):

60 mg Bovine Serum Albumin (BSA)

100 µl Pyruvate stock

300 µl Heparin stock

Before use, the medium was supplemented with BSA, pyruvate and heparin, and was equilibrated at 39 °C at 5% CO_2 for at least 1 hour.

3.2.7.5 Synthetic Oviductal Fluid (SOF) medium for *in vitro* culture

Synthetic Oviductal Fluid (SOF 500 ml):

500 ml Cell Culture Water

3146.0 mg NaCl

267.0 mg KCl

81.0 mg KH_2PO_4

123.9 mg $CaCl*2H_2O$

48.3 mg $MgCl_2*6H_2O$

1.053 g $NaHCO_3$

0.7 mg Phenol red

181.5 mg Na-Pyruvate

2.5 ml L-glutamine 200 mM stock

235.3 µl Na lactate sirup (60%)

The solution presented an osmolarity between 270-280 mOsmol and a pH of 7.2-7.3. It was sterile filtered, stored at 4 °C and used within two months.

Supplementation at the same day of start culture (10 ml):

400 µl BME Amino acid solution

100 µl MEM Amino acid solution

5.0 % OCS

Before use, the medium was supplemented with BME, MEM and OCS, and was equilibrated at 39 °C at 5% CO_2 for at least 2 hour.

3.2.8 Samples fixation solution

The samples were fixed in Albertini fixation solution as shown in (Table 2). This solution was chosen due to its content in taxol, an inhibitor of tubulin depolymerization. This fixative enables to analyze the changes in the microtubules in the immature oocyte up to the third cleavage. The ingredients of this solution except of aprotinin and taxol were mixed at room temperature and then incubated for few minutes at 37 °C until the Triton X appeared completely dissolved. Afterwards, aprotinin and taxol were added. The solution was then equilibrated at 37 °C for 5-7 minutes.

Reagents	**Volume (µl)**	**Final concentration**
Pipes (0.5 M)	200	0,1 M
$MgCl_2$ (50 mM)	100	5 mM
EGTA (50 mM)-	50	2.5 mM
Deuteriumoxid	445	50%
10% Paraformaldehyde	200	2%
Triton X-100	5	0.5%
Aprotinin (3-7 TIU/mg protein; 5-10 TIU/ml solution)	1	0.01%
Taxol (5 mM)	0.2	1 µM
Total:	1001.2	

Table 2: Fixation solution
According to (HERMAN et al., 1983; MESSINGER & ALBERTINI, 1991).

3.2.9 Washing and storing solution after fixation

After incubation in the fixative solution, the samples were washed in a PBS solution supplemented with 0.1% Polyvinil alcohol (PVA). The same solution was

used for preserving the fixed oocytes/embryos at 4 °C before undergoing immunostaining.

3.3 Methods

3.3.1 Recovery of non-matured oocytes from ovaries and *in vitro* maturation

Ovaries were collected from cows and heifers at the local slaughterhouses and transported within 1 hour in a PBS solution at room temperature to the laboratory. To remove the remaining blood and to avoid further contaminations, the ovaries were washed three times in PBS at room temperature. The cumulus-oocyte-complexes (COCs) were aspirated from 2-8 mm follicles with a vacuum pump (80-120 mmHg) attached to an 18-Gauge needle. The follicular fluid was collected in 50 ml Falcon tubes and the sediment was aspirated with a 1 ml Pasteur pipette and transferred into a 70 mm Petri dish. The COCs were then recovered into a 35 mm Petri dish containing 2 ml of Modified Parker's Medium added with 0.025 U/ml of FSH and 0.0125 U/ml of LH (IVM medium). COCs were divided into four morphological classes of quality, based on cytoplasm homogeneity, cytoplasm color and number of cumulus cells layers surrounding the oocyte (Table 3). The COCs were washed three times in 35 mm Petri dishes containing 2 ml of IVM medium. *In vitro* maturation was started in groups of 40 to 50 oocytes per well in 4-well dishes containing each 400 µl at a controlled temperature of 39 °C and an atmosphere of 5% CO_2. In this study, only high quality COCs were used grouped as class I and II oocytes. The experiments took place all over the year thereby seasonal influences were not analyzed.

Class	Cumulus Cells Layers	Cytoplasm
I	>5 complete layers	Homogenous color, not granulated, neither dark nor soft
II	3-5 complete layers	Homogenous color
III	<3 layers with gaps	Granulated and not homogenous color
IV	Completely or partially denuded	Small, granulated and not homogenous color

Table 3: Oocyte quality classification.
According (BERG & BREM, 1989).

3.3.2 *In vitro* fertilization

In this study, the sire "Mindel" was selected due to its known fertility for *in vitro* fertilization previously tested. The method of choice for selecting the best

spermatozoa in our laboratory was the “Swim up” procedure using the Sperm TALP medium added with BSA and pyruvate. The 500 µl sperm paillette stored in liquid nitrogen was thawed at 38 °C for 10 seconds in a water bath. Then, the sperm was transferred into a 10 ml centrifuge plastic tube and gently mix with a pipette. 100 µl of the semen were aspirated with a pipette and set into a 10 ml centrifuge plastic tube containing 1 ml Sperm TALP swim up medium. This handling was performed for 4 tubes. The centrifuge tubes were then incubated at 39 °C in 5% CO_2 for 90 minutes. Afterwards 850 µl of the supernatant of each tube were transferred into a new centrifuge tube, resulting in a final volume of 3.4 ml, and the tube was centrifuged at 1800 rpm at 28 °C. Then, 3.3 ml of the supernatant was aspirated and the residual 100 µl pellet was gently mixed with a pipette. The spermatozoa concentration was checked using an improved Neubauer chamber under a normal light microscope (10x) in order to obtain the final concentration of 1,000,000/ml spermatozoa in the Fert TALP medium for *in vitro* fertilization.

In our laboratory, the time point 23 hours after starting *in vitro* maturation was chosen as standard time point for insemination. Therefore, the immature oocytes were allowed to mature for 23 hours. Then, the matured oocytes were washed three times in 35 mm Petri-dishes containing each 2 ml of fertilization medium composed of Fert TALP added with BSA, pyruvate and heparin. They were then transferred into 4-well dishes containing 400 µl of Fert TALP medium each and inseminated. After addition of sperm, the oocytes were co-incubated for variable time intervals at 39 °C at a 5% CO_2 atmosphere.

3.3.3 *In vitro* culture of inseminated oocytes

The inseminated oocytes were incubated for 20 hours in the Fert TALP medium for *in vitro* fertilization. Then, the fertilized oocytes were transferred into a centrifuge tube containing 1 ml of SOF medium for *in vitro* culture composed of SOF added with essential and non-essential amino acids and OCS and were freed of cumulus cells by vortexing for 3 minutes. After denudation, the oocytes were washed twice in Petri dishes containing 2 ml of the SOF medium in order to remove any cumulus cell rest. The samples were then cultured in groups of 40 oocytes per well in 4-wells dishes containing 400 µl of SOF *in vitro* culture medium, covered by 400 µl of mineral oil per well, at 39 °C in a 5% CO_2 and 5% O_2 atmosphere.

3.3.4 Fixation of *in vitro* matured oocytes

In order to investigate the morphological changes of the chromatin and the microtubules during the maturation process, we fixed oocytes at 2-hours intervals from 0 to 28 hours after starting incubation for *in vitro* maturation (0, 2, 4, 6, 8, 10, 12, 14, 16, 18, 20, 22, 24, 26 and 28 hours maturation). Additionally, the time point of 23 hours incubation was also selected to analyze oocyte morphology and maturation grade, as in our laboratory the oocytes at this time point were rountinely inseminated.

In detail, to obtain representative samples, the oocytes were matured in groups of 40 to 50 in 400 µl maturation medium each and, at every time point chosen, the entire group was fixed. Just before fixation, the oocytes were freed from cumulus cells. The groups fixed at 0, 2, 4 and 6 hours incubation were denuded only by vortexing the samples in a centrifuge tube containing 1 ml of PBS 0.1% PVA solution for 3 minutes whereas the groups fixed between 8 and 28 hours underwent 20 minutes incubation in a centrifuge plastic tube containing 1 ml PBS supplemented with 6 mg hyaluronidase and 4 mg of BSA followed by 7 minutes vortexing. The denuded oocytes were fixed for 20 minutes at 37 °C in 400 µl Albertini solution and then washed twice in 400 µl PBS 0.1% PVA solution. The fixed samples were stored at 4 °C in 400 µl PBS 0.1% PVA solution and stained within two weeks. The experiments were designed in order to obtain at least 80 oocytes per time point, therefore at least two experiments were performed for each time point. Only the time points 24, 26 and 28 hours maturation were performed once.

3.3.5 Fixation of *in vitro* fertilized zygotes

The monitoring of the fertilization process was performed by fixation, staining and morphological analyses of zygotes at different time points from 4 hours after the semen addition up to 12 hours post insemination. A group of 40 zygotes were fixed for every time point analyzed. Just before fixation, the cumulus cells were removed. The samples underwent incubation in 1 ml PBS supplemented with 6 mg hyaluronidase and 4 mg of BSA followed by 7 minutes vortexing and then, they were washed twice. The denuded samples were fixed for 20 minutes at 37 °C in 400 µl Albertini solution and then washed twice in 400 µl PBS 0.1% PVA solution. The fixed samples were stored at 4 °C in 400 µl PBS 0.1% PVA solution and stained within two weeks. To avoid bias in *in vitro* culture, fixation and

staining, experiments of culture and fixation of oocytes and zygotes to every time point analyzed were undertaken on at least two independent experiments. The samples were fixed at 4, 5, 6, 7, 8, 10 and 12 hours post insemination (hpi).

3.3.6 Immunofluorescence staining

All oocytes analyzed in this study and encompassing *in vitro* oocyte maturation and the first steps of the fertilization, except of *in vitro* fertilized IVF oocytes of the second experiments at 12 and 28 hpi of the TMEM95 study, were immunostained to label i) α-tubulin marking the microtubules, ii) the phosphorylation of the histone 3 at serine 10 (H3S10p) as marker for chromatin condensation, iii) the cortical f-actin for defining the cell borders (phalloidin) and iv) DAPI marking the DNA (deoxyribonucleic acid).

3.3.6.1 α-tubulin-DAPI-H3S10p-phalloidin multicolor staining

The fixed samples were incubated for one hour at room temperature in a permeabilization solution composed of PBS 0.1% PVA supplemented with 0.5% Triton X-100 and then washed twice in a PBS 0.1% PVA solution. Any blocking step was omitted due to the well-known high specific binding of the antibodies used.

The following primary antibodies (Table 4) diluted in a PBS 0.1% PVA solution were used:

Antibody	**Dilution**	**Final Concentration**
Monoclonal mouse-anti α-tubulin	1:500	2.0 µg/ml
Polyclonal rabbit-anti-H3S10p	1:500	1.0 µg/ml

Table 4: Primary antibodies used and their final concentrations.

The samples were incubated for 30 minutes at 37 °C in groups of 10 zygotes in 50 µl droplets of primary antibody solution overlaid by 3.5 ml mineral oil.

After this step, the samples were washed three times in a PBS 0.1% PVA solution and incubated for 30 minutes at 37 °C in a solution composed of secondary antibodies, phalloidin and PBS 0.1% PVA (Table 5).

Antibody	**Dilution**	**Final Concentration**

Goat-anti-mouse-IgG(H+L)-Alexa-Fluor 488	1:500	3 µg/ml
Goat-anti-rabbit-IgG(H+L)-Cy5	1:500	3 µg/ml
Phalloidin-TRITC	1:250	2 µg/ml

Table 5: Secondary antibodies used and their final concentrations.

The samples were incubated in groups of 10 oocytes in 50 µl droplets as described for the primary antibody.

After incubation in the second antibodies solution, the oocytes/zygotes were washed three times in PBS 0.1% PVA solution. For the analysis at the confocal laser scanning microscope (CLSM), the samples were mounted singularly in holes created by a PVC film piece attached to a coverslip of 76x26 mm. At the end of the staining process the cells were put in a drop of Vectacshield solution containing DAPI (4′,6-Diamidin-2-phenylindol) and allowed to assume a transparent color. The samples were then aspirated by a stripper and every hole was filled up with mounting medium and a single cell. The coverslip was then overlaid by a smaller coverslip of the dimension of 26x21 mm and then sealed with a transparent nail varnish in all four coverslip borders. The slides were then store at 4 °C in light protected boxes.

3.3.7 CLSM analysis

The samples were recorded scanning the entire oocyte in optical section at an interval of 1 µm at a 40x magnification by an oil immersion Plan-Neofluar 40x objective with a numerical aperture (N.A.) of 1.3. The pixel size used was 125x125 nm. For more detailed images, the interval between two optical sections was reduced to 0.25 µm enabling an higher resolution. The optical sections were casted into 8-bit grayscale images. For the analysis, the obtained snapshots were additionally converted into three-dimensional (3D) videos of the entire oocyte/embryo or of sections of them. The samples were recorded with different laser intensity of the fluorochrome DAPI depending on the chromatin condensation status of the cells thereby the obtained signal intensity in the snapshots cannot be compared in the figures showed in this study. In Table 6 and Table 7 the parameters of the two confocal laser scanning microscopes are illustrated.

Laser (nm)	Fluorochrome	Max Excitation	Max Emission	Filter (nm)
Argon (364)	DAPI	365	440	385 LP
Argon/Crypton (488)	Alexa Fluor 488	485	530	505 LP
Helium-Neon 1 (633)	Cy5	645	660	650 LP
Helium-Neon 2 (543)	TRITC	535	590	560 LP

Table 6: Parameters of the CLSM 510 META.

Laser (nm)	Fluorochrome	Max Excitation	Max Emission	Filter (nm)
Argon (405)	DAPI	365	440	410-504 BP
Argon/Crypton (488)	Alexa Fluor 488	485	530	504-533 BP
Helium-Neon 1 (633)	Cy5	645	660	634-759 BP
Helium-Neon 2 (561)	TRITC	535	590	601-631 BP

Table 7: Parameters of the CLSM 710.

4 RESULTS

4.1 Experimental design

The main aims of this study were:

1. to obtain a reference image collection and microscopic atlas of normal and abnormal bovine oocyte maturation and early stages of fertilization

2. to determine a timetable of bovine oocyte maturation and early stages of fertilization

3. to characterize and classify the stages of normal oocyte maturation and fertilization and to detect and categorize anomalies

4. to evaluate the incidence (and potential relevance) of the detected anomalies.

The experimental approach is summarized in Figure 1.

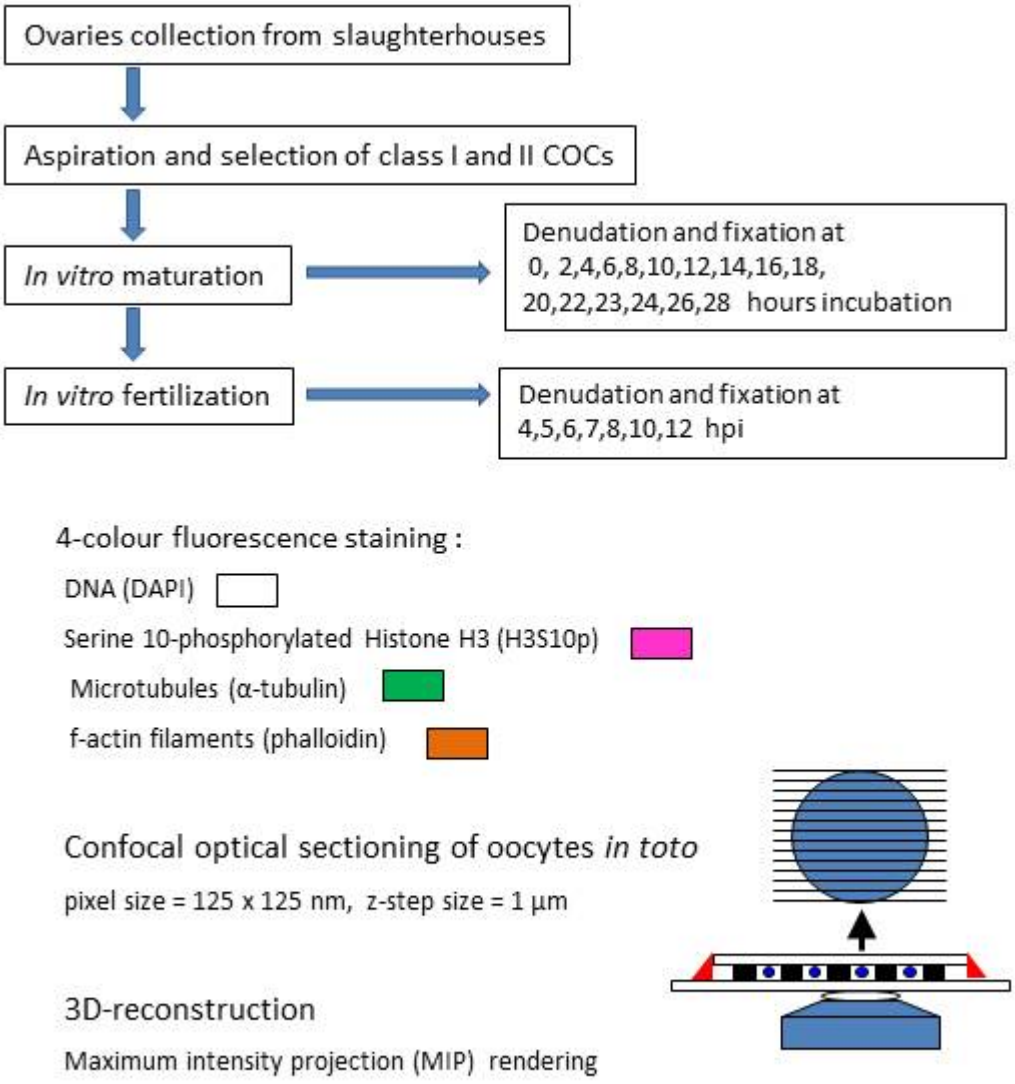

Figure 1: Experimental design.

4.2 Analysis of *in vitro* maturation (IVM) of oocytes

To investigate bovine oocyte maturation, class I and II oocytes were fixed at 16 time points from 0 to 28 hours of IVM, stained and imaged *in toto* by serial confocal sections. Oocyte denudation, immunostaining and embedding for microscopy include several tricky steps. Over all experiments, the proportion of oocytes that were lost or could not be analyzed due to insufficient preparation was in the range of 13 percent. In total, 1078 and between 31 and 126 oocytes per time point could be analyzed (Table 8).

The morphological characterization of IVM oocytes encompassed i) the analysis of the individual optical sections and ii) the three-dimensional (3D) reconstruction

of the entire image stack or oocyte slices e.g. containing the GV or the meiotic spindle by maximum intensity projection (MIP) rendering. 3D reconstruction was used to view details of interest from different angles. The four different stainings were analyzed separately in the single-color mode or together in two-, three and four-color overlay images.

h IVM	**0**	**2**	**4**	**6**	**8**	**10**	**12**	**14**	**16**	**18**	**20**	**22**	**23**	**24**	**26**	**28**
Series 1	22	18	22	40	32	29	35	36	44	30	32	22	32	31	35	32
Series 2	24	48	39	37	35	40	45	38	38	41	41	43	37			
Series 3	42															
Series 4	38															
TOTAL	126	66	61	77	67	69	80	74	82	71	73	65	69	31	35	32

Table 8: Number of oocytes analyzed per experiment and per time point.
The table indicates the number of independent experiments performed and the number of oocytes analyzed per experiment and time point. h IVM: hours of *in vitro* maturation.

4.2.1 Germinal vesicle (GV) stage and meiosis resumption

4.2.1.1 Classification oocyte maturation stages

The oocytes analyzed in this study were classified into the following stages: the GV stage (types 1-3), the germinal vesicle breakdown (GVBD), the prometaphase I (ProMI) stage, the metaphase I (MI), the ana-/telophase I (AI), the meiosis II transition (MI-II), the prometaphase II (ProMII) and the metaphase II (MII).

4.2.1.2 Classification of GV stages

Notably, in all oocytes analyzed, the GV was located in the oocyte periphery. Three different GV oocytes were observed and classified in three different groups based on chromatin configuration (Table 9, Figure 2 and Figure 3).

	GV1	**GV2**	**GV3**
Chromatin configuration	Long filamentous chromosomes spanning the entire GV Chiasmata sometimes visible Chromatin contacts to GV membrane	Chromatin cloud Chromosome condensation and aggregation in the GV center No chromatin contacts to the GV membrane	Small condensed chromatin cluster in the center of the GV No chromatin contacts to the GV membrane
H3S10p	Negative		

Table 9: Classification of GV stages based on the chromatin configuration.

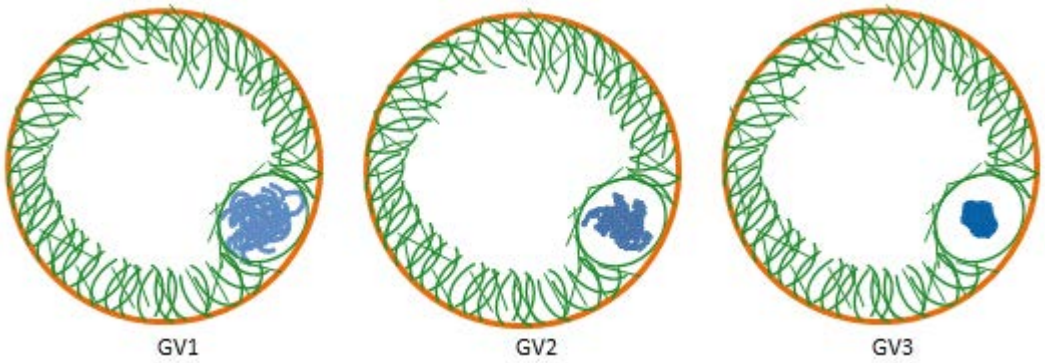

Figure 2: Schematic illustration of the chromatin patterns characterizing the GV stages 1, 2 and 3.
The chromatin is colored in blue, cortical f-actin is in orange, the microtubules in green.

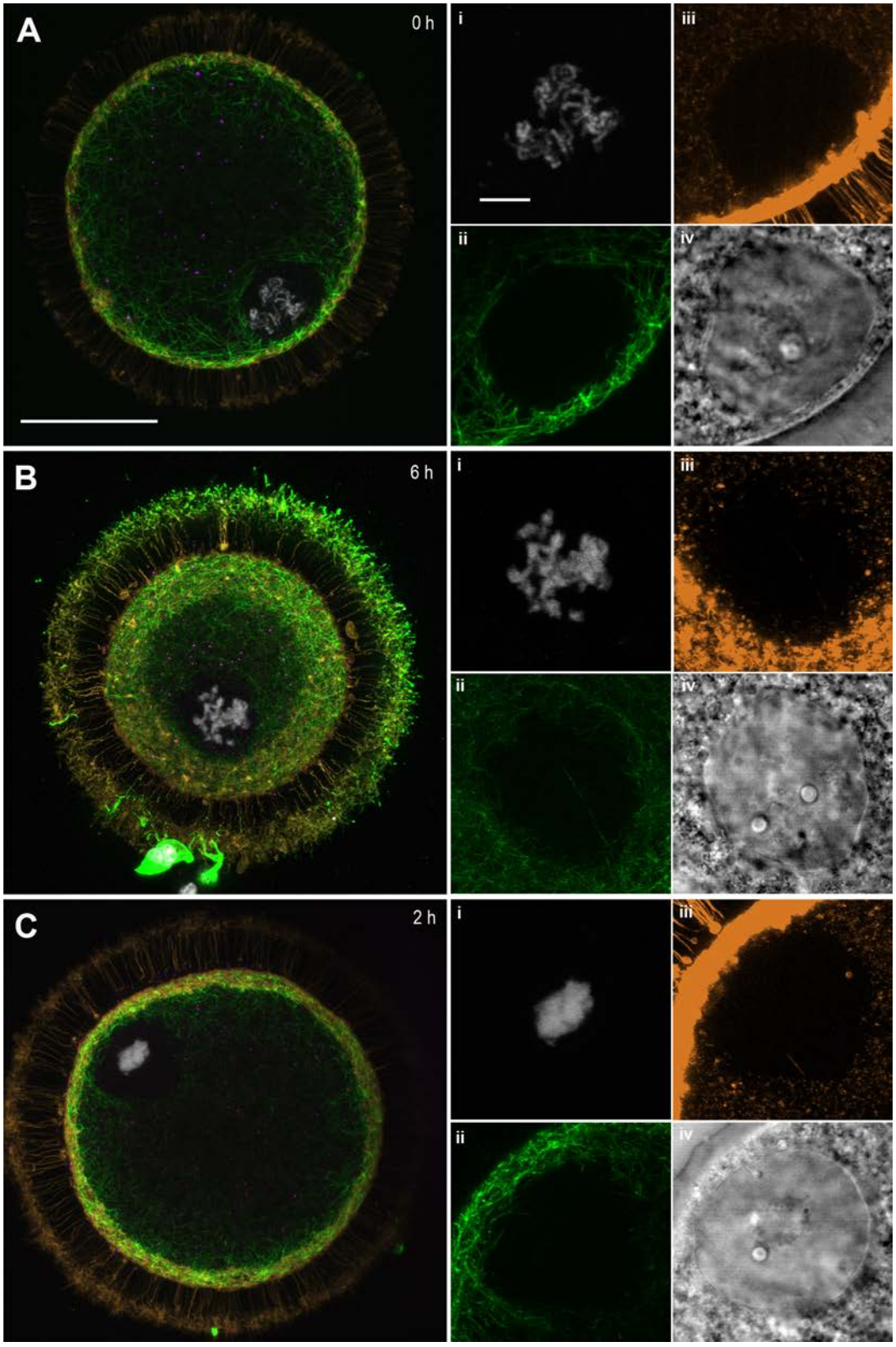

Figure 3: Examples of oocytes in different late GV stages.
(A) GV stage 1. **(B)** GV stage 2. **(C)** GV stage 3. DAPI-stained DNA is depicted in white, α-tubulin in green, f-actin in orange and H3S10p in magenta. The images are maximum intensity projections of subsets of the optical sections. Each panel presents an overview image **(A, B, C)** and details of the GV and the surrounding cytoskeleton i.e. (i) DAPI-stained chromatin alone, (ii) microtubules, (iii) f-actin microfilaments and (iv) the GV membrane in the transmission scan. The chromatin was consistently H3S10p-negative, signals in the cytoplasm and the perivitelline space were unspecific. To demonstrate the fine cytoplasmic f-actin meshwork in the detail views (iii), the image brightness has been enhanced. Scale bar= 50 µm (oocyte overviews A, B, C) and 10 µm (details i - iv).

4.2.1.3 Degenerating oocytes

Especially, some of the oocytes fixed before IVM (i.e. 0 h IVM) showed a patchy or fragmented cortical f-actin cytoskeleton, without any cytoplasmic microtubule (MT) network. Representative examples are shown in Figure 4. These oocytes were considered as degenerating and excluded from further analysis. In most cases, the GV seemed to be still intact in the transmission scan images and the chromatin configuration appeared to be normal.

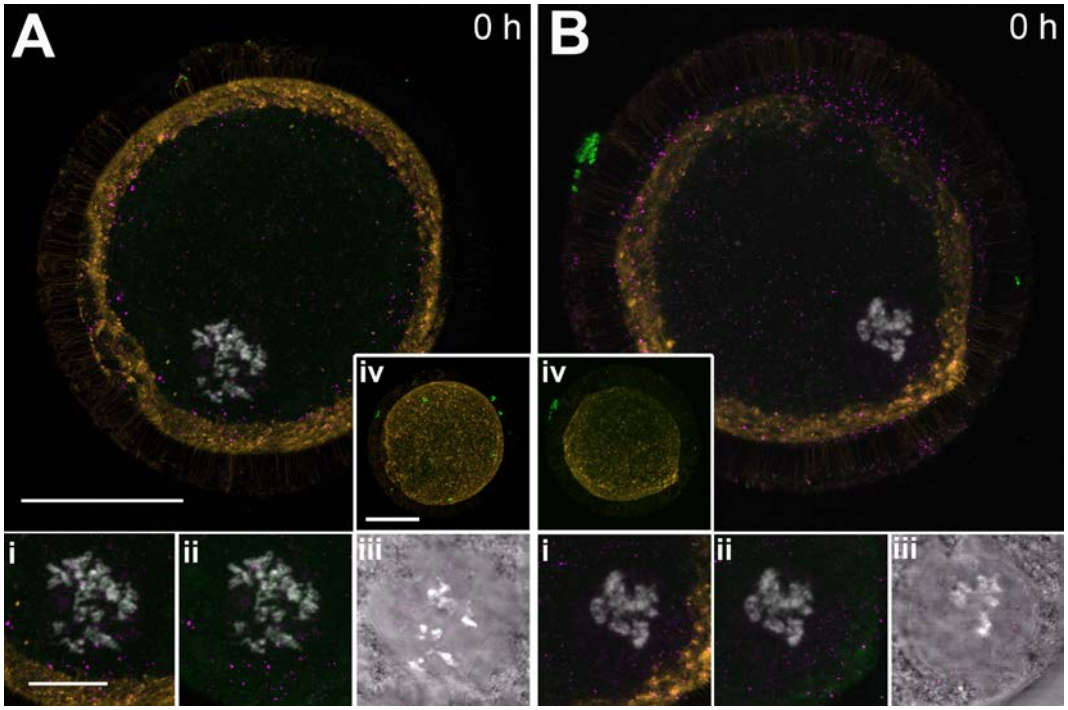

Figure 4: Examples of degenerating oocytes at 0 h *in vitro* maturation.
Degenerating oocytes were characterized by the complete loss of the cytoplasmic microtubules network and a partial or complete disintegration of the cortical f-actin. DAPI-stained DNA is depicted in white, α-tubulin in green, f-actin in orange and H3S10p in magenta. The images are maximum intensity projections of subsets of the optical sections. The chromatin was consistently H3S10p-negative, signals in the cytoplasm and the perivitelline space were unspecific. **(A)** Oocyte displaying a GV1 chromatin configuration. **(B)** Oocyte exhibiting a GV2 chromatin configuration. (i-iii) Detail views of the GV: (i) 4-color overlay, (ii) overlay of DNA, α-tubulin and H3S10p and (iii) Transmission scan and DAPI-stained DNA. (iv) Maximum intensity projection of the complete oocyte. Scale bar = 50 µm (oocyte overviews A, B, iv) and 20 µm (details i, ii, iii).

4.2.1.4 Classification of stages of meiotic maturation of bovine oocytes

The collection of three-dimensional image stacks was used to classify the stages of oocyte maturation at the resolution level of confocal laser scanning microscopy. The classification of the stages is summarized in Table 10. Schematic illustration of the stages are illustrated in Figure 5, whereas representative microscopic images are shown in Figure 6. The clearly first visible sign of meiosis resumption, the germinal vesicle breakdown (GVBD), mainly occurred between 4 and 8 hours of IVM. In oocytes, which apparently had been recorded immediately

after GVBD, the chromosomes formed a single highly compacted chromatin aggregate directly surrounded by the cytoplasmic MT network, while no GV membrane was seen in the transmission scan. Notably, at this stage, the highly dense chromatin was H3S10p negative (see Figure 6A).

In the earliest stage of the formation of the metaphase I (MI) spindles, in prometaphase I-A (proMI-A), the cytoplasmic MT network had disappeared, the chromosomes were intensely H3S10p-positive, and around the chromosomes, first few microtubules were visible (see Figure 5A up and 6B).

In prometaphase I-B (proMI-B), a MT aster had formed, and the individualization of the (bivalent) chromosomes had started (see Figure 5B up and 6C).

In late prometaphase I-C (proMI-C) the chromosomes had moved into the metaphase plate and appeared to be embedded in a single disk-shaped MT array (see Figure 5C up and 6D).

In metaphase I oocytes, the chromosomes appeared more or less regularly aligned in the metaphase plate between two flat MT arrays of a bipolar disk-shaped metaphase I spindle (see Figure 7A).

In mid-to-late anaphase I, the cylindrical central MT spindle had formed moving the separated homologous chromosomes apart from each other, and the first polar body was extruded. No MTs were seen at the spindle poles (see example in Figure 7B). Notably, in late anaphase I consistently an asymmetrical elongation of the central spindle was seen. The distal half of the central spindle towards the first polar body was approximately twice as long as the proximal one.

The meiosis-I-II transition was characterized by (i) complete extrusion of the first polar body inclusive the complete central spindle and (ii) a highly compacted H3S10p-positive chromosome aggregate in the oocyte directly below the cortical f-actin (see example in Figure 7C).

The stages of prometaphase II were similar to those of prometaphase I (see Figure 5A down, 5B down, 7D, 8A and 8B).

Stage		**Chromosome configuration**	**Spindle microtubules**	**Polar body I**
Prometaphase I	proMI A	Compacted chromosome aggregate	Few MTs around the chromosome aggregate	
	proMI B	Individualization of the bivalent chromosomes	MT aster	
	proMI C	Congression of the bivalent chromosomes to the metaphase plate	MT assembly between and around the chromosomes and formation of a disc-shaped MT array	
Metaphase I	MI	Alignment of the bivalent chromosomes in the metaphase plate	Disk-shaped bipolar MI spindle	
Ana-/telophase I	AI	Two separate chromosome sets	Formation and elongation of the central spindle	Formation of the first polar body
Meiosis I-II transition	MI-II	Compacted chromosome aggregate	No MTs; Few MTs around the chromosome aggregate	First polar body and central spindle extruded
Prometaphase II	proMII A	Chromosome individualization	MT aster	
	proMII B	Chromosome congression to the metaphase plate	MT assembly between and around the chromosomes and formation of a disc-shaped MT array	
Metaphase II	MII	Alignment of the chromosomes in the metaphase plate	Disk-shaped bipolar spindle	

Table 10: Stage classification of bovine oocyte meiotic maturation.

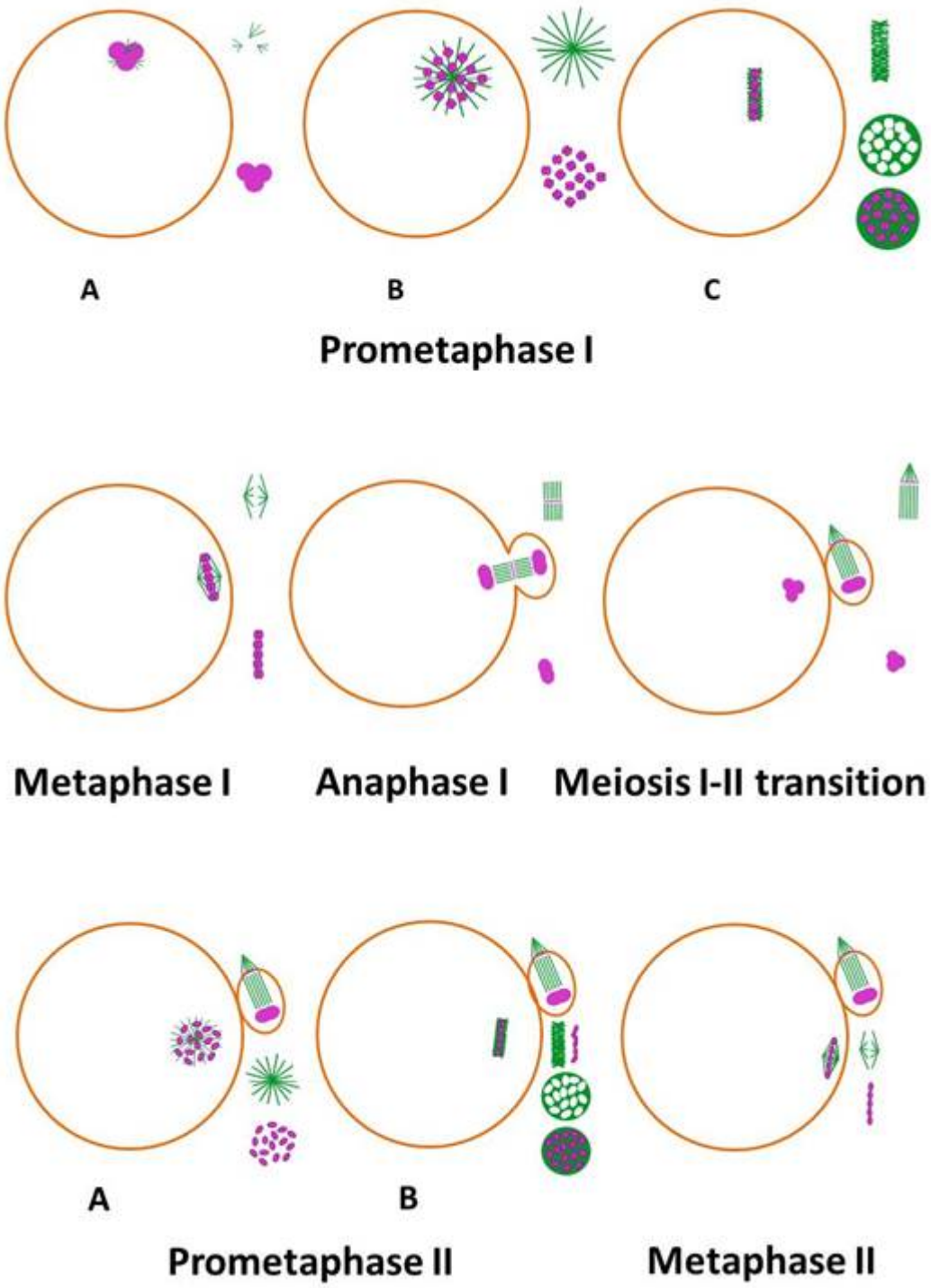

Figure 5: Schematic illustration of stages of bovine oocyte meiotic maturation.
Schematic illustration of the meiotic stage from prometaphase I to metaphase II. Chromatin is depicted in magenta, microtubules in green and f-actin in orange.

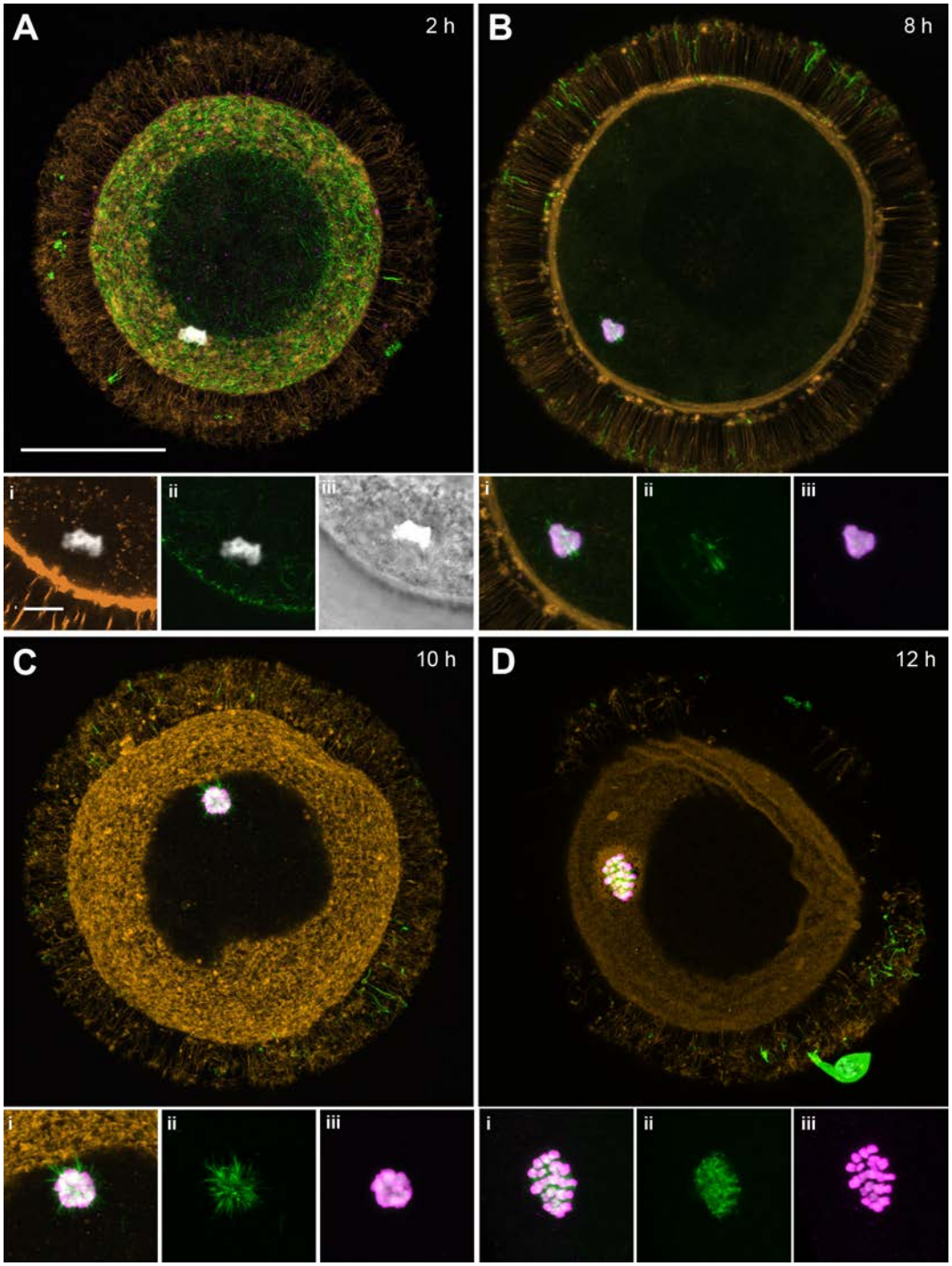

Figure 6: Examples of stages from the germinal vesicle breakdown to prometaphase I. **(A)** Oocyte immediately after the germinal vesicle breakdown (GVBD). The condensed chromosomes has formed a single compact aggregate which is H3S10p negative. **(B)** Prometaphase I-A oocyte: the compact chromosomes aggregate has condensed further and has become H3S10p+. The onset of spindle formation has started by MT nucleation around the chromatin. **(C)** Prometaphase I-B oocyte (later stage of spindle formation): MT-aster and start of the individualization of the bivalent chromosomes. **(D)** Late prometaphase I-C oocyte: chromosomes have moved into the metaphase plate, and a single disk-shaped MT array has formed. DAPI-stained DNA is depicted in white, α-tubulin in green, f-actin in orange and H3S10p in magenta. The images are maximum intensity projections of subsets of the optical sections. Each panel presents an overview image (A, B, C, D) and details (i-iii) i.e. (i) an overlay of DNA, H3S10p, MTs, and f-actin, (ii) microtubules alone and (iii) an overlay of DAPI and H3S10p. (Aiii) presents an overlay image of a transmission scan and the DAPI-stained chromosomes. Scale bar = 50 µm (overviews) or 10 µm (details).

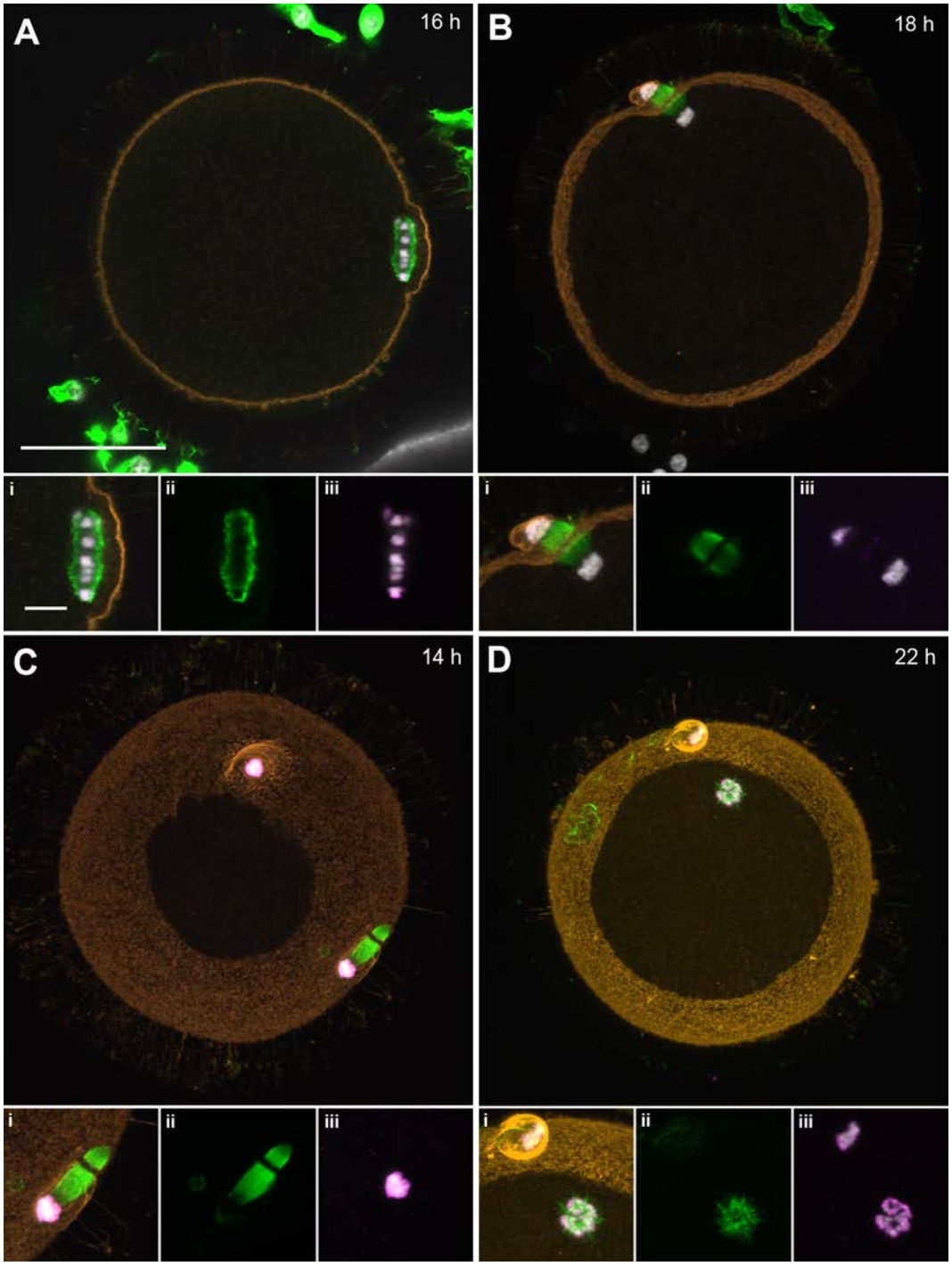

Figure 7: Examples of stages from metaphase I to early prometaphase II.
(A) Metaphase I oocyte: the (bivalent) chromosomes are aligned in the metaphase plate between two flat MT arrays forming a flat a bipolar disk-shaped spindle. Shown are single optical sections. **(B)** Anaphase I oocyte: expulsion of the first polar body. **(C)** Oocyte at the meiosis I-II transition. **(D)** Prometaphase II-A oocyte: A MT aster has formed and the chromosomes become separated from each other. DAPI-stained DNA is depicted in white, α-tubulin in green, f-actin in orange and H3S10p in magenta. Panel **A** shows single optical sections, all other images are maximum intensity projections of subsets of the optical sections. Each panel presents an overview image (**A, B, C, D**) and details (i-iii) i.e. (i) an overlay of DNA, H3S10p, MTs, and f-actin, (ii) microtubules alone and (iii) an overlay of DAPI and H3S10p. Scale bar = 50 µm (overviews) or 10 µm (details).

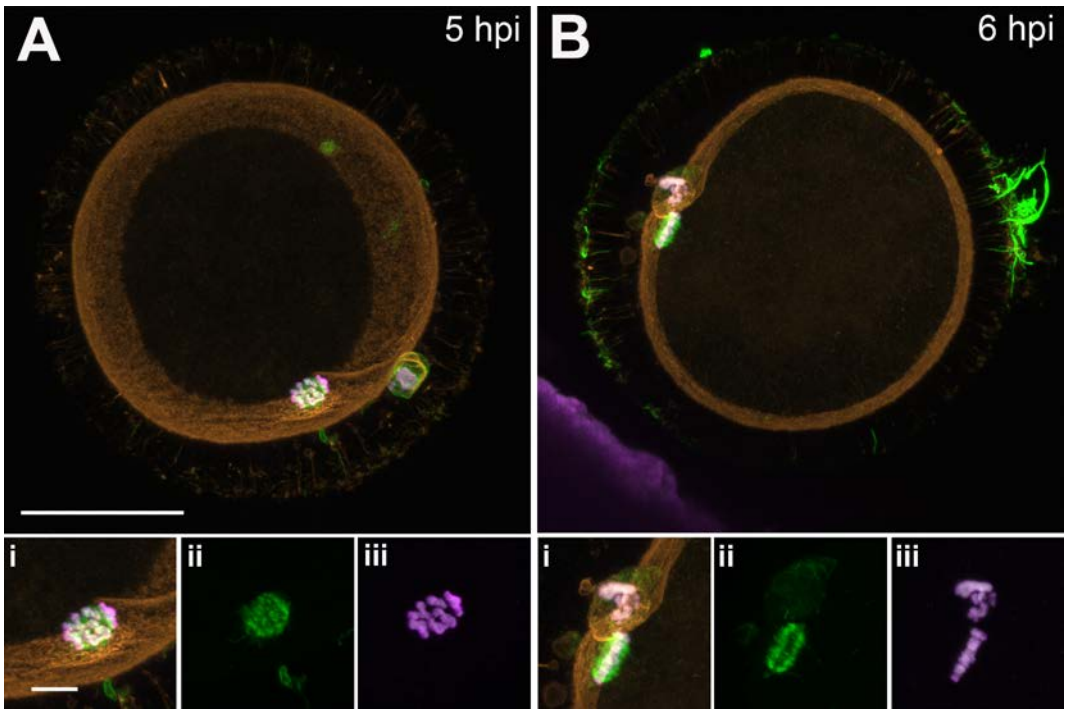

Figure 8: Examples of stages from prometaphase II to metaphase II.
(A) Prometaphase II-B oocyte. Similar as in prometaphase I, the (single-chromatid) chromosomes have moved into the metaphase plate. The spindle consists of a single disk-shaped MT array. **(B)** Metaphase II arrest: a flat bipolar spindle has formed and the chromosomes have been aligned between two disk-shaped MT arrays. DAPI-stained DNA is depicted in white, α-tubulin in green, f-actin in orange and H3S10p in magenta. The images are maximum intensity projections of subsets of the optical sections. Panels **A** and **B** present overview images and detail views (i-iii). (i) Overlay of DNA, H3S10p, MTs, and f-actin, (ii) microtubules alone and (iii) overlay of DAPI and H3S10p. Scale bar = 50 µm (overviews) or 10 µm (details).

Unexpectedly, the bipolar spindle of both metaphase I and metaphase II had a flat disk-like shape (see schematic drawing in Figure 9).

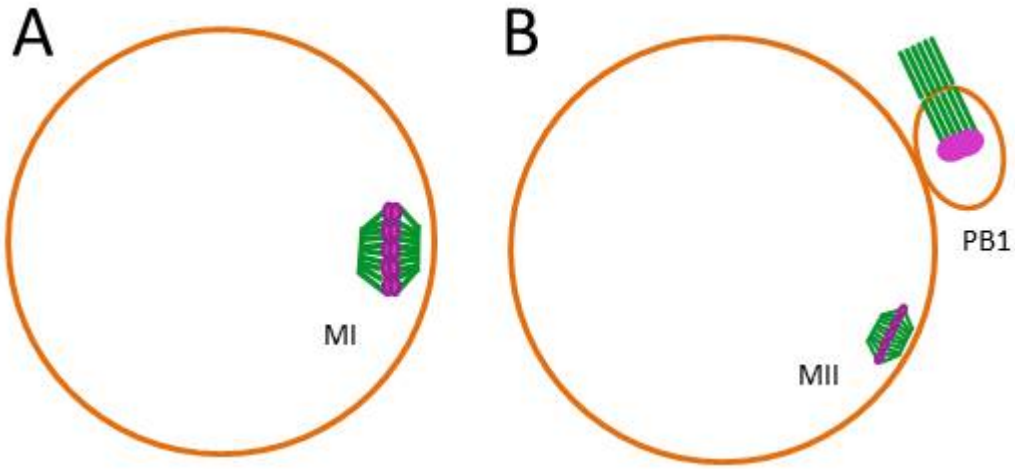

Figure 9: Schematic illustration of the disk-shaped bipolar metaphase I and II spindle.
(A) Metaphase I, **(B)** Metaphase II with the first polar body.

4.2.2 Evaluation of the kinetics of *in vitro* oocyte maturation

4.2.2.1 Oocyte maturation stages from 0 to 6 hours of IVM

To assess the quality and maturation status of class I and II oocytes before *in vitro* maturation, a total of 126 oocytes from four different weeks was fixed and analyzed at 0 h IVM i.e. immediately after isolation and selection. The classification procedure is illustrated in Figure 10.

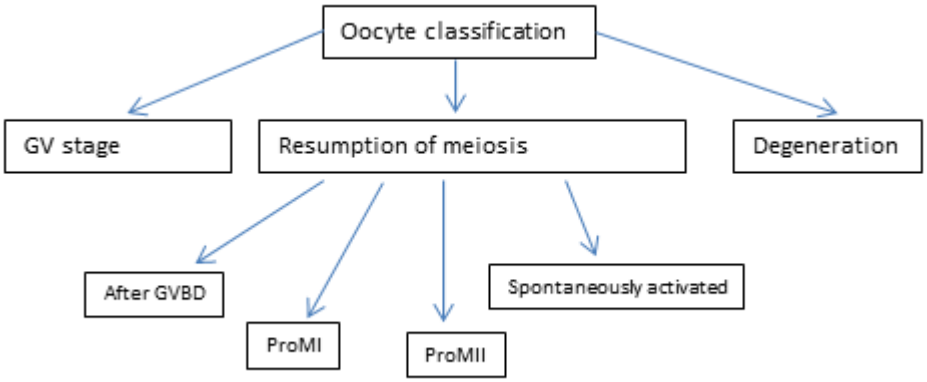

Figure 10: Scheme illustrating the oocyte stage classification at 0 h IVM.

As shown in Table 11 and Table 12, at 0 h IVM, 96.8% of the oocytes were still in the germinal vesicle stage and only few oocytes (3.2%) were found, which had already resumed meiosis. 15.9% (20/126) of the oocytes analyzed before IVM were degenerating and all of them were in the GV stage (Table 11). Next, we investigated in detail the groups of oocytes presenting a relevant presence of GV stages corresponding to the time interval 0-6 h IVM.

	0 h IVM		**2 h IVM**		**4 h IVM**		**6 h IVM**	
Degenerated	20	*(15.9)*	3	*(4.6)*	6	*(9.8)*	3	*(3.9)*
GV	102	*(80.9)*	57	*(86.4)*	54	*(88.6)*	34	*(44.2)*
GVBD	1	*(0.8)*	1	*(1.5)*	1	*(1.6)*	9	*(11.7)*
ProMI	2	*(1.6)*	3	*(4.6)*	0	*(0)*	30	*(39)*
ProMII	1	*(0.8)*	1	*(1.5)*	0	*(0)*	0	*(0)*
Activated	0	*(0)*	1	*(1.5)*	0	*(0)*	1	*(1.3)*
Total	126	*(100)*	66	*(100)*	61	*(100)*	77	*(100)*

Table 11: Frequency of oocyte stages from 0 to 6 hours of IVM.
Shown are the oocytes number and (in brackets) the weighted average values (%) from 4 (0 h IVM) or 2 (2–4 h IVM) independent experiments.

h IVM	Experiment	Total	GV	Degenerated	GVBD	ProMI	ProMII	Activated
0	1	22	20	0	0	1	1	0
0	2	24	13	9	1	1	0	0
0	3	42	36	6	0	0	0	0
0	4	38	33	5	0	0	0	0
2	1	18	15	2	0	1	0	0
2	2	48	42	1	1	2	1	1
4	1	22	17	4	1	0	0	0
4	2	39	37	2	0	0	0	0
6	1	40	7	3	7	23	0	0
6	2	37	27	0	2	7	0	1

Table 12: Frequency of oocyte stages from 0 to 6 hours of IVM in individual experiments.
Shown are the oocytes numbers of the individual experiments.

4.2.2.2 Kinetics of chromatin configuration changes in the GV

Notably, in all oocytes analyzed, the GV was located in the oocyte periphery. The spectrum of different GV phenotypes were divided into three different stages (see Table 9 and Figures 2 and 3). As shown in Table 13 and Figure 11, between 4 and 6 h IVM a marked decrease of presence of GV1 oocytes was detected while an increase of GV2 and GV3 oocytes was observed.

	0 h IVM		2 h IVM		4 h IVM		6 h IVM	
GV1	47	*(46.1)*	28	*(49.1)*	32	*(59.3)*	6	*(17.6)*
GV2	42	*(41.2)*	20	*(35.1)*	14	*(25.9)*	15	*(44.1)*
GV3	13	*(12.8)*	9	*(15.8)*	8	*(14.8)*	13	*(38.2)*
Total	102	*(100)*	57	*(100)*	54	*(100)*	34	*(100)*

Table 13: Frequency of GV stages 1, 2 and 3 from 0 to 6 hours of IVM.
Shown are the oocytes number and (in brackets) the weighted average values (%) from 4 (0 h IVM) or 2 (2–4 h IVM) independent experiments. Only oocytes classified as viable were included.

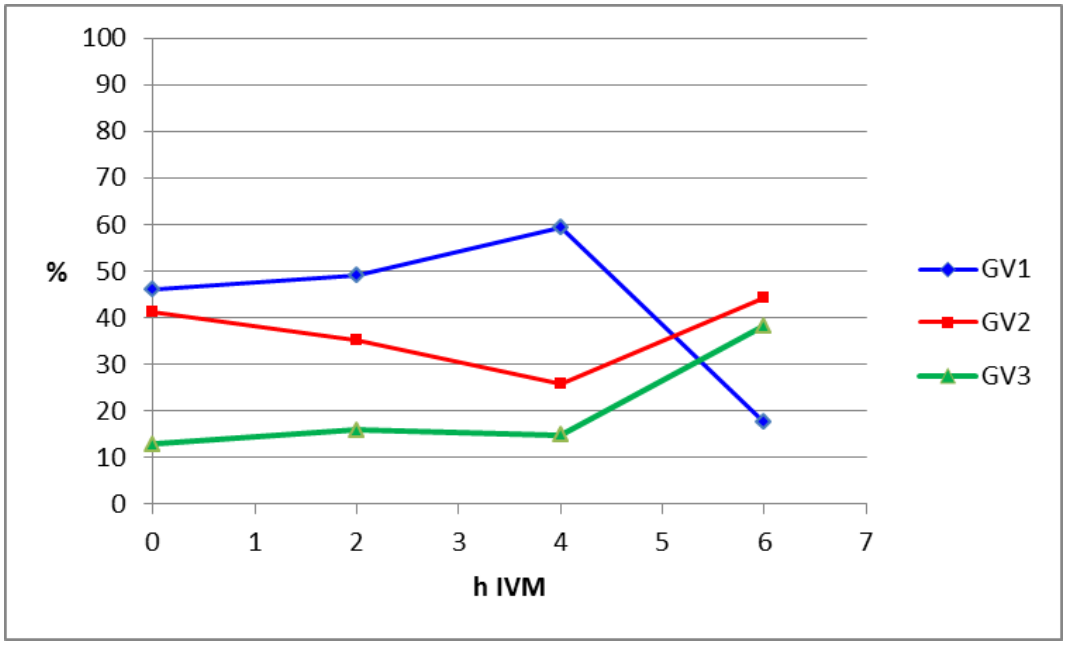

Figure 11: Frequency of GV stages 1, 2 and 3 from 0 to 6 hours of IVM.

4.2.2.3 Kinetics of the GVBD and progression of meiosis to MII

The GVDB occurred between 4 and 10 hours of IVM (Table 14, Figure 12). The proportion of GV oocytes dropped from close to 100% at 4 h IVM to only 3.8% at 8 h IVM. From 10 h IVM on, virtually all oocytes analyzed had exited the GV stage.

h IVM	Total oocytes	GV	GV (%)
0	106	102	96.2
2	62	57	91.9
4	55	54	98.2
6	64	34	53.1
8	53	2	3.8
10	64	0	0
12	74	0	0
14	67	1	1.5
16	73	0	0
18	63	0	0
20	66	1	1.5
22	58	0	0
23	57	0	0
24	29	0	0
26	34	0	0
28	29	0	0

Table 14: Frequency of GV oocytes from 0 to 28 hours of IVM.
Shown are the oocytes number and the weighted average values (%) from 4 (0 h IVM) and 2 (6-23 h IVM) independent experiments. Only oocytes classified as morphologically normal were included.

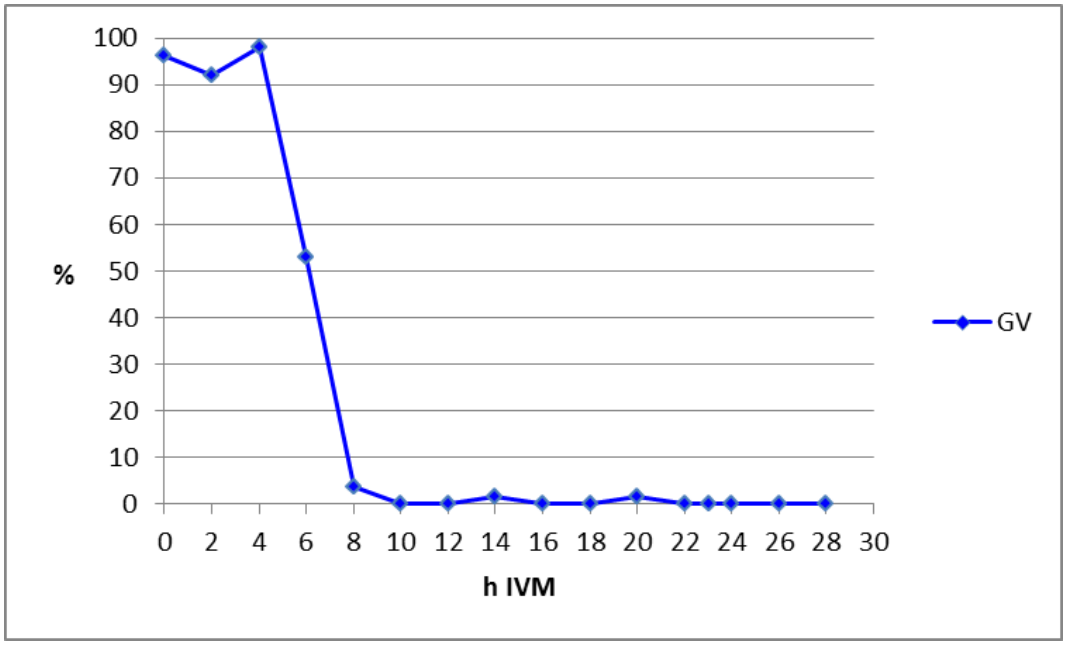

Figure 12: Frequency of GV oocytes from 0 to 28 h IVM.

Accordingly, the frequency of prometaphase I (proMI) oocytes increased from virtually zero at 4 h IVM to the highest levels between 8 and 14 hours (Table 15, Figure 13). At 10 h IVM, all oocytes had resumed meiosis and reached the ProMI stage. At 18 h IVM the proportion of ProMI oocytes had dropped down to 6.3% (Table 16, Figure 14). The first MI cells were documented at 12 h IVM, and accordingly, the minimum duration of ProMI was at least 6 hours. In the morphological analysis of the confocal image stacks, the ProMI was divided in three sub-stages as described in Table 10 and Figure 5. To reconstruct the process of the formation of the metaphase I spindle and of chromosome congression and alignment, the frequency of the ProMI sub-stages at the different time points was determined. The maximum of MI oocytes was observed at 16 h IVM. In parallel to the first MI oocytes, already a single AI oocyte with a first polar body was detected at 12 h IVM (Table 17, Figure 15). The highest ratio of MI oocytes was recorded at 16 hours, in parallel to the peak of oocytes in anaphase I (AI). At the time points 23, 24, 26 and 28 h IVM, 10 of 167 IVM oocytes (6%) had not reached meiosis II.

h IVM	N.oocytes	ProMI		MI		AI		ProMII		MII	
0	106	3	*(2.8)*	0	*(0)*	0	*(0)*	1	*(0.9)*	0	*(0)*
2	62	4	*(6.4)*	0	*(0)*	0	*(0)*	1	*(1.6)*	0	*(0)*
4	55	1	*(1.8)*	0	*(0)*	0	*(0)*	0	*(0)*	0	*(0)*
6	64	30	*(46.9)*	0	*(0)*	0	*(0)*	0	*(0)*	0	*(0)*
8	53	51	*(96.2)*	0	*(0)*	0	*(0)*	0	*(0)*	0	*(0)*
10	64	64	*(100)*	0	*(0)*	0	*(0)*	0	*(0)*	0	*(0)*
12	74	66	*(89.2)*	5	*(6.7)*	1	*(1.3)*	2	*(2.7)*	0	*(0)*
14	67	54	*(80.6)*	5	*(7.4)*	4	*(6)*	3	*(4.5)*	0	*(0)*
16	73	38	*(52.1)*	10	*(13.7)*	11	*(15.1)*	14	*(19.2)*	0	*(0)*
18	63	4	*(6.3)*	5	*(7.9)*	6	*(9.5)*	48	*(76.2)*	0	*(0)*
20	66	11	*(16.7)*	3	*(4.6)*	5	*(7.7)*	46	*(69.7)*	0	*(0)*
22	58	2	*(3.5)*	6	*(10.4)*	0	*(0)*	49	*(84.5)*	1	*(1.7)*
23	57	8	*(14)*	0	*(0)*	0	*(0)*	49	*(86)*	0	*(0)*
24	29	0	*(0)*	0	*(0)*	0	*(0)*	29	*(100)*	0	*(0)*
26	34	1	*(2.9)*	0	*(0)*	0	*(0)*	33	*(97.1)*	0	*(0)*
28	29	1	*(3.4)*	0	*(0)*	0	*(0)*	21	*(72.4)*	7	*(24)*

Table 15: Timetable of the progression of meiosis in morphologically normal oocytes. Shown are the oocytes number and (in brackets) the weighted average values (%) from 4 (0 h IVM) or 2 (2–23 h IVM) independent experiments. Only oocytes (954 in total) classified as morphologically normal were included.

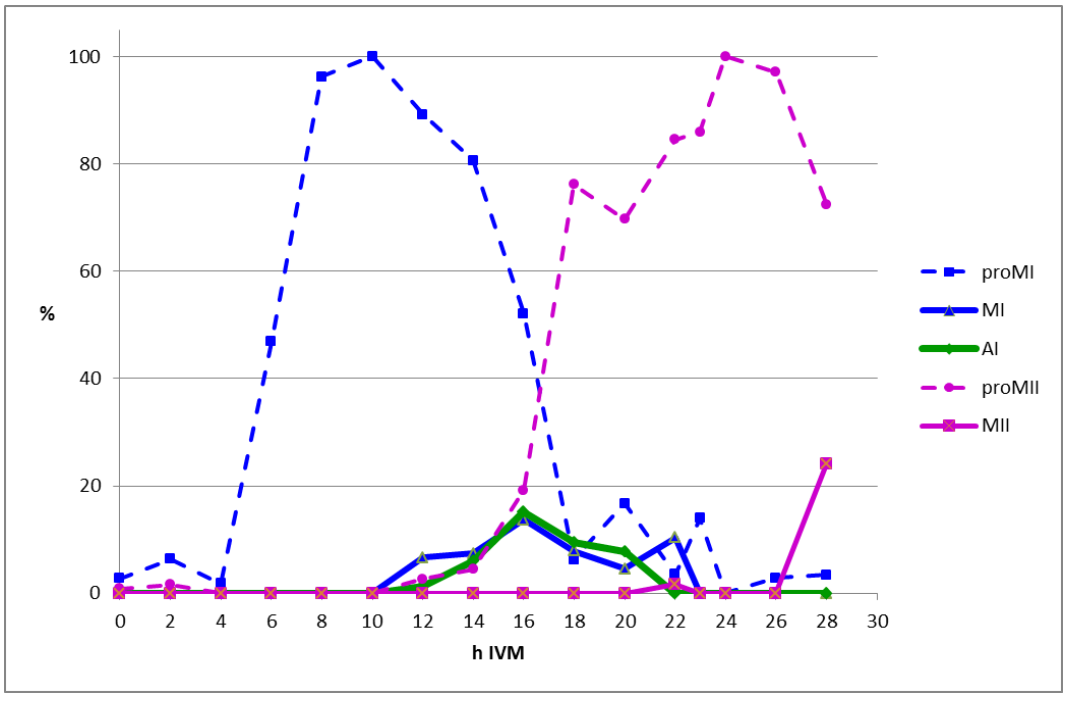

Figure 13: Time course of meiotic progression of morphologically normal oocytes. Shown is the percentage of oocytes at the different meiotic stages. The exact values are shown in Table 15.

h IVM	N. oocytes	GVBD		ProMI-A		ProMI-B		ProMI-C	
0	106	1	*(0.9)*	0	*(0)*	2	*(1.9)*	0	*(0)*
2	62	1	*(1.6)*	0	*(0)*	3	*(4.8)*	0	*(0)*
4	55	1	*(1.8)*	0	*(0)*	0	*(0)*	0	*(0)*
6	64	9	*(14.1)*	14	*(21.9)*	7	*(10.9)*	0	*(0)*
8	53	2	*(3.8)*	16	*(30.2)*	33	*(62.2)*	0	*(0)*
10	64	0	*(0)*	0	*(0)*	49	*(76.6)*	15	*(23.4)*
12	74	0	*(0)*	0	*(0)*	30	*(40.6)*	36	*(48.6)*
14	67	0	*(0)*	0	*(0)*	25	*(37.3)*	29	*(43.3)*
16	73	1	*(1.4)*	0	*(0)*	17	*(23.3)*	20	*(27.4)*
18	63	0	*(0)*	0	*(0)*	1	*(1.6)*	3	*(4.7)*
20	66	1	*(1.5)*	0	*(0)*	5	*(7.6)*	5	*(7.6)*
22	58	0	*(0)*	0	*(0)*	0	*(0)*	2	*(3.5)*
23	57	1	*(1.7)*	0	*(0)*	3	*(5.3)*	4	*(7)*
24	29	0	*(0)*	0	*(0)*	0	*(0)*	0	*(0)*
26	34	0	*(0)*	0	*(0)*	0	*(0)*	1	*(2.9)*
28	29	0	*(0)*	0	*(0)*	0	*(0)*	1	*(3.4)*

Table 16: Timetable of the GVBD and the prometaphase I-A, -B and –C stages in morphologically normal oocytes.
Shown are the oocytes number and (in brackets) the weighted average values (%) from 4 (0 h IVM) or 2 (2–23 h IVM) independent experiments. Only oocytes classified as morphologically normal were included.

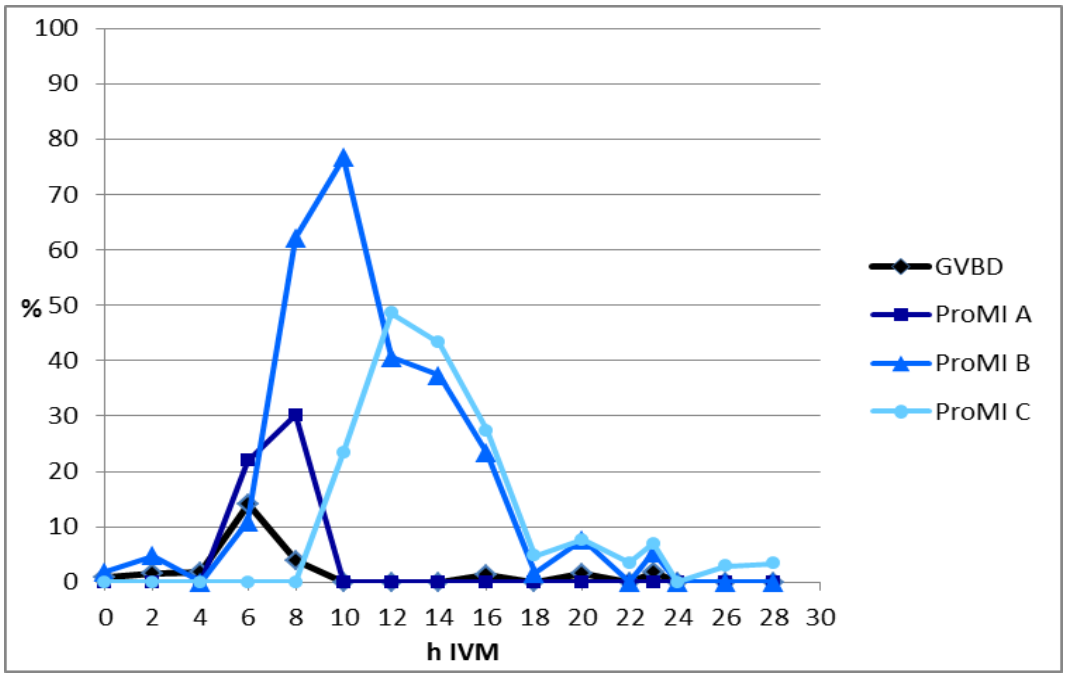

Figure 14: Frequency of oocytes at the GVBD and prometaphase I sub-stages.
Shown is the percentage of oocytes at the different meiotic stages. The exact values are shown in Table 16.

h IVM	Total oocytes	MI		A/TI		Mei I-II	
0	106	0	*(0)*	0	*(0)*	0	*(0)*
2	62	0	*(0)*	0	*(0)*	0	*(0)*
4	55	0	*(0)*	0	*0()*	0	*(0)*
6	64	0	*(0)*	0	*(0)*	0	*(0)*
8	53	0	*(0)*	0	*(0)*	0	*(0)*
10	64	0	*(0)*	0	*(0)*	0	*(0)*
12	74	5	*(6.7)*	1	*(1.3)*	1	*(1.3)*
14	67	5	*(7.4)*	4	*(6)*	2	*(3)*
16	73	10	*(13.7)*	11	*(15.1)*	9	*(12.3)*
18	63	5	*(7.9)*	6	*(9.5)*	10	*(15.8)*
20	66	3	*(4.6)*	5	*(7.6)*	4	*(6.2)*
22	58	6	*(10.4)*	0	*(0)*	0	*(0)*
23	57	0	*(0)*	0	*(0)*	0	*(0)*
24	29	0	*(0)*	0	*(0)*	0	*(0)*
26	34	0	*(0)*	0	*(0)*	0	*(0)*
28	29	0	*(0)*	0	*(0)*	0	*(0)*

Table 17: Timetable of the metaphase I, the ana-/telophase I and the meiosis I-II transition.
Shown are the oocytes number and (in brackets) the weighted average values (%) from 4 (0 h IVM) or 2 (2–23 h IVM) independent experiments. Only oocytes classified as morphologically normal were included.

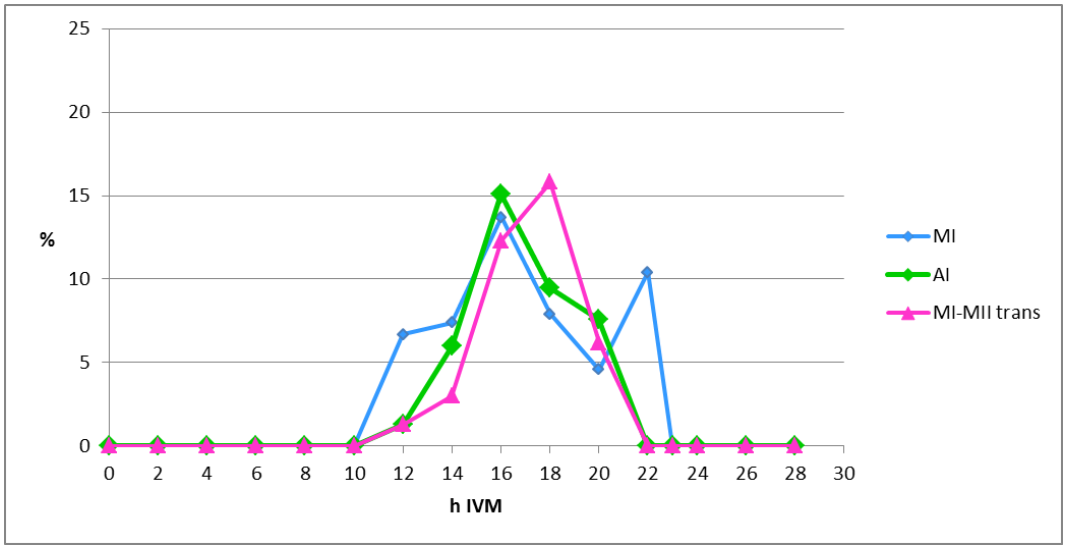

Figure 15: Time course of the metaphase I, the ana-/telophase I and the meiosis I-II transition.
Shown is the percentage of oocytes at different meiotic stages. The exact values are shown in Table 17

Prometaphase II (proMII) started shortly after the expulsion of the first polar body and seems to need at least 14 hours (Table 18, Figure 16). Notably, at 23 h IVM, a duration of IVM usually used for bovine oocytes, we could not detect metaphase II oocytes, characterized by regularly aligned between two half-spindles. The IVM duration had to be extended to 28 hours, to obtain the first MII oocytes

showing a regular alignment of chromosomes between the two flat MT arrays of a disk-shaped bipolar spindle (Table 18, Figure 16; see also Figure 8B).

h IVM	Total oocytes	ProMII-A		ProMII-B		MII	
0	106	1	*(0.9)*	0	*(0)*	0	*(0)*
2	62	0	*(0)*	1	*(1.6)*	0	*(0)*
4	55	0	*(0)*	0	*(0)*	0	*(0)*
6	64	0	*(0)*	0	*(0)*	0	*(0)*
8	53	0	*(0)*	0	*(0)*	0	*(0)*
10	64	0	*(0)*	0	*(0)*	0	*(0)*
12	74	1	*(1.3)*	0	*(0)*	0	*(0)*
14	67	1	*(1.5)*	0	*(0)*	0	*(0)*
16	73	3	*(4.1)*	2	*(2.7)*	0	*(0)*
18	63	25	*(39.7)*	13	*(20.6)*	0	*(0)*
20	66	28	*(42.4)*	14	*(21.2)*	0	*(0)*
22	58	26	*(44.8)*	23	*(39.7)*	1	*(1.7)*
23	57	38	*(66.7)*	11	*(19.3)*	0	*(0)*
24	29	22	*(75.9)*	7	*(24.1)*	0	*(0)*
26	34	26	*(76.5)*	7	*(20.6)*	0	*(0)*
28	29	13	*(44.8)*	8	*(27.6)*	7	*(24.1)*

Table 18: Timetable of the prometaphase II - metaphase II stages.
Shown are the oocytes number and (in brackets) the weighted average values (%) from 4 (0 h IVM) or 2 (2–23 h IVM) independent experiments. Only oocytes classified as morphologically normal were included.

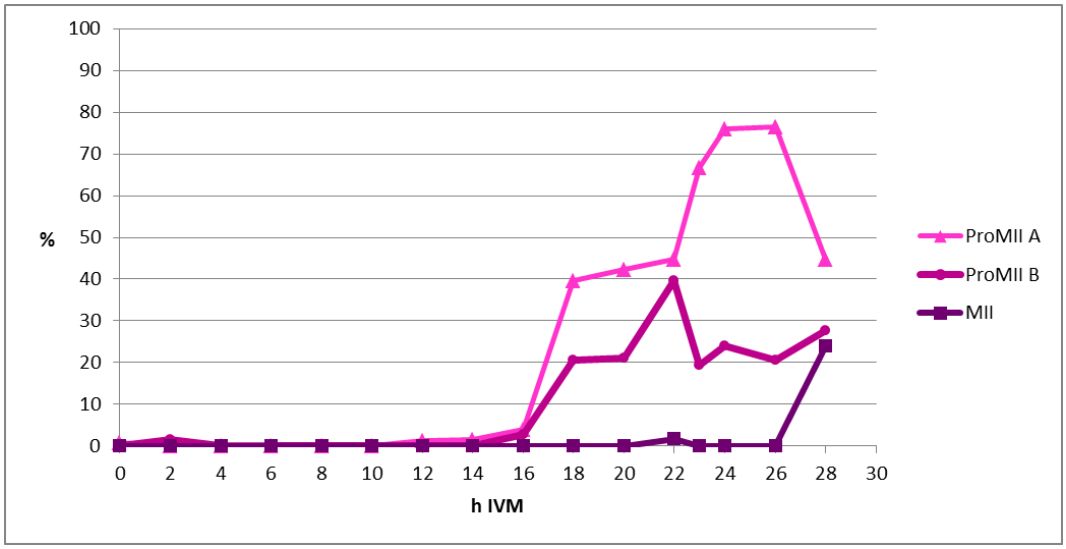

Figure 16: Time course of prometaphase II and metaphase II stages.
Shown is the percentage of oocytes at different meiotic stages. The exact values are shown in Table 18.

4.2.3 Characterization and classification of anomalies of oocyte maturation

The three-dimensional microscopic analysis revealed a broad spectrum of abnormalities, which were divided in five groups:

1) Spontaneous oocyte activation
2) Separate chromosome aggregates at prometaphase I
3) Irregular prometaphase I/II spindle
4) Multipolar metaphase I spindle
5) Irregular ana-/telophase I:
    a) Irregular chromatin segregation:
        i) Unaligned chromosomes
        ii) Lagging chromosomes
        iii) Chromatin bridges
    b) Abnormal positioning and/or orientation of the meiosis I spindle
    c) Irregular chromosome segregation and meiosis I spindle:
        i) Meiotic self-enucleation.
        ii) Multipolar ana-/telophase I with chromatin bridges.
        iii) Unaligned chromosomes combined with spindle anomalies
        iv) Lagging chromosomes combined with spindle anomalies
        v) Chromatin bridges combined with spindle anomalies

Most of the abnormalities identified in this study were combinations of abnormal chromosome segregation and spindle anomalies.

4.2.3.1 Spontaneous oocyte activation

Sporadically, we found oocytes which had already been activated independent of sperm cells. A schematic illustration and two examples from the study are shown in Figure 17 and representative microscopic image stacks are exhibited in Figure

18.

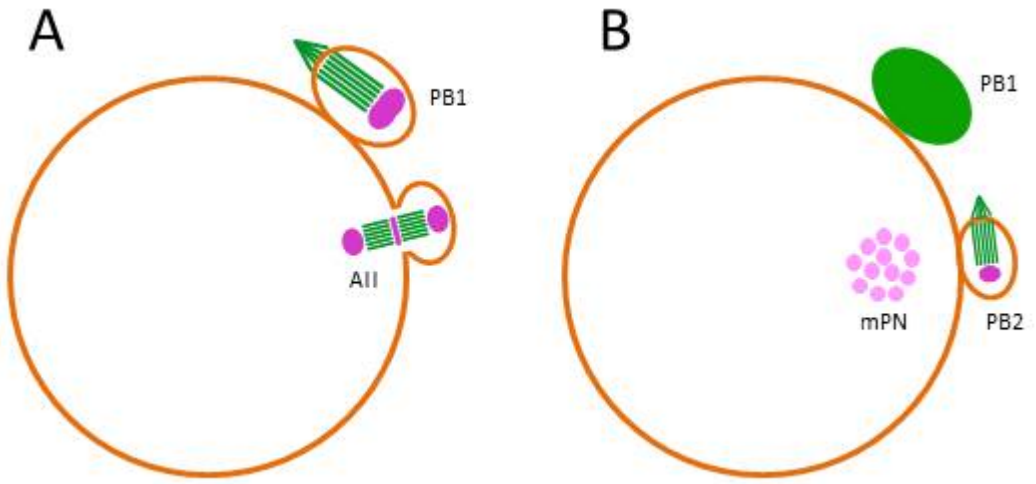

Figure 17: Schematic illustration of spontaneous oocyte activation.
(A) Anaphase II and **(B)** pronuclear stage. PB=polar body, mPN= maternal pronucleus.

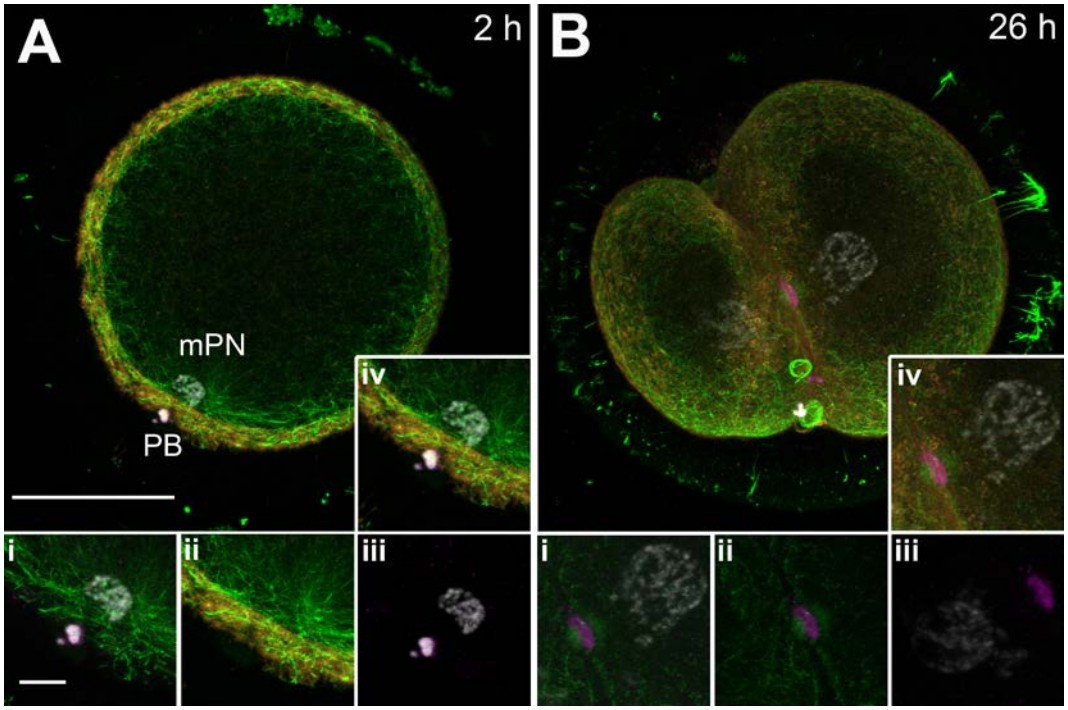

Figure 18: Spontaneous oocyte activation.
(A) Spontaneously activated oocyte in the pronuclear stage. **(B)** Parthenogenetic two-cell embryo. DAPI-stained DNA is depicted in white, α-tubulin in green, f-actin in orange and H3S10p in magenta. The images are maximum intensity projections of subsets of the optical sections. The two panels present overview images **(A, B)** and detail views (i-iv) i.e. overlay images of (i) DNA, H3S10p and MTs, (ii) microtubules and f-actin, (iii) DNA and H3S10p and (iv) all four stains. The chromatin of the maternal pronucleus and the nuclei of the two-cell embryo are H3S10p negative. The midbody of the first cleavage division is intensely H3S10p-positive. Scale bar = 50 µm (overviews) or 10 µm (details) PB=polar body, mPN= maternal pronucleus.

4.2.3.2 Separate chromatin particles at chromosome aggregation before the GVBD and at later stages of meiosis I

During the characterization of GV phenotypes, we noted GV2 and GV3 oocytes showing one or more chromatin particles separate from the main aggregating and condensing chromatin mass in the GV. Notably, we detected oocytes after the GBDV and in early stages of prometaphase I, where we found two or more unevenly sized condensed chromatin masses which seemed to start independently the formation of a MT spindle. Moreover, we recorded separate unaligned chromatin particles in late prometaphase I and metaphase I. Figure 19 presents a schematic illustration, how a disturbed chromosome aggregation at the late GV stage before the GVBD might be linked to separate unaligned chromosomes in meiosis I.

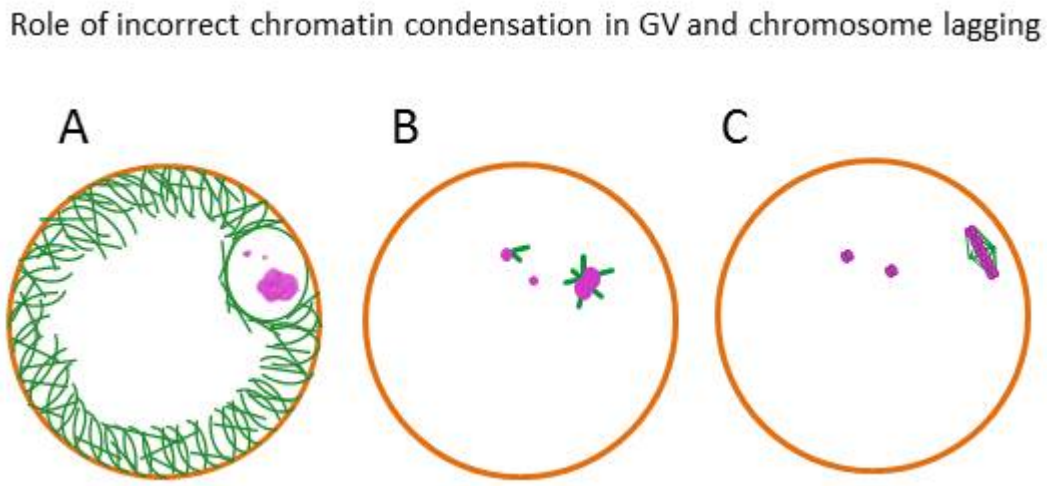

Figure 19: Schematic illustration of how a disturbed chromosome aggregation at the late GV stage might be linked to separate unaligned chromosomes in meiosis I.

(**A**) GV oocyte with small chromatin particles separate from the major chromosomes aggregate in the center of the GV; (**B**) Oocyte after GVBD showing the onset of prometaphase spindle formation. Separate chromosomes are not included in MI spindle formation. (**C**) Metaphase I with unaligned bivalent chromosomes far away from the MI plate.

Figure 20 shows representative microscopic image stacks of separate chromosomes in prometaphase I (proMI-A).

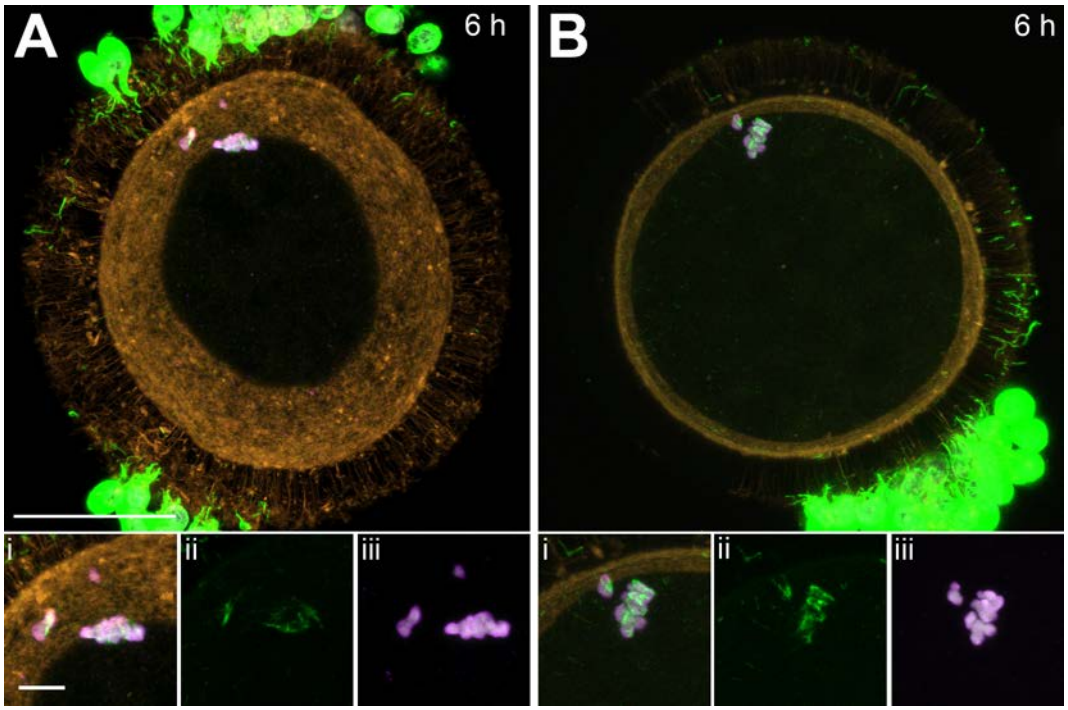

Figure 20: Examples of separate chromosomes in early prometaphase I.
(**A**) Oocyte presenting a remarkable distance between the two small chromatin particles and the main chromosomes aggregate. **(B)** Oocyte containing one small separate chromosomes aggregate. DAPI-stained DNA is depicted in white, α-tubulin in green, f-actin in orange and H3S10p in magenta. The images are maximum intensity projections of subsets of the optical sections. The two panels present overview images (A, B) and detail views (i-iii) i.e. overlay images of (i) all four stains, (ii) microtubules alone and (iii) DNA and H3S10p. Scale bar: 50 µm (overview) and 10 µm (details).

4.2.3.3 Multipolar (pro-)metaphase I spindle

At late time points from 20 to 28 h IVM, we found severely delayed and possibly arrested oocytes in metaphase I with an abnormal multipolar spindle and irregularly arranged chromosomes due to the MT nucleation from three or more MT organizing centers (MTOCs).

We also could document cases of a multipolar prometaphase I combined with unaligned distant chromatin particles (Figure 21 and Figure 22), which might be linked to disturbances of the chromosome aggregation at the late GV stage before the GVBD (see Figure 19).

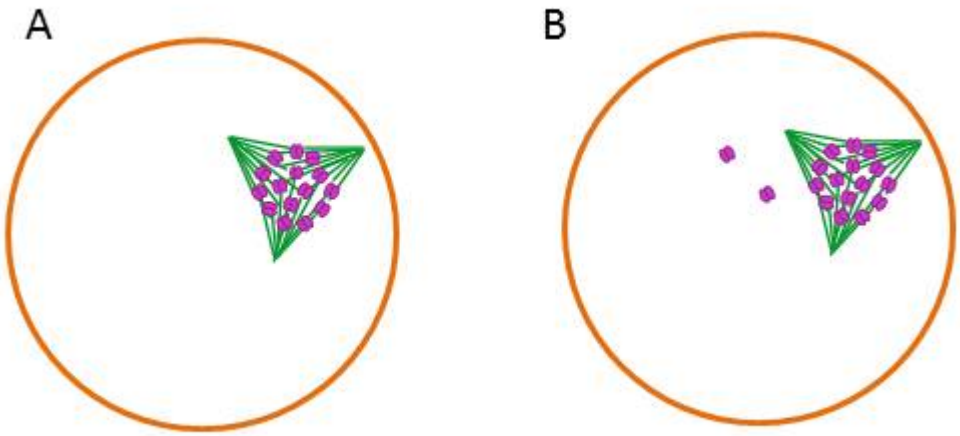

Figure 21: Schematic illustration of a multipolar (pro-)metaphase I spindle.
(**A**) Multipolar ProMI spindle with three microtubular organization centers. (**B**) Multipolar ProMI spindle with distant unaligned chromosomes.

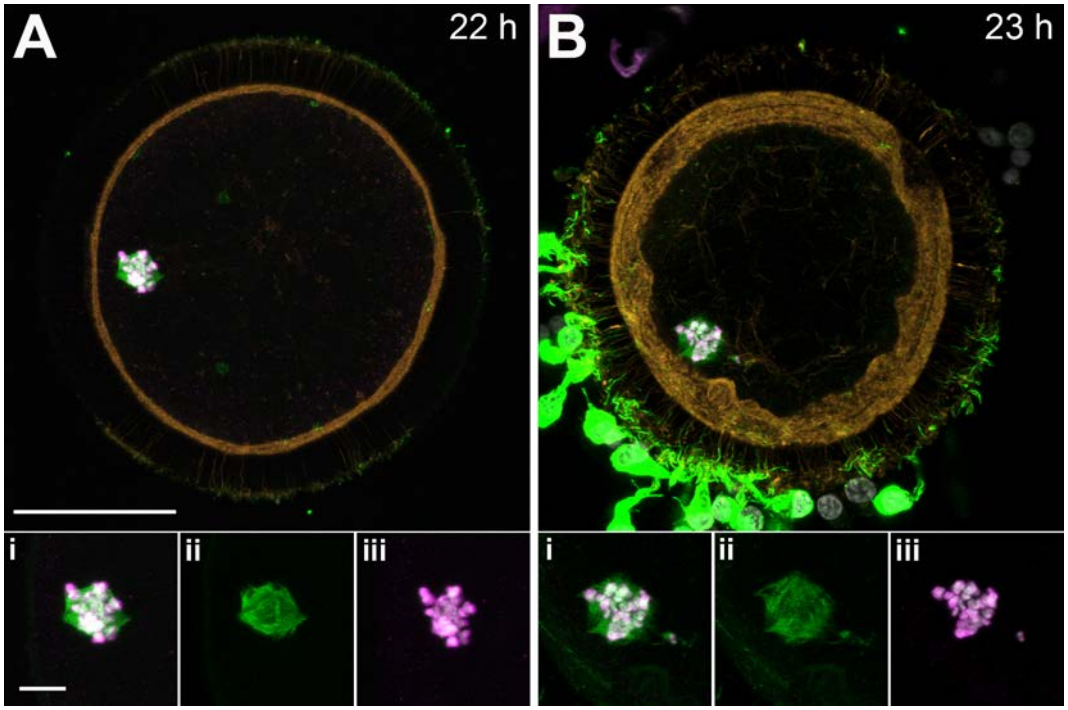

Figure 22: Multipolar (pro-)metaphase I.
(A) Multipolar (pro-)metaphase I: in this case, the oocyte seems to present a tripolar spindle organization. **(B)** Oocyte with a multipolar (pro-)metaphase I spindle and a distant unaligned chromosome. Oocytes with a multipolar metaphase I spindle were observed from 20 to 28 h IVM and severely delayed. DAPI-stained DNA is depicted in white, α-tubulin in green, f-actin in orange and H3S10p in magenta. The images are maximum intensity projections of subsets of the optical sections. The two panels present overview images (A, B) and detail views (i-iii) i.e. overlay images of (i) DNA, MTs and H3S10p, (ii) MTs alone and (iii) DNA and H3S10p. Scale bar: 50 µm (overview) and 10 µm (details).

4.2.3.4 Anaphase I aberrations:

Morphologically, the aberrations observed at anaphase I stage were divided in three groups: (i) abnormal chromosome segregation, (ii) spindle anomalies and (iii) aberrations involving both the chromatin and the spindle apparatus.

4.2.3.4.1 Abnormal chromosome segregation

The aberrations of chromosomes segregation without apparent spindle anomalies were divided into three types: (i) unaligned chromosomes, (ii) lagging (anaphase) chromosomes and (iii) chromatin bridges. A schematic illustration of the three types of chromosome segregation errors and confocal images of representative oocytes are presented in Figure 23 and Figure 24.

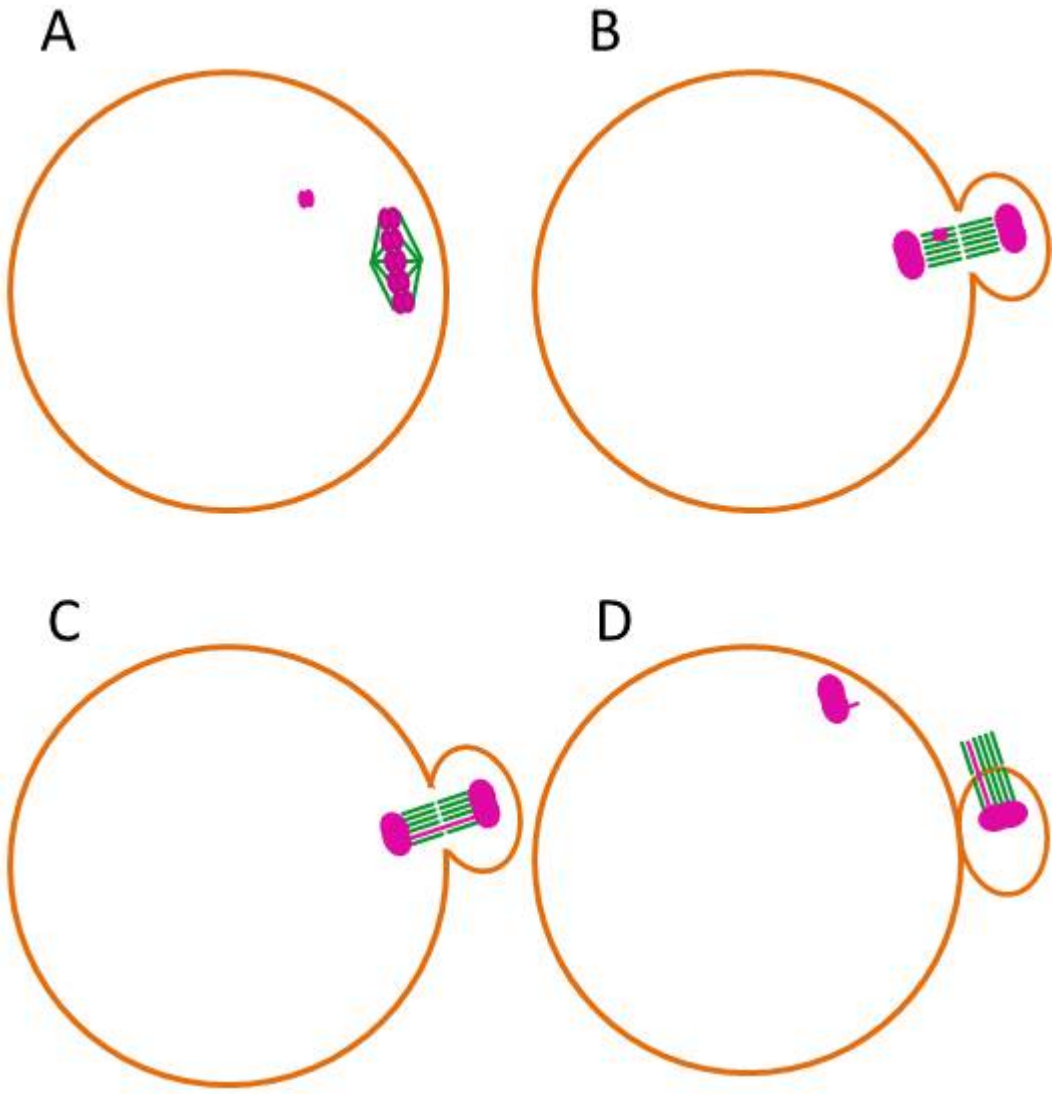

Figure 23: Schematic illustration of chromosome segregation errors in meiosis I without spindle anomalies.
(A) Distant unaligned chromosome. **(B)** Lagging chromosome at anaphase I. **(C)** Intact and **(D)** broken chromatin bridge.

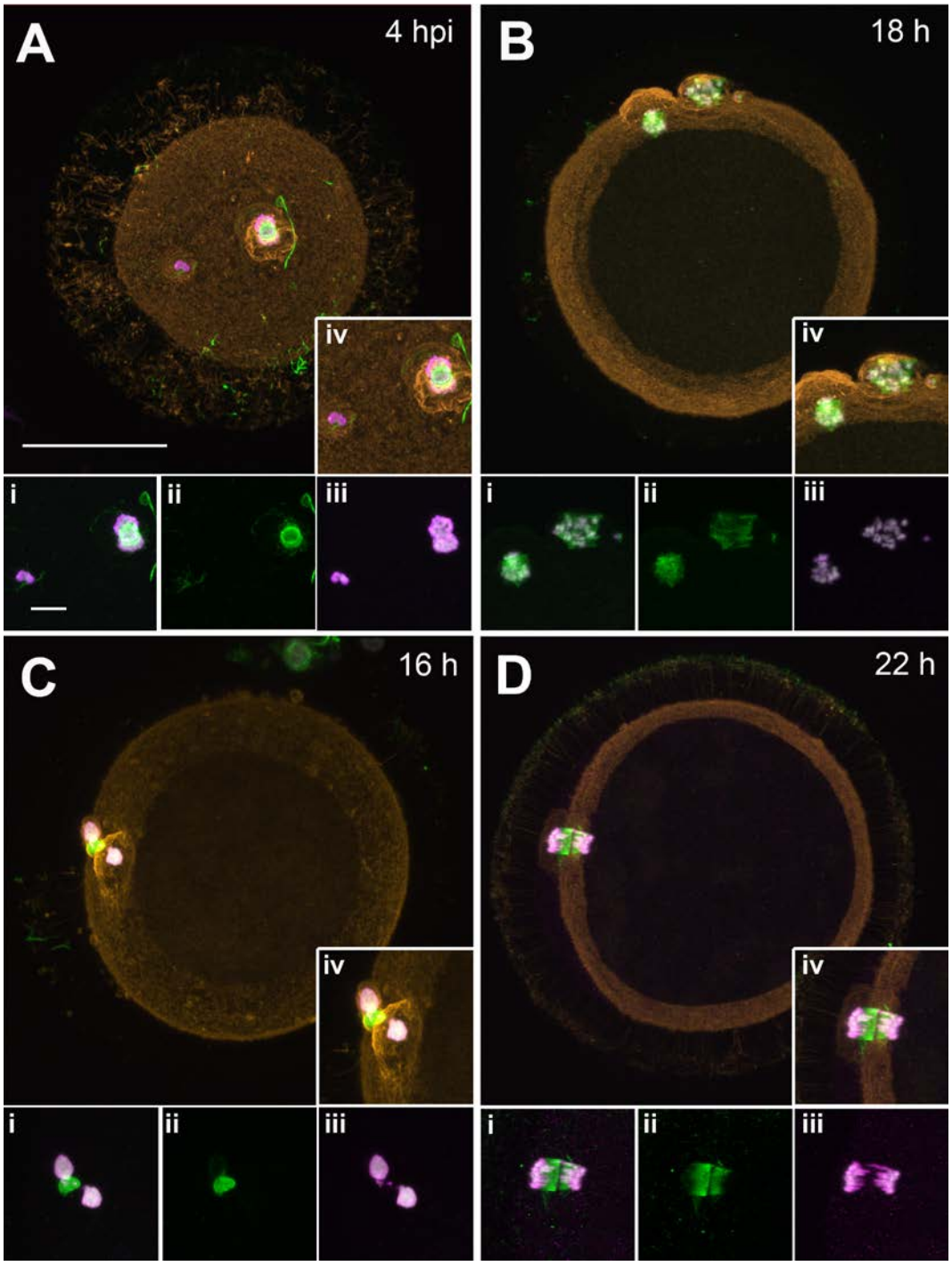

Figure 24: Unaligned chromosomes, lagging chromosomes and chromatin bridges.
(A) Distant unaligned chromosomes at a delayed anaphase I. **(B)** Early prometaphase II oocyte with a lagging chromosome which has been lost during polar body extrusion. **(C)** Chromatin bridge at ana/telophase I. The chromatin bridge is intensely H3S10p positive. **(D)** Multiple chromatin bridges at anaphase I. The chromatin bridges are intensely H3S10p positive. DAPI-stained DNA is depicted in white, α-tubulin in green, f-actin in orange and H3S10p in magenta. The images are maximum intensity projections of subsets of the optical sections. Each panel presents: overview images (A, B) and detail views (i-iv) i.e. overlay images of (i) DNA, MTs and H3S10p, (ii) MTs alone, (iii) DNA and H3S10p and (iv) all four stains. Scale bar: 50 µm (overviews) and 10 µm (details).

4.2.3.4.2 Incorrect positioning and orientation of the anaphase I spindle

In our experiments, we could document oocytes showing an irregular position of the anaphase I spindle i.e. too far away from the oocyte surface or showing an incorrect spindle orientation (parallel instead of perpendicular to the oocyte surface). In both cases, no polar body can be extruded and two separate haploid sets of (two-chromatid) chromosomes remain in the oocyte. A schematic illustration is presented in Figure 25. Incorrect orientation of the anaphase spindle and dysfunctions of the oocyte cortex may also result in the self-enucleation of the oocyte by segregating all chromosomes in the polar body. Confocal image stacks of representative oocytes are shown in Figure 26.

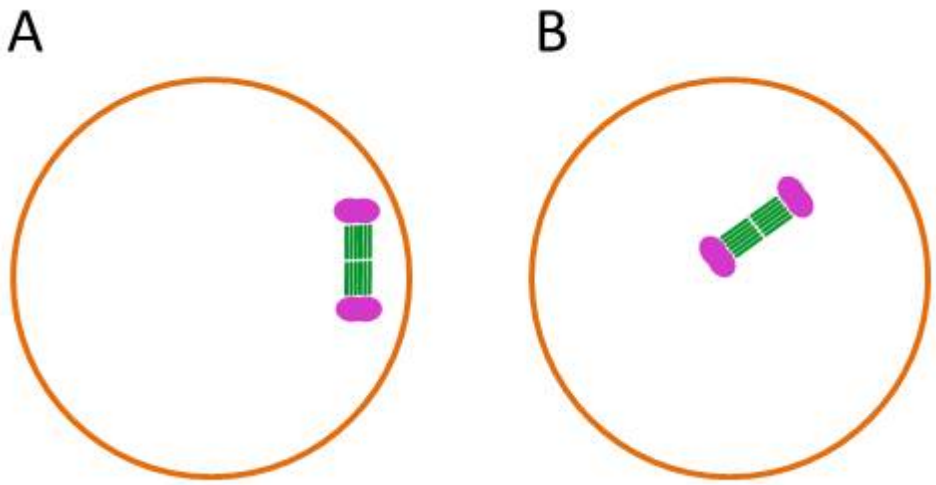

Figure 25: Schematic illustration of irregular orientation and irregular positioning of the anaphase I spindle.
(A) Irregular orientation and **(B)** irregular positioning of the anaphase I spindle. In both cases, no polar body is extruded.

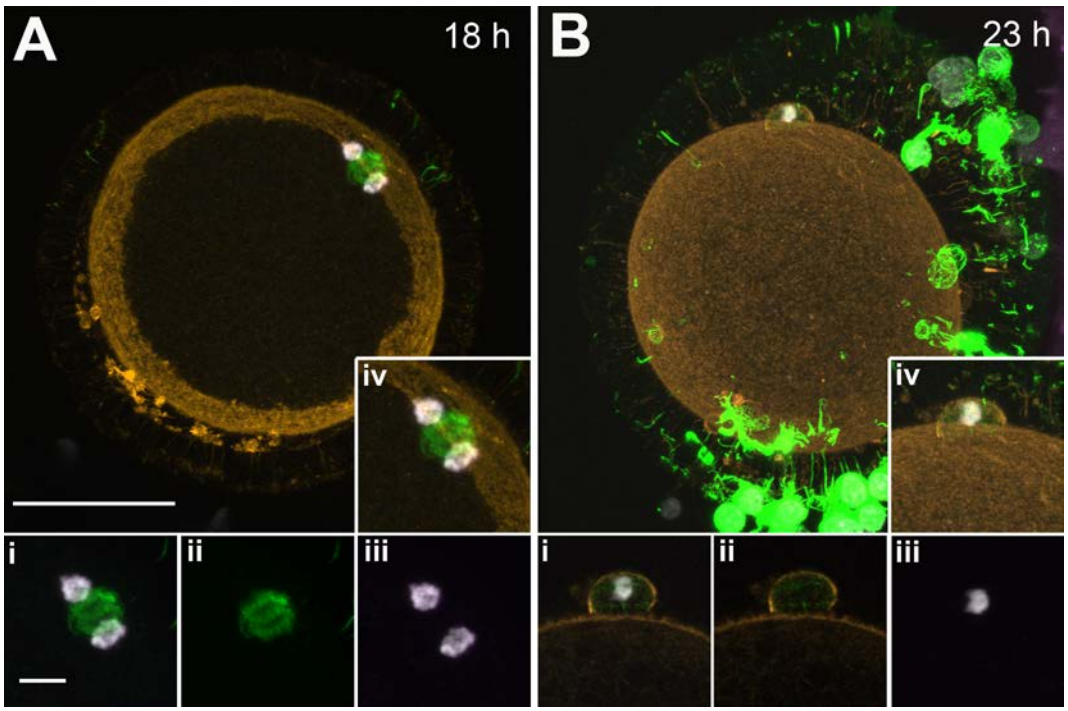

Figure 26: Examples of the failure of the extrusion of the first polar body and meiotic self-enucleation of the oocyte.
(A) Failure of polar body extrusion due to an incorrect orientation of the anaphase I spindle. **(B)** Self-enucleation at meiosis I: all chromosomes have been segregated into the first polar body. DAPI-stained DNA is depicted in white, α-tubulin in green, f-actin in orange and H3S10p in magenta. The images are maximum intensity projections of subsets of the optical sections. Only (Bi-iii) show a detail of a single optical section. Both panels show: overview images (A, B) and detail views (i-iv) i.e. overlay images of (i) DNA, MTs and H3S10p, (ii) MTs alone, (iii) DNA and H3S10p and (iv) all four stains. Scale bar: 50 µm (overviews) and 10 µm (details).

4.2.3.4.3 Irregular anaphase I spindle and chromatin segregation errors

In this study, the majority of the anaphase I aberrations detected involved both chromosome segregation and MI/AI spindle (Figure 27 and Figure 28).

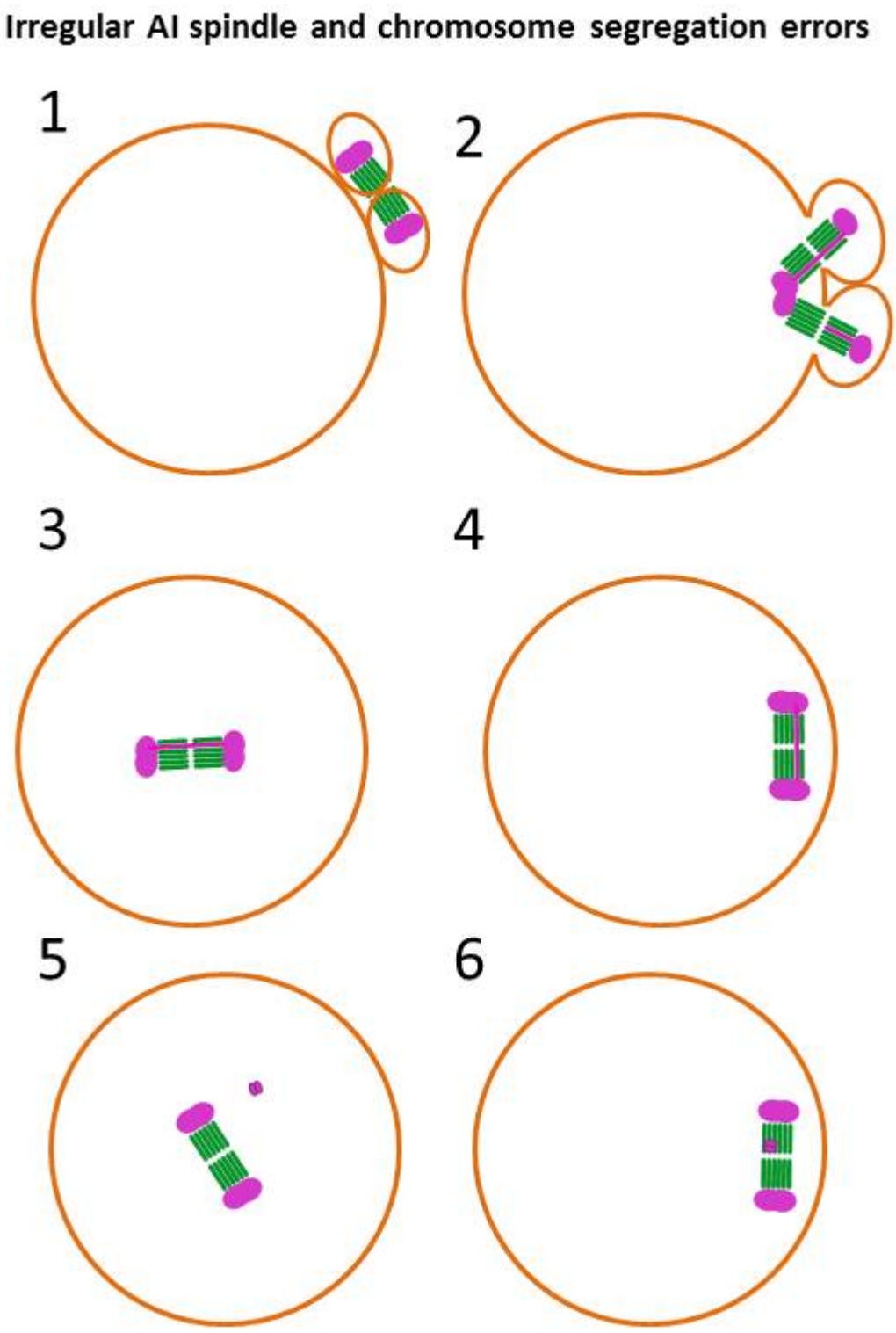

Figure 27: Schematic illustration of spindle anomalies and abnormal chromosomes segregations at meiosis I.

(1) Self-enucleation at meiosis I. **(2)** Multipolar anaphase I spindle and multiple chromatin bridges both intact and broken. **(3)** Irregular AI spindle positioning and chromatin bridge. **(4)** Irregular AI spindle orientation and chromatin bridge. **(5)** Irregular AI spindle positioning and distant unaligned bivalent chromosome. **(6)** Irregular AI spindle orientation and lagging chromosome.

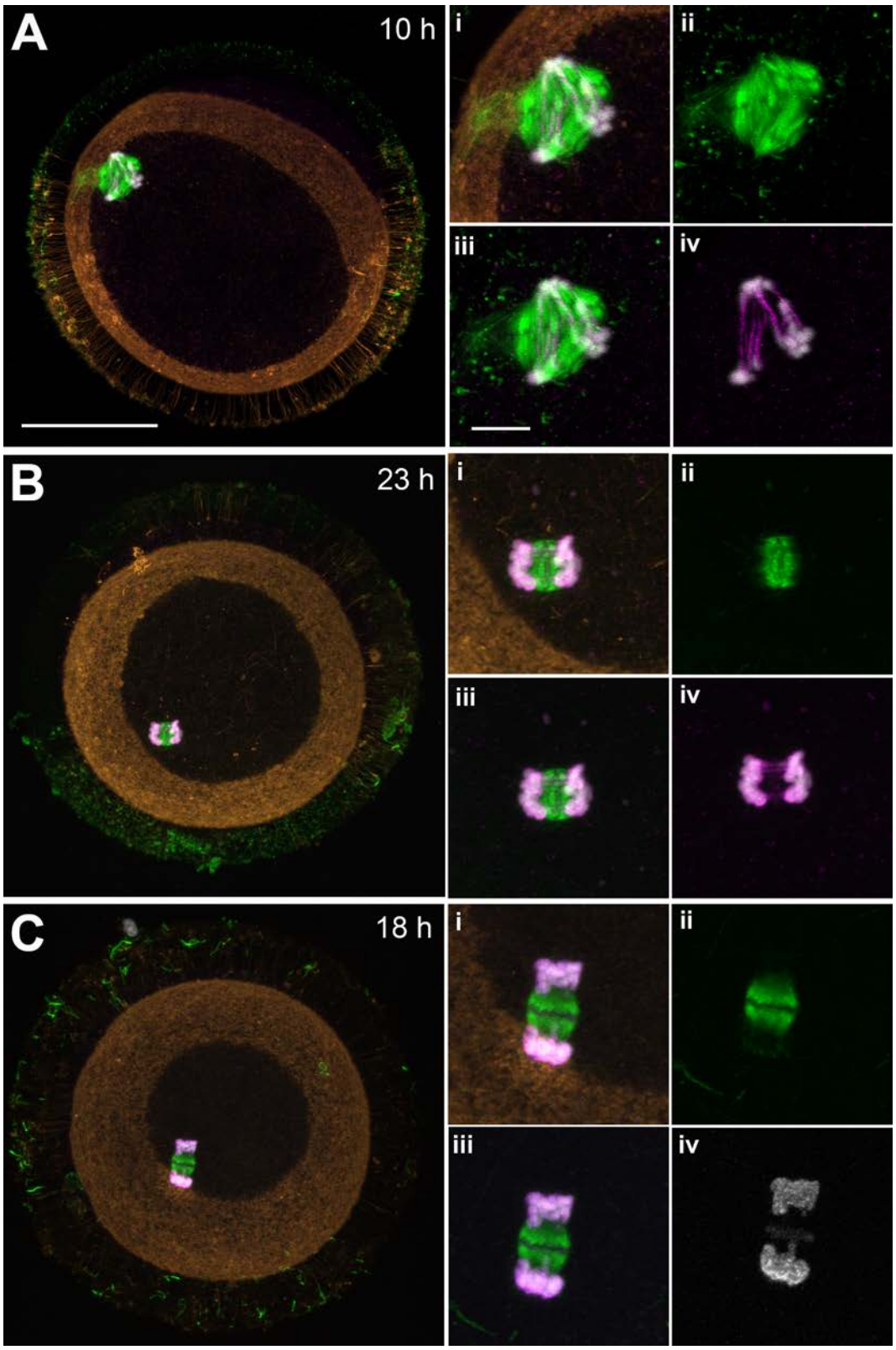

Figure 28: Examples of irregular anaphase I.
(A) Multipolar anaphase I combined with irregular spindle positioning and multiple chromatin bridges. **(B)** Irregular positioning of anaphase I spindle combined with multiple chromatin bridges. **(C)** Irregular anaphase I spindle with multiple chromatin bridges and irregular spindle orientation. DAPI-stained DNA is depicted in white, α-tubulin in green, f-actin in orange and H3S10p in magenta. The images are maximum intensity projections of subsets of the optical sections. Each panel presents (A, B, C) an overview image and (i-iv) details i.e. (i) an overlay of all four stains, (ii) microtubules alone, (iii) an overlay of DNA, H3S10p and α-tubulin stainings, and (iv) an overlay of DNA and H3S10p stainings. For better presentation of the chromatin bridge and the midbody, figure (Civ) shows only the H3S10p labeling. Scale bar: 50 µm (overviews) and 10 µm

(details).

4.2.4 The incidence of the detected anomalies

In total, over all experiments, 41 of 1078 oocytes (3.8%) were classified as degenerated and not further characterized. In total 84 i.e. 7.79% of the 1078 oocytes analyzed showed anomalies as described above. Table 19 gives an overview of the total incidence of the detected anomalies subdivided in five types. Table 20 presents the incidences of the five types of anomalies at the different time points of IVM. Four oocytes were found to have been spontaneously activated. 28 oocytes presented separate chromatin aggregates after GVBD. Eight oocytes were classified as displaying an irregular microtubule organization in prometaphase I. A multipolar (pro-)metaphase I (multipolar MI) was detected in 10 oocytes. Oocytes with a multipolar MI were only found from 20-28 h IVM and severely delayed. Anomalies of ana- and telophase I could be documented in 34 oocytes.

Type of anomaly	**Number of oocytes**
Spontaneous oocyte activation	4
Separate chromosome aggregates at prometaphase I	28
Irregular prometaphase MI spindle	8
Multipolar metaphase I spindle	10
Irregular anaphase I	34
TOTAL	84

Table 19: Incidence of the five types of anomalies over all experiments.
In total, over all experiments, 1078 oocytes were analyzed from 0 to 28 hours of IVM.

h IVM	n	Spontaneous activation		Separate chromatin aggregates		Irregular proMI-/MII spindle		Multipolar MI spindle		Irregular AI	
0	126	0	*(0)*	0	*(0)*	0	*(0)*	0	*(0)*	0	*(0)*
2	66	1	*(1.5)*	0	*(0)*	0	*(0)*	0	*(0)*	0	*(0)*
4	61	0	*(0)*	0	*(0)*	0	*(0)*	0	*(0)*	0	*(0)*
6	77	1	*(1.3)*	9	*(11.7)*	0	*(0)*	0	*(0)*	0	*(0)*
8	67	0	*(0)*	12	*(17.9)*	0	*(0)*	0	*(0)*	0	*(0)*
10	69	0	*(0)*	3	*(4.3)*	1	*(1.4)*	0	*(0)*	1	*(1.4)*
12	80	0	*(0)*	0	*(0)*	1	*(1.3)*	0	*(0)*	4	*(5)*
14	74	0	*(0)*	0	*(0)*	0	*(0)*	0	*(0)*	4	*(5.4)*
16	82	1	*(1.2)*	0	*(0)*	2	*(2.4)*	0	*(0)*	6	*(7.3)*
18	71	0	*(0)*	1	*(1.4)*	1	*(1.4)*	0	*(0)*	6	*(8.4)*
20	73	0	*(0)*	1	*(1.3)*	2	*(2.8)*	1	*(1.4)*	1	*(1.3)*
22	65	0	*(0)*	1	*(1.5)*	0	*(0)*	3	*(4.6)*	4	*(6.2)*
23	69	0	*(0)*	0	*(0)*	0	*(0)*	3	*(4.3)*	8	*(11.6)*
24	31	0	*(0)*	1	*(3.2)*	1	*(3.2)*	1	*(3.2)*	0	*(0)*
26	35	1	*(2.9)*	0	*(0)*	0	*(0)*	0	*(0)*	0	*(0)*
28	32	0	*(0)*	0	*(0)*	0	*(0)*	2	*(6.3)*	0	*(0)*

Table 20: Incidences of the five types of anomalies detected by CLSM analysis.
Shown are the oocytes number (n) and (in brackets) the weighted average values (%) from 4 (0 h IVM) or 2 (2–23 h IVM) independent experiments.

Table 21 gives an overview of the incidence of the different ana- and telophase I anomalies. The incidences of the abnormalities detected at the different time points of IVM are presented in Table 22 and Table 23. Notably, in 21 of 34 cases of an abnormal ana- and telophase I, chromatin bridges alone or combined with spindle anomalies were found.

In this study, at the time points 23, 24, 26 and 28 h IVM, 10 of 167 IVM oocytes (6%) had not reached meiosis II.

Anomalies of ana- and telophase I	Number of oocytes
Chromatin bridges	8
Unaligned and lagging chromosomes	3
Irregular spindle orientation/positioning	3
Multipolar anaphase I spindle	2
Irregular anaphase I spindle and lagging chromosomes	2
Irregular anaphase I spindle and chromatin bridge	13
Self-enucleation	3
Total	34

Table 21: Incidence of anomalies of ana- and telophase I among all experiments.
In total, among all experiments, 1078 oocytes were analyzed from 0 to 28 hours of IVM.

h IVM	n	Chromatin bridges		Unaligned and lagging Chromosomes		Irregular spindle position/orientation	
0	126	0	*(0)*	0	*(0)*	0	*(0)*
2	66	0	*(0)*	0	*(0)*	0	*(0)*
4	61	0	*(0)*	0	*(0)*	0	*(0)*
6	77	0	*(0)*	0	*(0)*	0	*(0)*
8	67	0	*(0)*	0	*(0)*	0	*(0)*
10	69	0	*(0)*	0	*(0)*	0	*(0)*
12	80	1	*(1.2)*	0	*(0)*	1	*(1.3)*
14	74	2	*(2.7)*	0	*(0)*	0	*(0)*
16	82	1	*(1.2)*	0	*(0)*	1	*(1.2)*
18	71	0	*(0)*	1	*(1.4)*	1	*(1.4)*
20	73	1	*(1.3)*	0	*(0)*	0	*(0)*
22	65	1	*(1.5)*	1	*(1.5)*	0	*(0)*
23	69	2	*(2.9)*	1	*(1.4)*	0	*(0)*
24	31	0	*(0)*	0	*(0)*	0	*(0)*
26	35	0	*(0)*	0	*(0)*	0	*(0)*
28	32	0	*(0)*	0	*(0)*	0	*(0)*

Table 22: Incidences of anaphase I anomalies affecting only chromosome segregation.
Shown are the oocytes number (n) and (in brackets) the weighted average values (%) from 4 (0 h IVM) or 2 (2–23 h IVM) independent experiments.

h IVM	n	Multipolar anaphase spindle		Irregular spindle + lagging chromosomes		Irregular spindle + chromatin bridge		Self-enucleation	
0	126	0	*(0)*	0	*(0)*	0	*(0)*	0	*(0)*
2	66	0	*(0)*	0	*(0)*	0	*(0)*	0	*(0)*
4	61	0	*(0)*	0	*(0)*	0	*(0)*	0	*(0)*
6	77	0	*(0)*	0	*(0)*	0	*(0)*	0	*(0)*
8	67	0	*(0)*	0	*(0)*	0	*(0)*	0	*(0)*
10	69	1	*(1.4)*	0	*(0)*	0	*(0)*	0	*(0)*
12	80	0	*(0)*	0	*(0)*	2	*(2.5)*	0	*(0)*
14	74	0	*(0)*	0	*(0)*	2	*(2.7)*	0	*(0)*
16	82	0	*(0)*	1	*(1.2)*	3	*(3.6)*	0	*(0)*
18	71	0	*(0)*	0	*(0)*	4	*(5.6)*	0	*(0)*
20	73	0	*(0)*	0	*(0)*	0	*(0)*	0	*(0)*
22	65	0	*(0)*	1	*(1.5)*	1	*(1.5)*	0	*(0)*
23	69	1	*(1.4)*	0	*(0)*	1	*(1.4)*	3	*(4.4)*
24	31	0	*(0)*	0	*(0)*	0	*(0)*	0	*(0)*
26	35	0	*(0)*	0	*(0)*	0	*(0)*	0	*(0)*
28	32	0	*(0)*	0	*(0)*	0	*(0)*	0	*(0)*

Table 23: Incidences of anaphase I anomalies affecting both chromosome segregation and spindle.
Shown are the oocytes number (n) and (in brackets) the weighted average values (%) from 4 (0 h IVM) or 2 (2–23 h IVM) independent experiments.

4.3 Analysis of *in vitro* fertilization (4-12 hpi)

To investigate the first steps of fertilization i.e. the sperm penetration, the oocyte activation and the formation of the pronuclei, class I and II oocytes were matured, inseminated *in vitro* and fixed at different time points from 4-12 hours after insemination (hpi) to be stained and imaged *in toto* by serial confocal sections (for an overview of the experimental approach see Figure 1). Over all experiments, the proportion of oocytes that were lost during denudation, staining and embedding for microscopy was in the range of 18 percent. In total, 654 oocytes were analyzed (Table 24).

hpi	**4**	**5**	**6**	**7**	**8**	**10**	**12**
Series 1	33	36	39	31	33	11	28
Series 2		37	34	22	44	29	41
Series 3			55		26		36
Series 4					38	30	
Series 5			20		31		
TOTAL	33	73	148	53	172	70	105

Table 24: Number of oocytes analyzed per experiment and per time point (hpi).
The table indicates the number of independent experiments and the number of oocytes analyzed per experiment and time point. hpi = hours post insemination.

4.3.1 Kinetics of sperm head penetration and oocyte activation

For practical reasons, oocytes were designated as fertilized, when they (i) had been activated and at least progressed to anaphase II and (ii) a partial or complete entry of the sperm nucleus was seen. As presented in Table 25 and Figure 29, the first fertilized i.e. penetrated and activated oocytes were observed at 5 hpi. From hpi 5 to 12 hpi, the fertilization rate increased from 19.1 % to 89.5 % (Figure 29). In total, 334 sperm-penetrated and activated oocytes were analyzed. Monospermy was found in 295 oocytes (88.32 % among fertilized), polyspermy in 40 oocytes (6.11 % of all oocytes and 11.94 % of the fertilized oocytes). 245 fertilized oocytes (73.1 % of all fertilized oocytes) appeared to be morphologically normal.

hpi	n	Fertilized	Monospermy	Polyspermy
4	33	0	*0*	*0*
5	73	13	*21*	*0*
6	148	41	*42.3*	*5.4*
7	53	17	*46*	*3.7*
8	172	69	*59.5*	*7*
10	70	36	*76.6*	*11.4*
12	105	69	*93.3*	*9.5*

Table 25: Time table of sperm entry and oocyte activation.
Shown are the oocytes numbers and (in italic) the weighted average values (%).

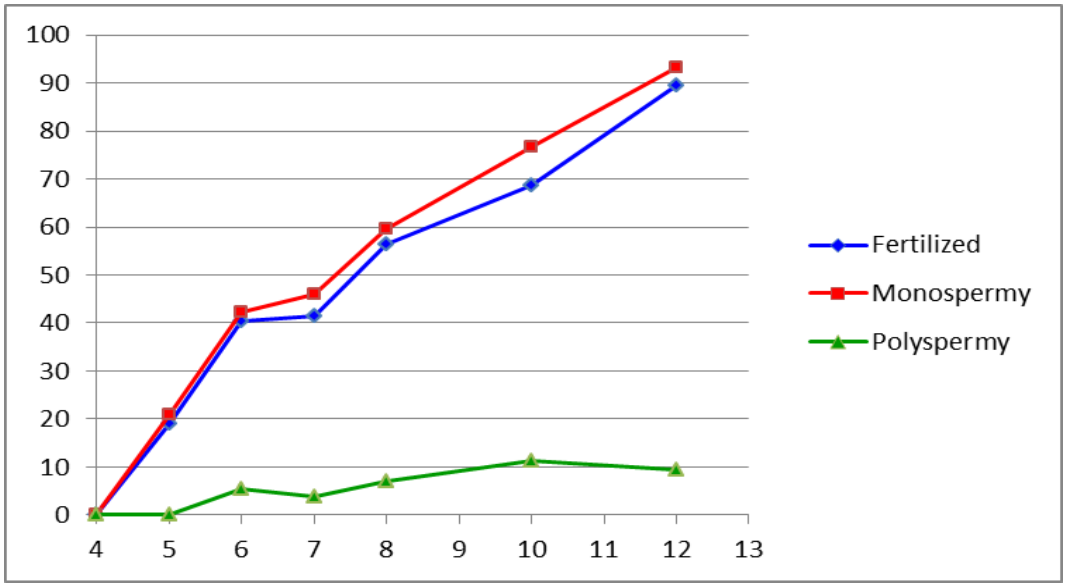

Figure 29: Time course of sperm entry and oocyte activation.

4.3.2 Morphological characterization of the sperm entry and oocyte activation

In this study, we could document a series of oocytes at different stages of sperm penetration and multiple stages from very early to late anaphase II and complete separation of the second polar body. The penetration of the sperm nucleus into the oocyte appeared to be immediately followed by oocyte activation and progression to anaphase II. Only three of the 355 inseminated oocytes, which were found to be penetrated by a sperm nucleus, were still arrested at MII. Notably, we could not detect any evidence for a correlation between the sperm entry site and the position of the meiosis II spindle. In numerous but not all anaphase II oocytes recorded, a pocket-like or long tube-like invagination of the cortical f-actin around the sperm nucleus which seemed to contribute to the inward transfer of the sperm nucleus deep into the oocyte was observed.

4.3.2.1 Formation of the maternal and the paternal pronucleus and of the sperm aster

The collection of confocal image stacks was used to gain detailed information on the gross morphological reorganization of the maternal and the paternal chromatin and on the time course after sperm penetration and oocyte activation. The formation of both the maternal and the paternal pronucleus was divided into five stages distinguished by the shape, the size, the condensation degree and morphological appearance of the DAPI-stained chromatin. The structural appearance of the chromatin was also used to distinguish between the maternal and the paternal pronucleus. The development of the sperm aster (SA), initiated by the proximal sperm centriole, was divided in four stages. The stages classification is listed in Table 26.

Stages of the formation of the maternal pronucleus

The first stage of the formation of the maternal pronucleus (mPN), the mPN0 stage, was seen after separation of the second polar body. The chromosomes of the oocyte formed an extremely compacted aggregate which was either still H3S10p-positive or already negative with a diameter of 3 – 5 µm. In numerous but not all oocytes, a bulge of the oocyte cortex above the dense maternal chromatin aggregate was seen. At stage mPN1, the maternal chromatin had partially decondensed forming a small spherical pronucleus with a diameter of 6 – 10 µm composed of coarse chromatin granules, which were always H3S10p-negative. Notably, from stage mPN1 to mPN2, an increasingly dense microtubule cytoplasmic network was rebuilt. Maternal pronuclei of stage mPN2 and mPN3 had a spherical shape and were characterized by progressive chromatin decondensation and enormous increase in size up to more than 20 µm in diameter. A granular chromatin structure was still visible in the mPN3 pronuclei and allowed to distinguish the maternal pronucleus from the paternal one (see Table 26 and Figure 30).

Stages of the formation of the paternal pronucleus and of the sperm aster

In analogy to the stage classification of maternal pronucleus, the formation of the paternal pronucleus was also divided in five stages (see Table 26 and microscopic images Figure 31). The first stage of paternal pronucleus formation, pPN0, was seen shortly after the entry of the sperm nucleus, concomitantly with (i) the

progression of the activated oocyte from ana- to telophase II, (ii) the separation of the second polar body and (iii) the maternal pronucleus stage mPN0. At stage pPN1, the paternal chromatin had recondensed to a small round to oval pronucleus with a diameter of 6 – 8 µm, which in part appeared weakly H3S10p positive. Stages pPN2 and pPN3 represent different stages of progressive chromatin decondensation and multiplication of the volume to a spherical paternal pronucleus with a diameter of over 20 µm. In parallel to paternal pronucleus formation, the development of the sperm aster (SA), initiated by the proximal sperm centriole, was observed and divided into four stages. The first visible structure, was a tiny MT focus at stage SA1 close to the posterior end of the decondensing sperm nucleus (i.e. stage pPN0). At stage SA2, two clearly separated small microtubule organizing centers were seen. Stage SA3 was characterized by two widely separated MT asters with a diameter of more than 10 µm and often small additional MT asters. At stage SA4, long fine MT structures emanating around the expanded paternal pronucleus at stage pPN2 or pPN3 were found, interlaced with the cytoplasmic MT network.

Stages of oocyte meiosis and the formation of the maternal pronucleus	
A/T II	Early anaphase II – telophase II/cytokinesis
mPN0	Extremely compacted chromatin aggregate; Ø 3 – 5 µm; DAPI ++++; H3S10p+/-; second polar body completely separated;
mPN1	Coarsely granular chromatin, Ø 6 – 10 µm; DAPI+++
mPN2	Granular chromatin; Ø 10 – 20 µm; DAPI++
mPN3	Granular chromatin. Ø > 20 µm: DAPI++
Stages of the formation of the paternal pronucleus	
SN	Non-decondensed sperm nucleus; DAPI +++++
pPN0	Elongated flat decondensing sperm nucleus; DAPI ++
pPN1	Round to oval, Ø 6 – 8 µm; dense chromatin; DAPI +++
pPN2	Spherical, diffuse chromatin distribution, Ø 10 – 20 µm, DAPI ++
pPN3	Spherical, diffuse chromatin distribution, Ø > 20 µm; DAPI+
Stages of the formation of the sperm aster	
SA1	Tiny α-tubulin spot
SA2	Two separate small MT asters
SA3	Two widely separated MT asters, Ø > 10 µm; small additional MT asters
SA4	Long radial MTs around the pPN, interlaced with the cytoplasmic MT network

Table 26: Stage classification of the formation of the pronuclei and the sperm aster.
A/T II = ana/-telophase II; mPN = maternal pronucleus; SN = sperm nucleus; pPN = paternal pronucleus; SA = sperm aster; Ø = diameter.

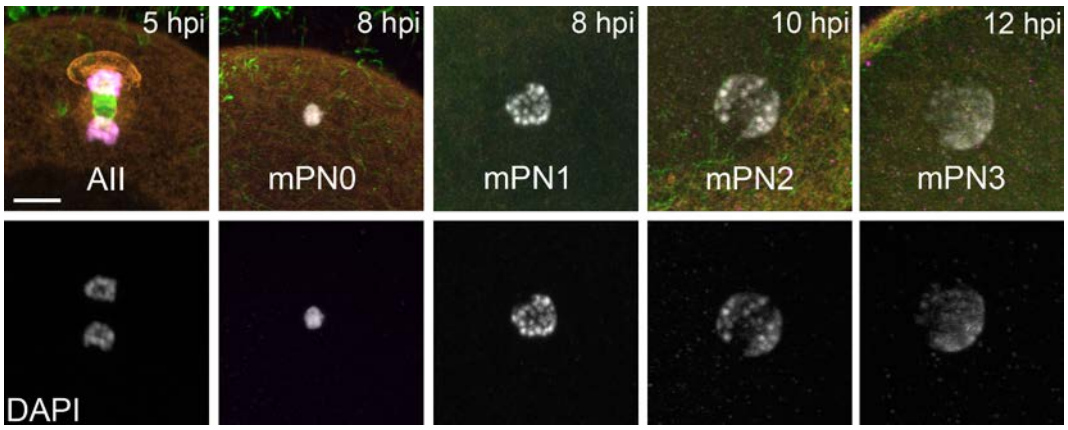

Figure 30: Early stages of maternal pronucleus formation.
Detail views from different oocytes representing the stages of maternal pronucleus formation from anaphase II to mPN3 as defined in Table 26. At mPN0 the maternal chromatin becomes H3S10p-negative. The upper panel shows 4-color overlay images of the DAPI-stained DNA (white), microtubules (green), f-actin (orange) and H3S10p (magenta). The lower panel separately presents the chromatin stained with DAPI. Due to the extensive decondensation of the DNA, the DAPI fluorescence intensity at mPN3 was much lower at the mPN0 stage. Accordingly, the DAPI images were recorded at different sensitivities. The time points after insemination (hpi) are indicated in the figure. AII = anaphase II; mPN0 – mPN3 = maternal pronucleus stage. Scale bar = 10 µm.

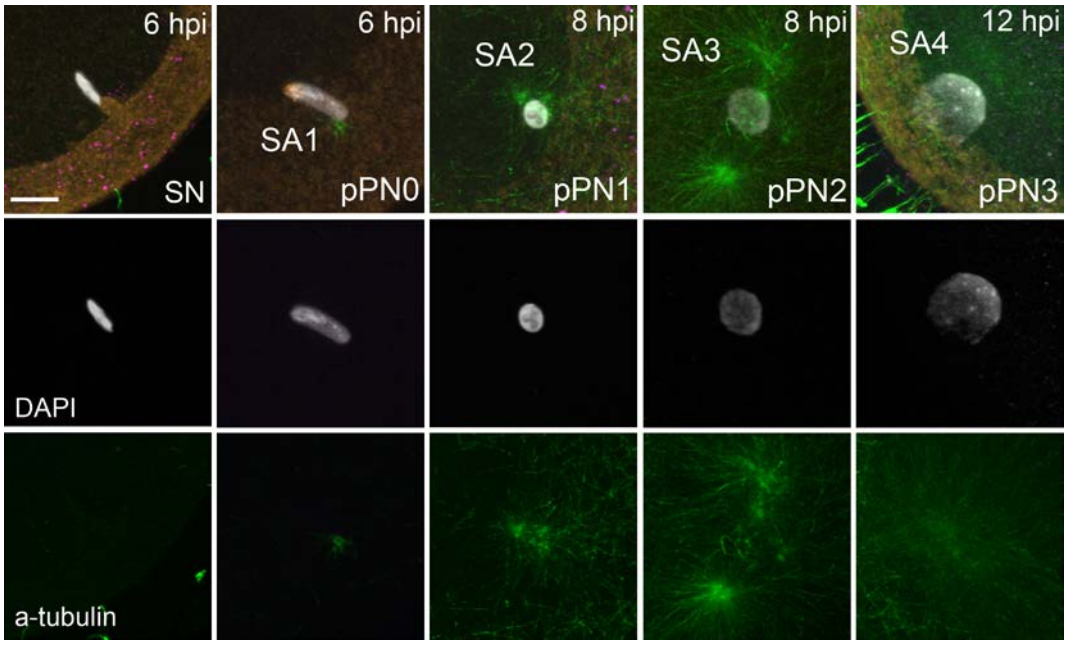

Figure 31: Early stages of paternal pronucleus formation.
The sequence of the paternal pronucleus formation with decondensation and conformational changes of the paternal DNA starting with sperm penetration and resulting in a pronucleus with a diameter of more than 20 µm as defined in Table 26. Upper panel: 4-color overlay images of the DAPI-stained DNA (white), microtubules (green), f-actin (orange) and H3S10p (magenta). The Mid panel separately presents the chromatin stained with DAPI. Due to the extensive decondensation of the DNA, the DAPI fluorescence intensity at pPN3 was much lower at the pPN0 stage. Accordingly, the DAPI images were recorded at different sensitivities. The lower panel separately shows the development of the sperm aster from a tiny α-tubulin spot at pPN0. The time points after inseminations (hpi) are indicated. pPN = paternal pronucleus; SA = sperm aster. Scale bar = 10 µm.

4.3.3 The kinetics of the formation of the pronuclei and of the sperm

aster

The 245 monospermic fertilized oocytes without apparent anomalies were included to evaluate the kinetics of presumably normal formation of the maternal and the paternal pronucleus and of the sperm aster.

The classification scheme defined in Table 26 was used to assess the mPN, pPN and SA stage in each oocyte and to determine their frequency distributions at the different time points after insemination. The results are presented in Table 27 and Figure 32.

Sperm penetration appeared to be followed by immediate oocyte activation, completion of meiosis II and immediate onset of sperm nucleus decondensation within less than 1 hour. At 4 hpi, still no sperm-penetrated and activated oocytes were observed while at 5 hpi already post-meiotic oocytes at mPN stage 0 and decondensing sperm nuclei were found. The decondensation of the maternal chromosomes and formation of a small round mPN1 pronucleus needed more time, at least three hours. The first mPN1 pronuclei appeared at 8 hpi, concomitantly with the first expanding mPN2 pronuclei. The first small dense oval to round paternal pronuclei of stage pPN1 were seen at 7 hpi, 2 hours after the first decondensing sperm nuclei. Large expanded paternal pronuclei of stage pPN3 occurred from 10 hpi. Large maternal mPN3 pronuclei were only found at 12 hpi.

hpi	n	A/T II		mPN0		mPN1		mPN2		mPN3	
5	13	9	*(69.2)*	4	*(30.8)*	0	*(0)*	0	*(0)*	0	*(0)*
6	41	33	*(80.5)*	8	*(19.5)*	0	*(0)*	0	*(0)*	0	*(0)*
7	17	4	*(23.5)*	13	*(76.5)*	0	*(0)*	0	*(0)*	0	*(0)*
8	69	15	*(21.7)*	46	*(66.7)*	6	*(8.7)*	2	*(2.9)*	0	*(0)*
10	36	5	*(13.9)*	19	*(52.8)*	4	*(11.1)*	8	*(22.2)*	0	*(0)*
12	69	3	*(4.3)*	11	*(15.9)*	7	*(10.1)*	25	*(36.2)*	23	*(33.3)*
Total	245	69	*(28.2)*	101	*(41.2)*	17	*(6.9)*	35	*(14.3)*	23	*(9.4)*
hpi	**n**	**SN**		**pPN0**		**pPN1**		**pPN2**		**pPN3**	
5	13	9	*(69.2)*	4	*(30.8)*	0	*(0)*	0	*(0)*	0	*(0)*
6	41	16	*(39)*	24	*(58.5)*	1	*(2.4)*	0	*(0)*	0	*(0)*
7	17	2	*(11.8)*	13	*(76.5)*	2	*(11.8)*	0	*(0)*	0	*(0)*
8	69	9	*(13.1)*	23	*(33.3)*	29	*(42)*	6	*(8.7)*	2	*(2.9)*
10	36	0	*(0)*	11	*(30.6)*	10	*(27.8)*	13	*(36.1)*	2	*(5.6)*
12	69	1	*(1.4)*	6	*(8.7)*	5	*(7.2)*	22	*(31.9)*	35	*(50.7)*
Total	245	37	*(15.1)*	81	*(33.06)*	47	*(19.18)*	41	*(16.73)*	39	*(15.91)*

Table 27: Kinetics of maternal and paternal pronucleus formation.
Shown are the numbers of oocytes displaying different maternal (up) and paternal (down) pronucleus stages and (in brackets) the respective weighted average values (%). n = total number of all fertilized oocytes analyzed per time point.

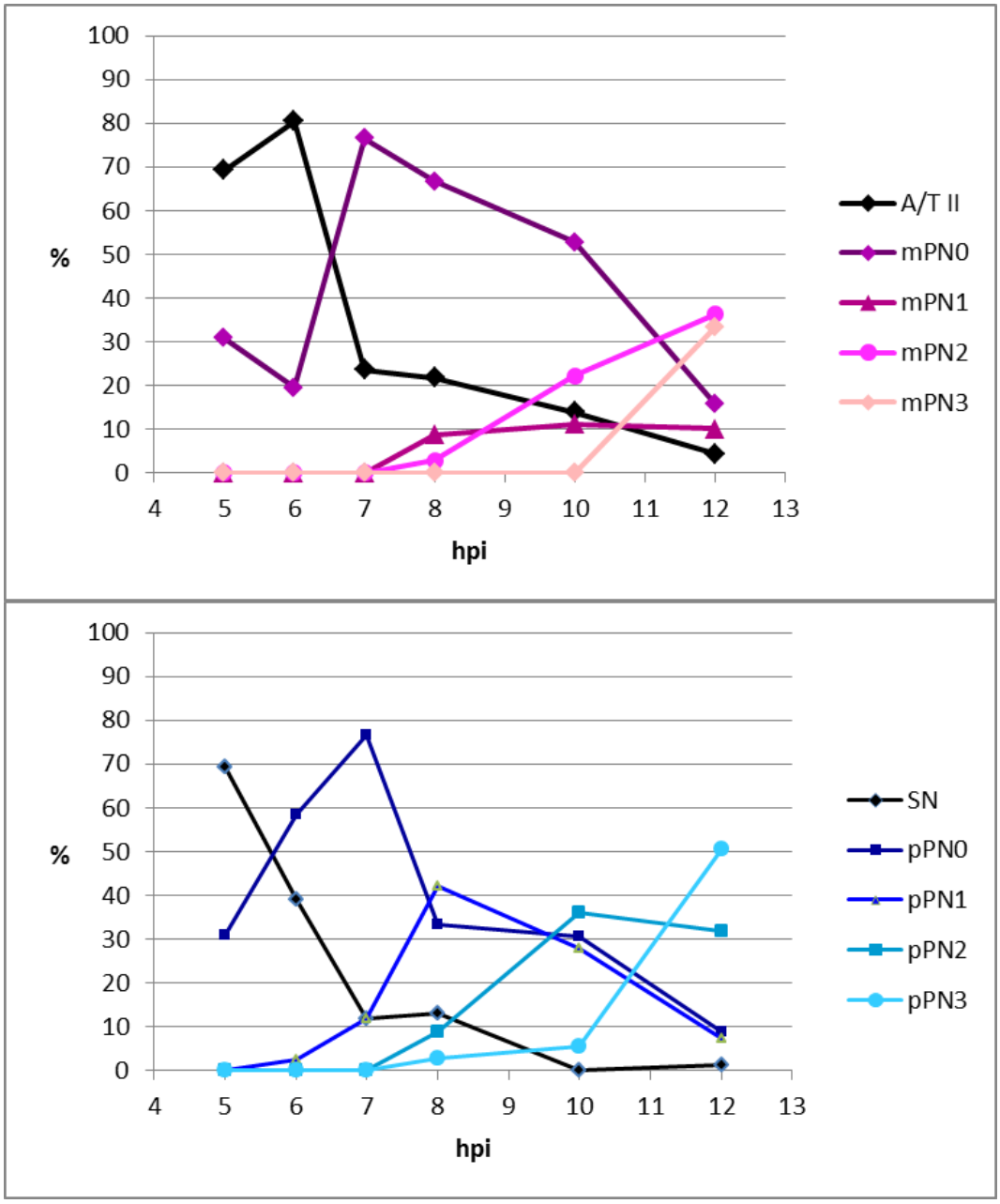

Figure 32: Time course of the formation of the maternal and the paternal pronucleus. Shown is the proportion of oocytes displaying different maternal (up) and paternal (down) pronucleus stages. For the exact values see Table 27. AII = anaphase II; mPN = maternal pronucleus; SN = sperm nucleus; pPN = paternal pronucleus.

The correlation between maternal and paternal pronucleus formation

To gain information on the correlation between the formation of the maternal and the paternal pronucleus, the mPN and pPN stage combinations of the individual oocytes were determined. The data for each time point from 5 to 12 hpi and over all time points are presented in Table 28A. The occurrence or absence of specific mPN and pPN stage combinations strongly suggests a high correlation between maternal and paternal pronucleus formation. 67 of 70 oocytes (96%) found in anaphase-/telophase II contained an undecondensed (SN) or elongating and

decondensing sperm nucleus (pPN0). In 83 of 100 oocytes with a segregated second polar body, the maternal pronucleus stage mPN0 was combined with paternal stages pPN0 and pPN1. 71 of 80 (89%) oocytes with an expanded paternal stage pPN2 or pPN3 pronucleus had at least reached mPN1. 57 of 58 (98%) oocytes with a large maternal mPN2 or mPN3 pronucleus contained a pPN2 or pPN3 counterpart.

The correlation between the stage of the paternal pronucleus and the sperm aster

To gain insights into the correlation between the formation of the paternal pronucleus and the sperm aster, the pPN and sperm aster stage combinations of the individual oocytes were determined. The data for each time point from 5 to 12 hpi and over all time points are presented in Table 28B. The onset of sperm aster formation appeared to depend on decondensation of the sperm nucleus. Only in one of the 38 oocytes with an undecondensed sperm nucleus, the first sperm aster stage SA1, a tiny α-tubulin spot, was detected. Sperm aster stage SA2 was in 55 of 58 cases combined with the sperm decondensation stage pPN0 or with pPN1. The development to sperm aster stage SA3, defined by two widely separated MT asters appeared to depend on recondensation of the decondensed sperm nucleus to the small dense pPN1 pronucleus. In 69 of the 80 oocytes with a large pPN2 or pPN3 pronucleus, a late sperm aster stage SA3 or SA4 was found. However, the development of the paternal pronucleus to stage pPN2 and pPN3 appeared not to depend on the formation of the sperm aster. In 7 of the 80 oocytes with a pPN2 and pPN3 pronucleus no sperm aster could be detected.

A schematic illustration of the stages of the fertilization reconstructed from the collection of the three-dimensional oocyte snapshots is presented in Figure 33. In Figure 34 and Figure 35 representative microscopic images are shown.

A

5 hpi	SN	pPN0	pPN1	pPN2	pPN3	n
A II	7	2				9
mPN0	2	2				4
mPN1						0
mPN2						0
mPN3						0
n	9	4	0	0	0	13

6 hpi	SN	pPN0	pPN1	pPN2	pPN3	n
A II	14	20				33
mPN0	3	4				8
mPN1						0
mPN2						0
mPN3						0
n	17	24	0	0	0	41

7 hpi	SN	pPN0	pPN1	pPN2	pPN3	n
A/T II	2	2				4
mPN0		11	2			13
mPN1						0
mPN2						0
mPN3						0
n	2	13	2	0	0	17

8 hpi	SN	pPN0	pPN1	pPN2	pPN3	n
A/T II	5	7	3			15
mPN0	3	15	25	3		46
mPN1	1	1	1	2	1	6
mPN2				1	1	2
mPN3						0
n	9	23	29	6	2	69

10 hpi	SN	pPN0	pPN1	pPN2	pPN3	n
A/T II		5				5
mPN0		6	9	4		19
mPN1				4		4
mPN2			1	5	2	8
mPN3						0
n	0	11	10	13	2	36

12 hpi	SN	pPN0	pPN1	pPN2	pPN3	n
A/T II	1	2				3
mPN0		4	5	2		11
mPN1				6	1	7
mPN2				13	12	25
mPN3				1	22	23
n	1	6	5	22	35	69

5-12 hpi	SN	pPN0	pPN1	pPN2	pPN3	n
A/T II	29	38	3			69
mPN0	8	42	41	9		100
mPN1	1	1	1	12	2	17
mPN2			1	19	15	35
mPN3				1	22	23
n	38	81	46	41	39	245

B

5 hpi	n.d.	SA1	SA2	SA3	SA4	n
SN	9					9
pPN0	3	1				4
pPN1						0
pPN2						0
pPN3						0
n	12	1	0	0	0	13

6 hpi	n.d.	SA1	SA2	SA3	SA4	n
SN	17					17
pPN0	10	10	4			24
pPN1						0
pPN2						0
pPN3						0
n	27	10	4	0	0	41

7 hpi	n.d.	SA1	SA2	SA3	SA4	n
SN	1	1				2
pPN0	2	5	6			13
pPN1		1	1			0
pPN2						0
pPN3						0
n	3	6	6	0	0	17

8 hpi	n.d.	SA1	SA2	SA3	SA4	n
SN	9					9
pPN0	3	11	8	1		23
pPN1	2	4	17	6		29
pPN2			2	2	2	6
pPN3				1	1	2
n	14	15	27	10	3	69

10 hpi	n.d.	SA1	SA2	SA3	SA4	n
SN						0
pPN0	1	3	7			11
pPN1		2	4	4		10
pPN2	2			9	2	13
pPN3				1	1	2
n	3	5	11	14	3	36

12 hpi	n.d.	SA1	SA2	SA3	SA4	n
SN	1					1
pPN0	2		4			6
pPN1	1		4			5
pPN2	2		2	14	4	22
pPN3	3			31	1	35
n	9	0	10	45	5	69

5-12 hpi	n.d.	SA1	SA2	SA3	SA4	n
SN	37	1				38
pPN0	21	30	29	1		81
pPN1	3	7	26	10		46
pPN2	4		4	25	8	41
pPN3	3			33	3	39
n	68	37	58	69	11	245

Table 28: Correlation between maternal and paternal PN stage and between paternal PN and sperm aster stage in individual morphologically normal oocytes.
For each time point and over all time points from 5 to 12 hpi, the number of oocytes displaying a specific combination of (**A**) mPN and pPN stage and (**B**) pPN and sperm aster (SA) stage is shown. A/T II = ana-/telophase II; n.d. = no sperm aster detectable, n = number of oocytes.

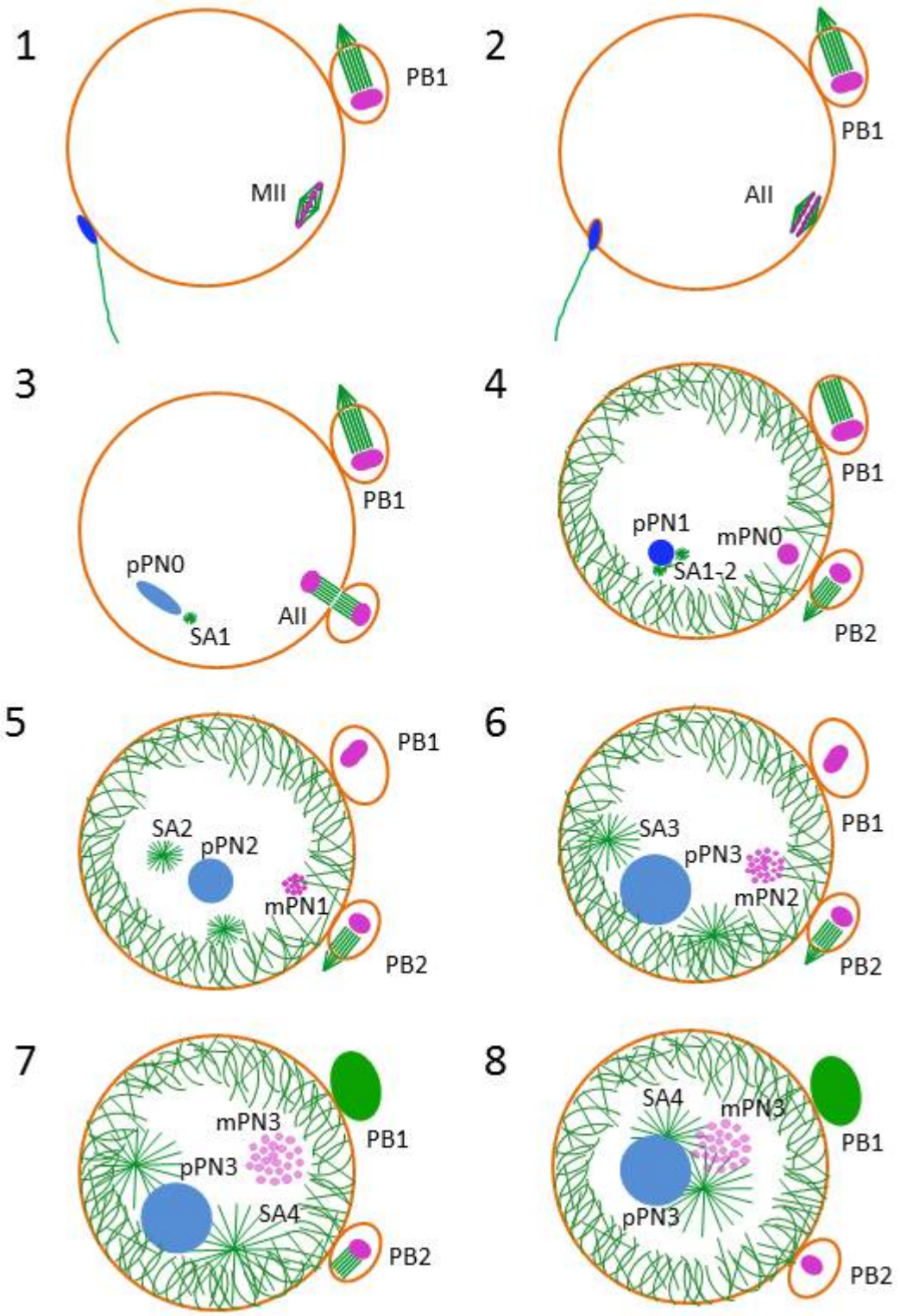

Figure 33: Schematic illustration of early stages of fertilization.
PB= polar body; SN = sperm nucleus; pPN0 – pPN3 = paternal pronucleus stages; A II = oocyte anaphase II; mPN0 – mPN3 = maternal pronucleus stages; SA= sperm aster. The color intensity is correlated to the condensation status of the chromatin both in maternal and paternal DNA.
As shown in this scheme, the cytoplasmic microtubular network is reconstituted concomitantly to the decondensation of the sperm nucleus and the formation of the early paternal pronucleus.

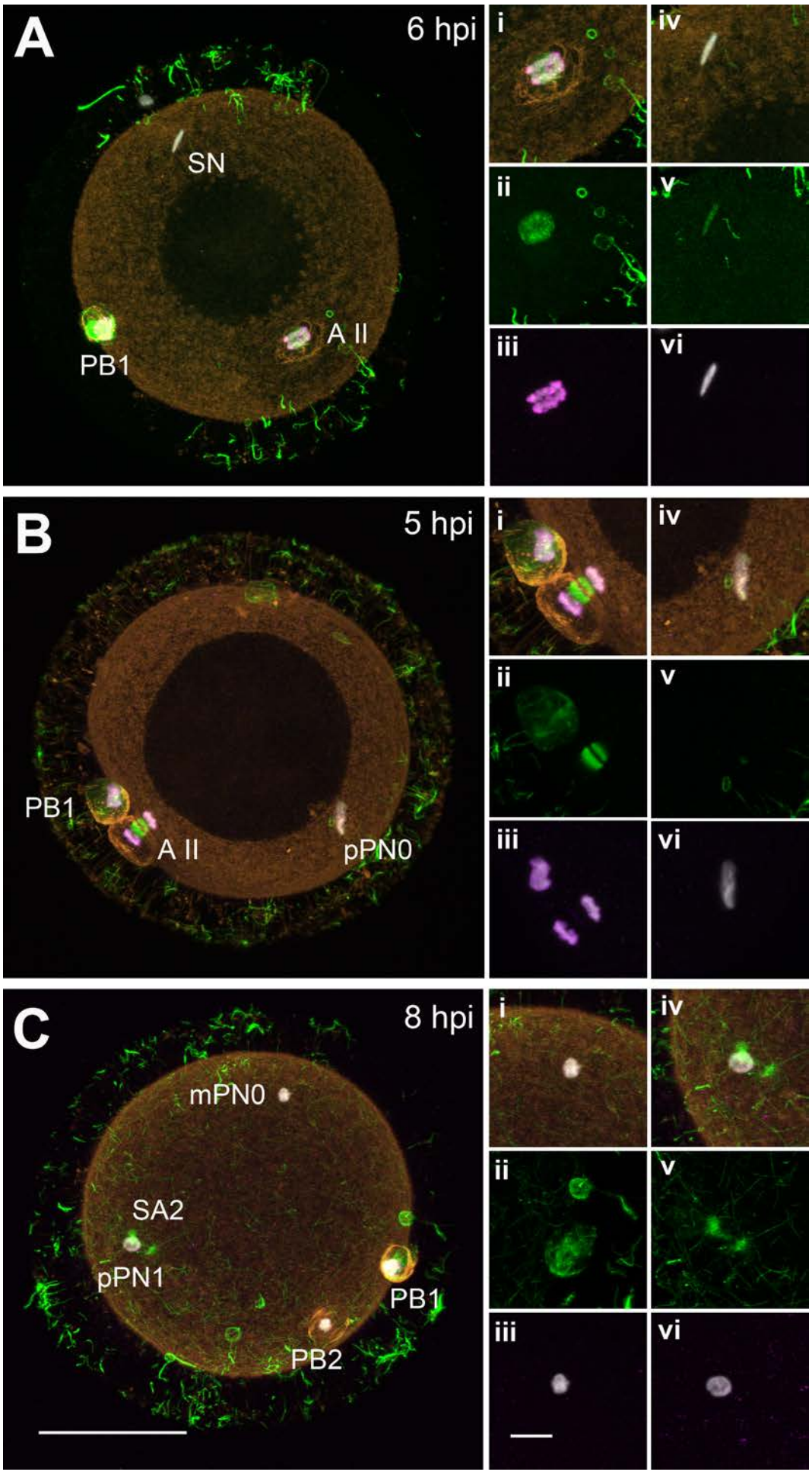
A
6 hpi
SN
PB1
A II
i
ii
iii
iv
v
vi
B
5 hpi
PB1
A II
pPN0
i
ii
iii
iv
v
vi
C
8 hpi
mPN0
SA2
pPN1
PB1
PB2
i
ii
iii
iv
v
vi

Figure 34: Examples of early stages of fertilization and of pronuclear formation.
(A) Penetrating sperm nucleus and sperm-induced oocyte activation (very early anaphase II), **(B)** Later stage of anaphase II: the central spindle has formed, at the spindle poles no MTs are detectable. In parallel, decondensation of the sperm nucleus has already started (pPN0). **(C)** Post telophase oocyte displaying a highly condensed maternal chromatin cluster (mPN0) and re-condensation of the paternal chromatin into a small round to oval pronucleus (pPN1). Nearby the paternal pronucleus, sperm aster stage 2 can be seen. DAPI-stained DNA is depicted in white, α-tubulin in green, f-actin in orange and H3S10p in magenta. The images are maximum intensity projections of subsets of the optical sections. The two panels present overview images (A, B, C) and detail views of stages of maternal (i-iii) and (iv-vi) paternal pronucleus formation. (i, iv) Overlay image of all four stains, (ii, v) microtubules alone and (iii, vi) overlay of DAPI and H3S10p. Scale bars = 50 µm (overviews) and 10 µm (details).

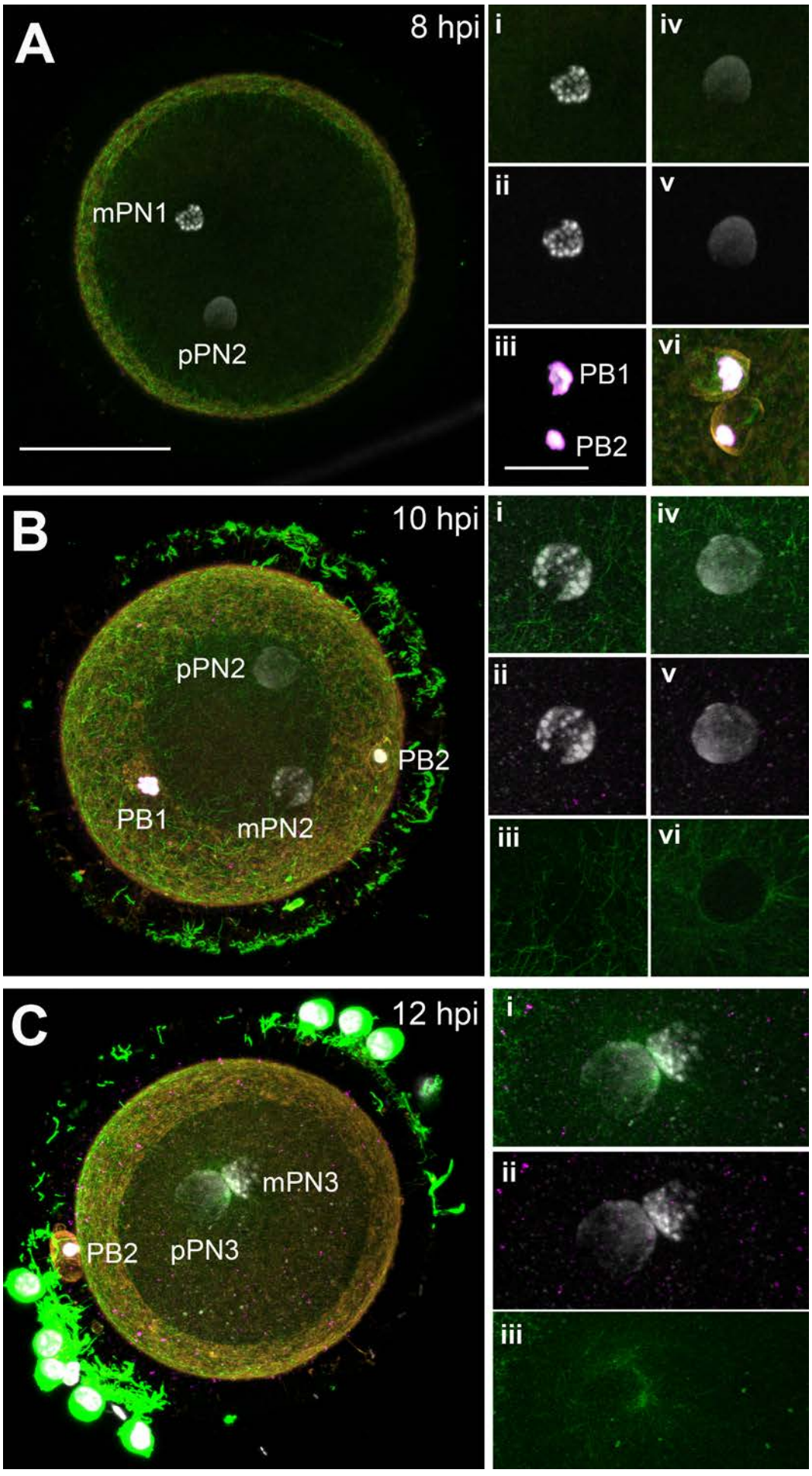
A
8 hpi
mPN1
pPN2
i
ii
iii
PB1
PB2
iv
v
vi
B
10 hpi
pPN2
PB2
PB1
mPN2
i
ii
iii
iv
v
vi
C
12 hpi
mPN3
PB2
pPN3
i
ii
iii

Figure 35: Examples of later stages of maternal and paternal pronuclear formation. **(A)** Early final decondensation of both maternal and paternal pronuclei (mPN1; pPN2), **(B)** Maternal pronucleus stage mPN2 and paternal pronucleus stage pPN2. **(C)** Maternal stage mPN3 and paternal stage pPN3. DAPI-stained DNA is depicted in white, α-tubulin in green, f-actin in orange and H3S10p in magenta. At these pronuclear stages, the chromatin was consistently H3S10p-negative, signals in the cytoplasm and the perivitelline space were unspecific. The images are maximum intensity projections of subsets of the optical sections. The panels present overview images (A, B, C) and detail views (i-vi) of maternal and paternal pronucleus stages. Scale bar = 50 µm (overviews) and 20 µm (details).

4.3.4 Errors of fertilization and oocyte meiosis

4.3.4.1 Error types observed from 4 to 12 hpi

The detected abnormalities were divided into two groups, based on the role played by the sperm. The first group includes oocyte anomalies which precede and preclude fertilization. The second group comprises aberrations occurring during and after sperm penetration and oocyte activation.

The first group of recorded abnormalities comprehends:

1) Spontaneously activated oocytes
    a) Spontaneous oocyte activation as single error detectable.
    b) Spontaneous oocyte activation where an irregular anaphase is visible.
    c) Spontaneous oocyte activation where a diploid nucleus is clear distinguishable.
2) Prometaphase I to prometaphase II oocytes morphologically normal
    a) Not penetrated by sperm
    b) Penetrated by sperm
3) Abnormal metaphase I
    a) Multipolar MI
        i) Not penetrated by sperm
        ii) Penetrated by sperm
    b) Multipolar MI with lagging chromosomes
        i) Not penetrated by sperm
        ii) Penetrated by sperm

The second group includes:

1) Polyspermy
    a) Oocyte penetrated by two or more sperm
    b) Oocyte penetrated by two or more sperm in addition to an irregular

anaphase I/II

2) Irregular ana-/telophase I/II

a) Irregular chromatin segregation

i. Lagging chromosomes

ii. Chromatin bridges

b) Abnormal MII-AII spindle positioning and/or orientation

c) Irregular chromosome segregation and MI/AII spindle

i. Self-enucleated oocytes

ii. Multipolar AI/AII with chromatin bridges

iii. Lagging chromosomes with irregular spindle formation, positioning and/or orientation

iv. Chromatin bridge with irregular spindle formation, positioning and/or orientation

d) Irregular maternal pronucleus

4.3.4.1.1 Spontaneous oocyte activation

In this study, spontaneous oocyte activation was defined as activation of the oocyte and progression to anaphase II without penetration by sperm. In our study, we observed also spontaneously activated oocytes that failed to expel the second polar body. Schematic representation and confocal images of parthenogenetic activated oocytes are presented in Figure 36 and Figure 37.

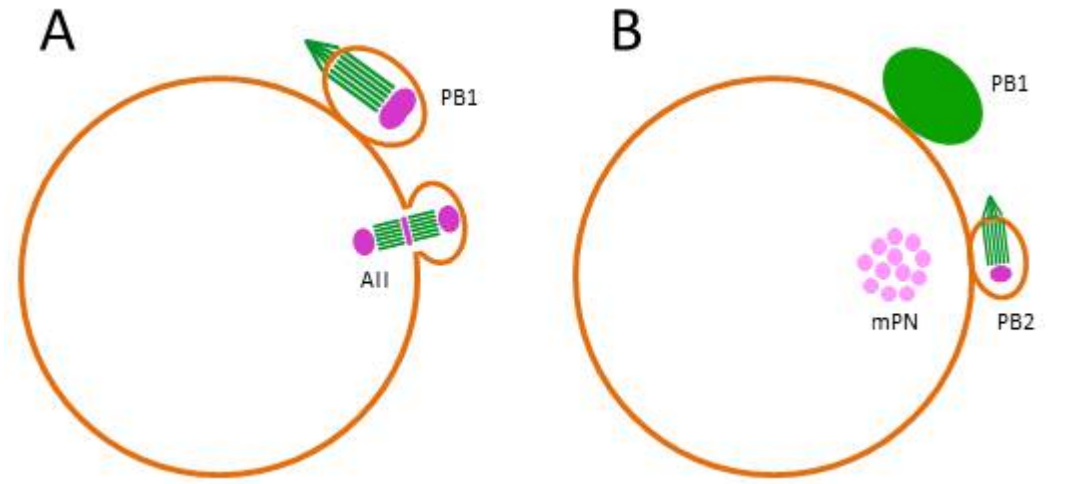

Figure 36: Spontaneously activated oocytes.
(A) Non-penetrated oocyte at anaphase II. **(B)** Oocyte at a pronuclear stage exhibiting a single maternal pronucleus.

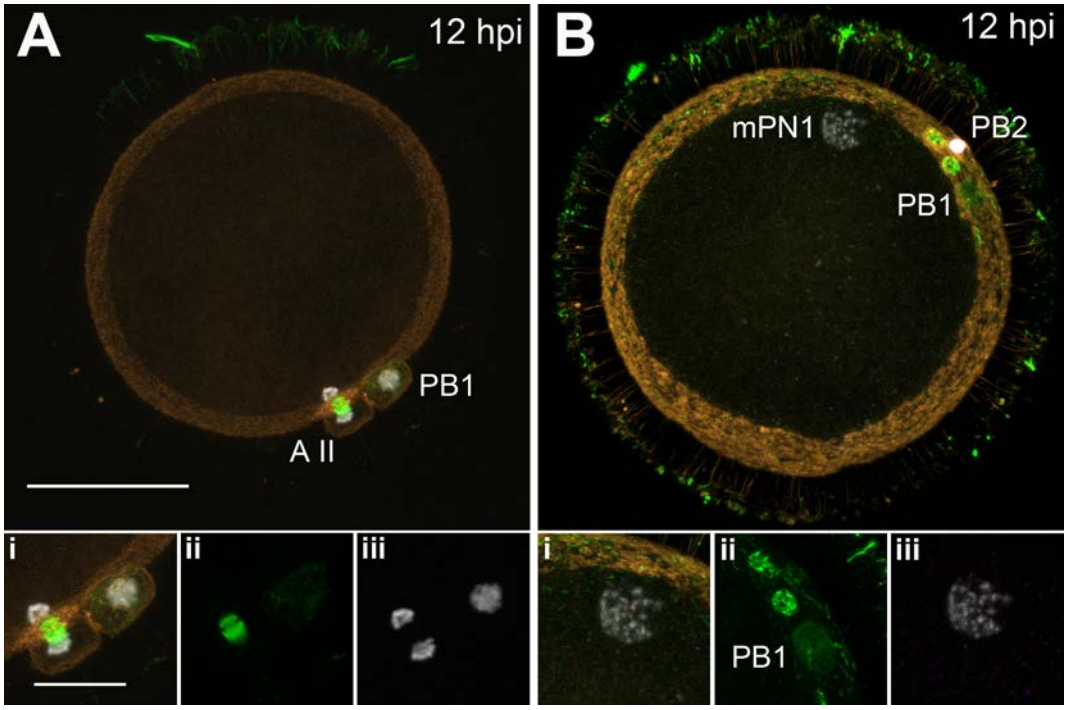

Figure 37: Examples of spontaneous oocyte activation.
(A) Anaphase II oocyte without sperm nucleus or paternal pronucleus. **(B)** Haploid maternal pronucleus after the extrusion of both polar bodies. DAPI-stained DNA is depicted in white, α-tubulin in green, f-actin in orange and H3S10p in magenta. The images are maximum intensity projections of subsets of the optical sections. The two panels present overview images (A, B) of the abnormal oocytes and (i-iii) details: (i) an overlay of DAPI, α-tubulin and f-actin, (ii) α-tubulin only and (iii) DAPI only. Scale bar = 50 µm (overviews) and 10 µm (details).

In our study, we observed also spontaneously activated oocytes that failed to expel the polar body. Examples are shown in Figure 38.

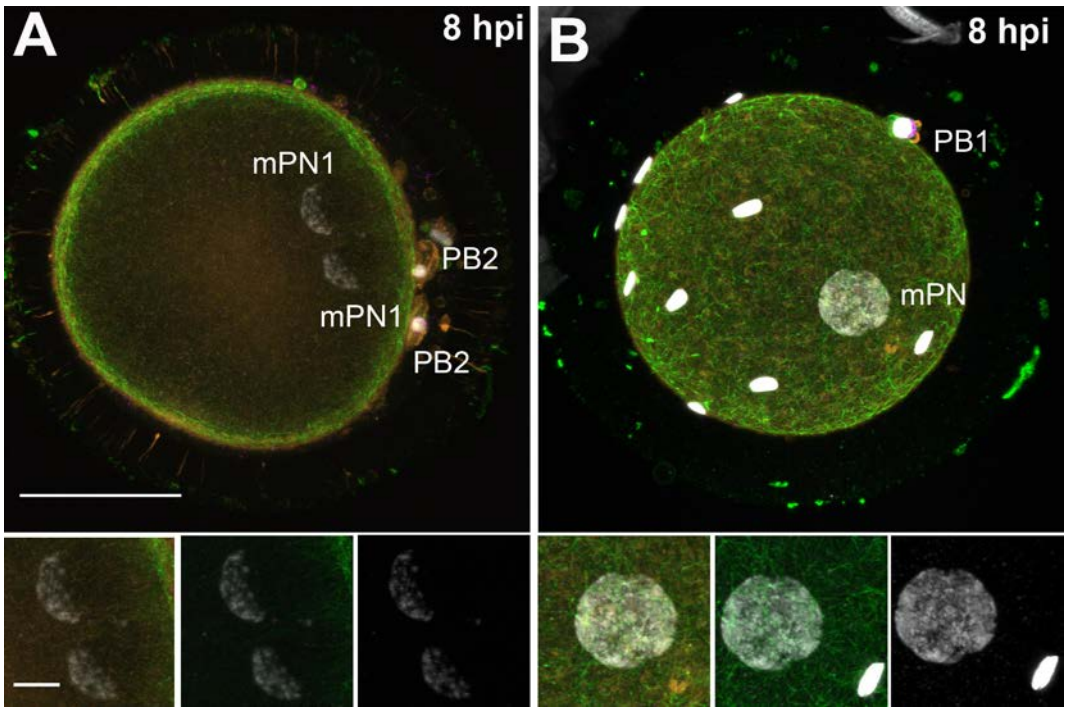

Figure 38: Two haploid and one diploid mPN in spontaneously activated oocytes.
(A) Spontaneously activated oocyte with 2 extruded polar bodies but exhibiting two pronuclei. **(B)** Spontaneously activated oocyte with a single large and presumably diploid maternal pronucleus due to a failure of second polar body extrusion. All sperm nuclei are located outside the oocyte. DAPI-stained DNA is depicted in white, α-tubulin in green, f-actin in orange and H3S10p in magenta. The images are maximum intensity projections of subsets of the optical sections. The two panels present overview images (A, B) and detail views (i-iii): (i) an overlay of DAPI, α-tubulin and f-actin, (ii) an overlay of DAPI and α-tubulin and (iii) DAPI only. Scale bar = 50 µm (overviews) or 10 µm (details).

4.3.4.1.2 Polyspermy

For practical reasons, polyspermy was defined as oocyte penetration and activation by two or more sperm. In this study, a series of oocytes at early stages of polyspermic fertilization without and in combination with anomalies of oocytes were imaged by 3D confocal microscopy. Thereby, we found dispermic oocytes (i) with two pPN at the same stage, (ii) two pPN at different stages together with two different sperm aster stages, or (iii) one pPN and one non-decondensed sperm nucleus. Figure 39 presents a scheme illustrating penetration of an oocyte by two sperm nuclei, the development of two paternal pronuclei and two sperm asters, the convergence of one paternal and the maternal pronucleus resulting in the formation of two metaphase spindles: one with a biparental diploid and one with a haploid paternal chromosome set. Notably, we also observed dispermic oocytes which contained two paternal and two maternal pronuclei (for microscopic images see Figure 41D, for a schematic illustration see Figure 40).

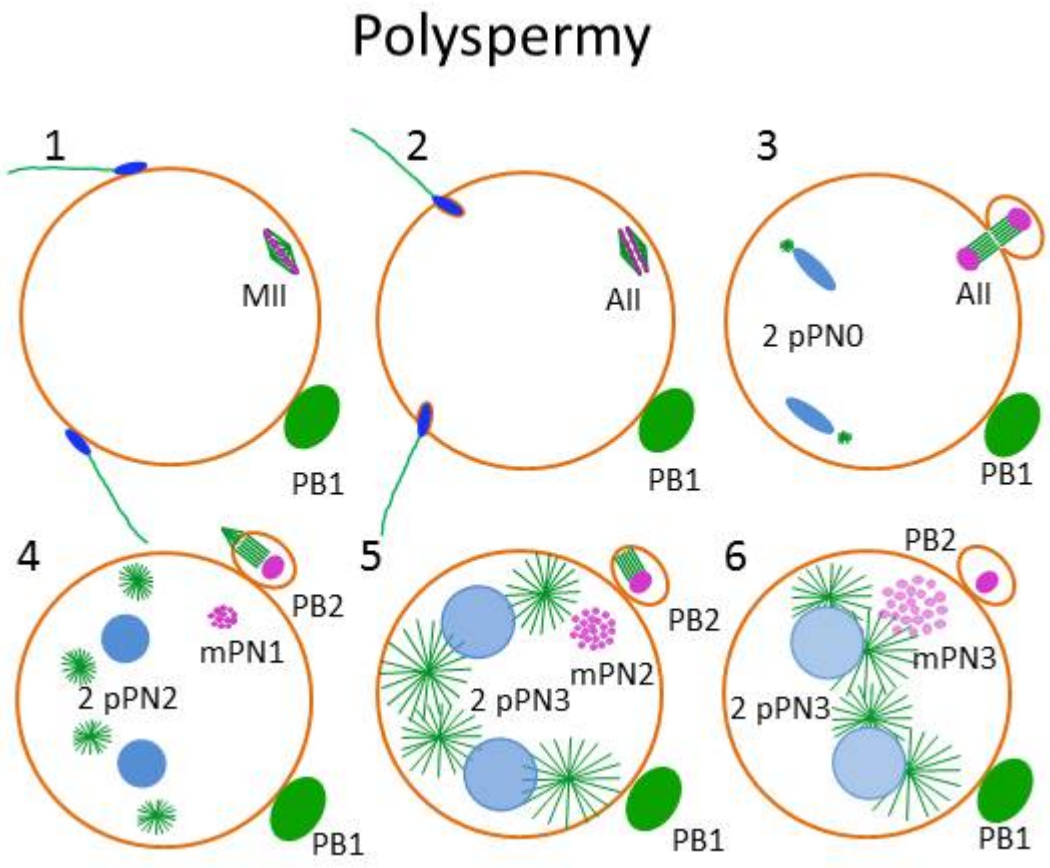

Figure 39: Schematic illustration of fertilization of a morphologically normal oocyte by two sperm.

In this scheme the progression from sperm adhesion to the late paternal pronucleus as well as from sperm-induced oocyte activation to the late maternal pronucleus stage is illustrated.

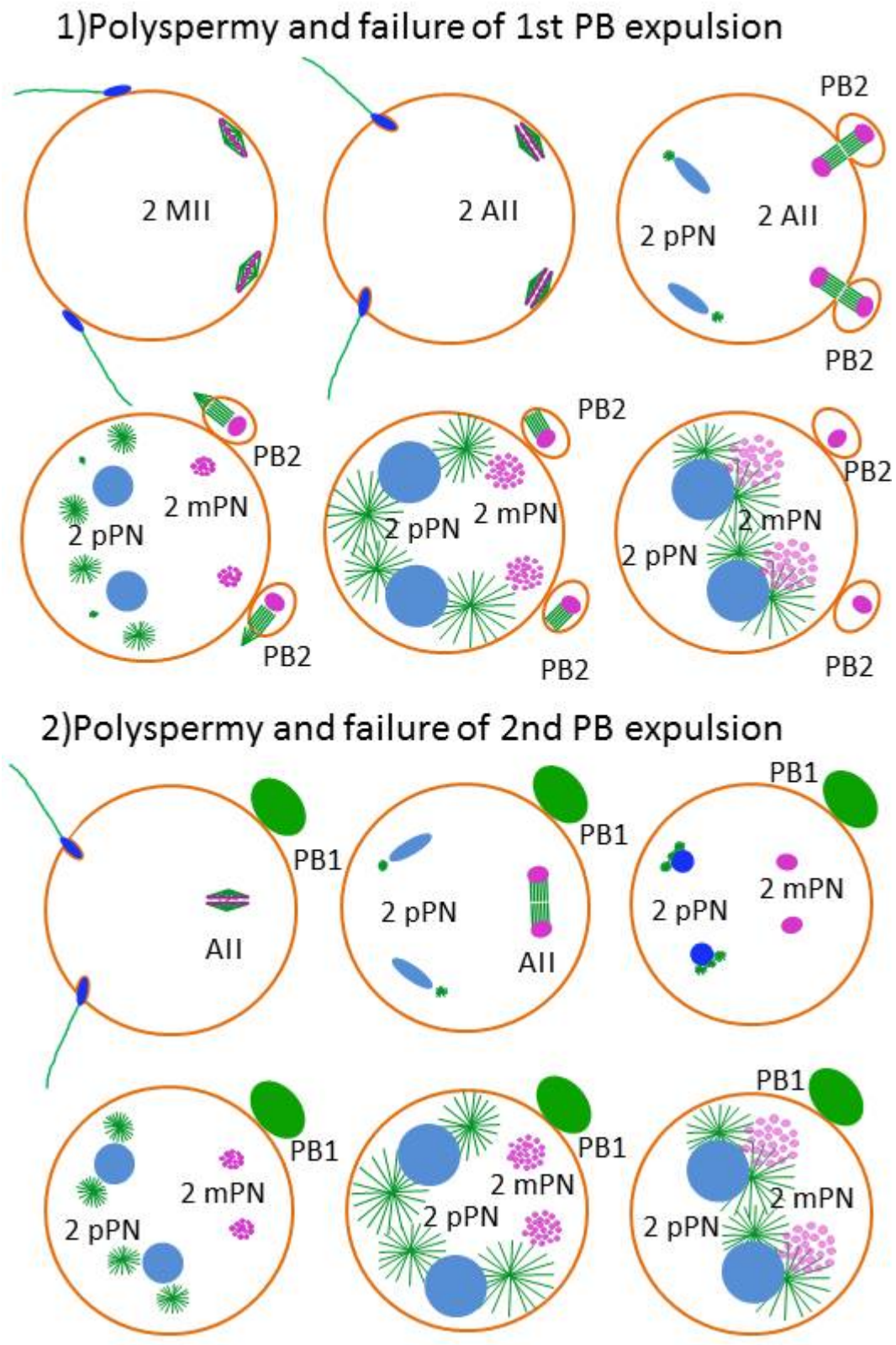

Figure 40: Schematic illustration of possible outcomes of dispermic fertilization combined with polar body extrusion failure.

(1) Penetration of two sperm nuclei into an oocyte, which failed to extrude the first polar body and contains two metaphase II spindles, can result in (i) the extrusion of two second polar bodies, (ii) the formation of two maternal and two paternal pronuclei, (iii) two syngamies and cleavage into a 4-cell embryo composed of two genetically different blastomere pairs. **(2)** Penetration of two sperm into an oocyte, which fails to extrude the second polar body, also can result in the formation of two maternal and two paternal pronuclei, two syngamies and cleavage into two genetically

different pairs of blastomeres.

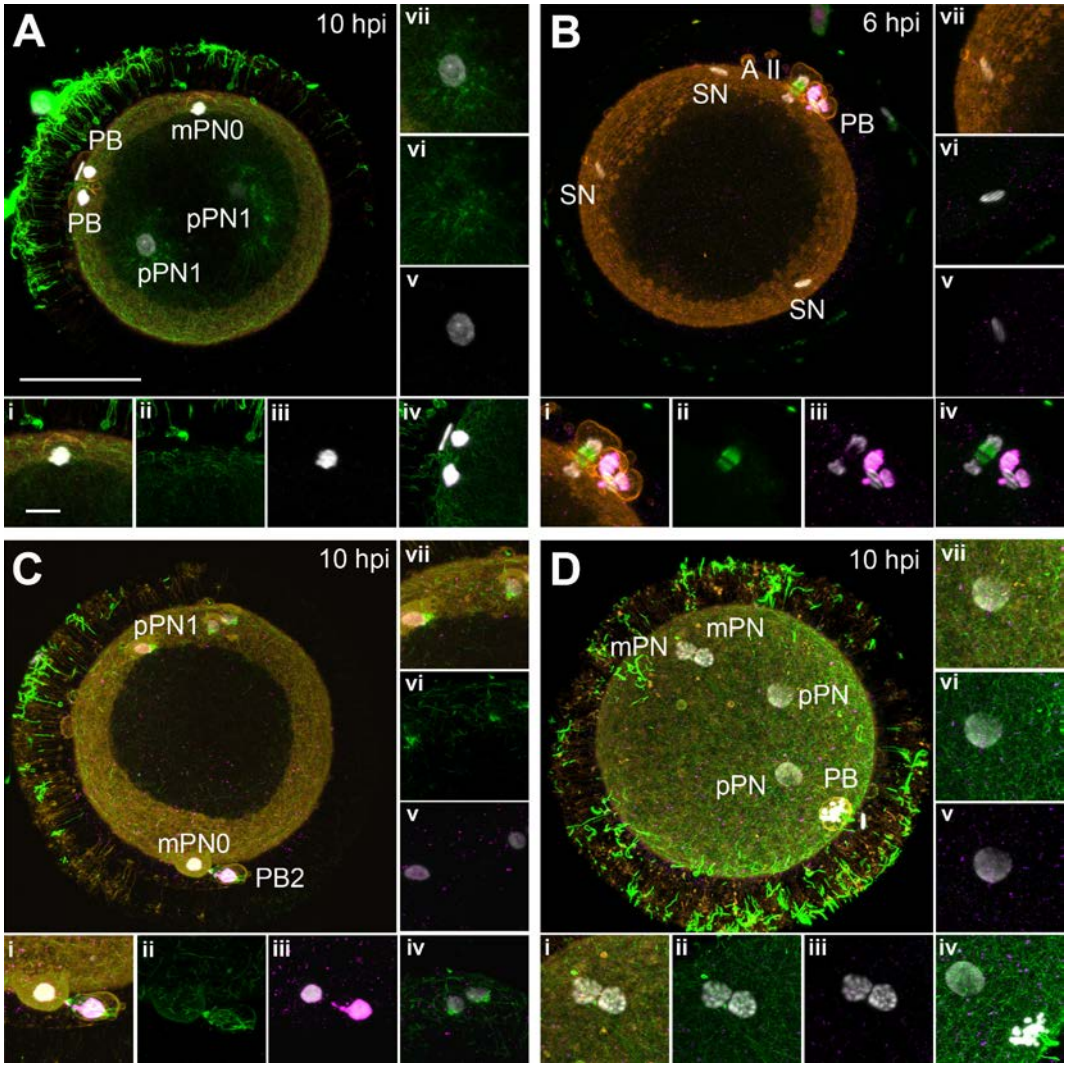

Figure 41: Cases of polyspermy without and with aberrations of oocyte meiosis.
(A) Penetration of two sperm nuclei and formation of two paternal pronuclei at stage pPN1.The activated oocyte displayed a normal post telophase I configuration with two extruded polar bodies. **(B)** Three non-decondensed sperm nuclei within an oocyte displaying an irregular anaphase II with multiple chromatin bridges and an irregular first polar body expulsion. **(C)** Penetration by three sperm nuclei, which have developed to stage pPN0 and pPN1, into an oocyte at late ana-/telophase II. The chromatin bridge between the mPN0 and the second polar body is clearly visible. **(D)** Oocyte containing two paternal pronuclei and two closely adjacent maternal pronuclei resulting from a failure of second polar body extrusion. Only a single (first) polar body can be detected. DAPI-stained DNA is depicted in white, α-tubulin in green, f-actin in orange and H3S10p in magenta. The images are maximum intensity projections of subsets of the optical sections. The four panels show overview images of the oocyte (A-D) and (i-vii) details. Scale bar = 50 µm (overviews) or 10 µm (details).

4.3.4.1.3 Abnormalities of anaphase II

As described in errors occurring during the *in vitro* maturation, the irregular anaphases detected during fertilization were classified based on the oocyte compartment affected. We distinguished three groups: (1) errors affecting only the chromatin segregation, (2) abnormal anaphase spindle and (3) abnormalities involving irregular MII/AII spindle in addition to chromosome segregation errors.

4.3.4.1.3.1 Irregular chromosome segregation

As presented in the previous chapter (IVM), the abnormalities affecting the DNA segregation could be divided into two groups: lagging chromosomes and chromatin bridges (Figure 42).

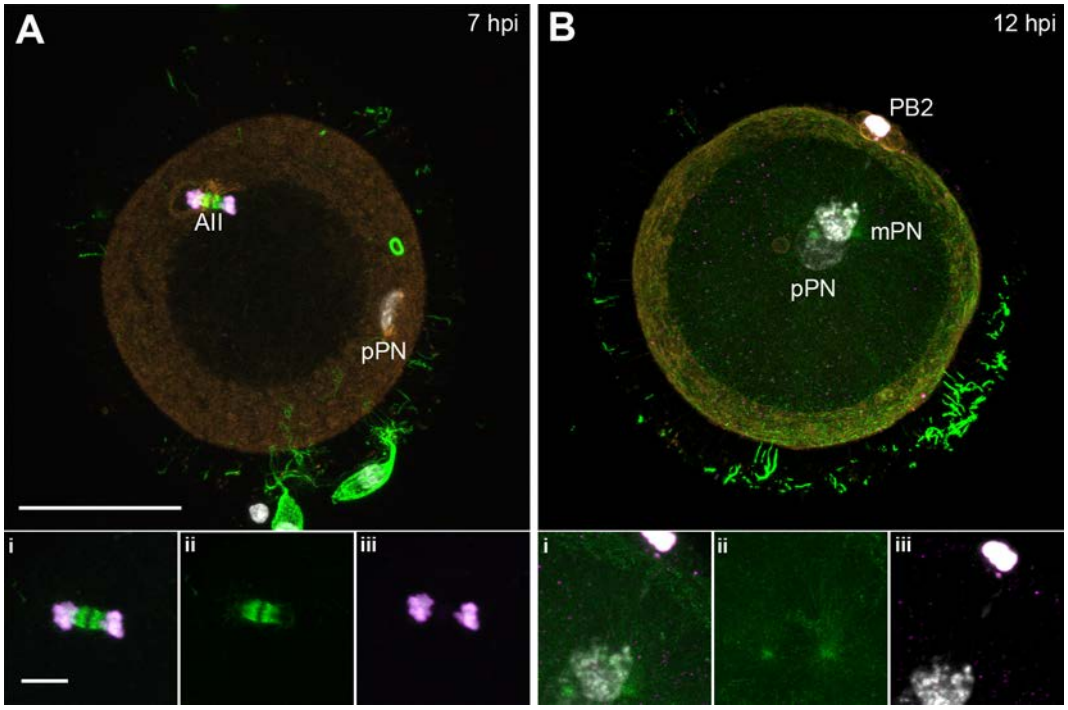

Figure 42: Irregular chromosome segregation.
(A) Oocyte presenting a lagging chromosome detected during anaphase II. **(B)** Oocyte displaying a chromatin bridge bounding the maternal pronucleus to the second polar body. DAPI-stained DNA is depicted in white, α-tubulin in green, f-actin in orange and H3S10p in magenta. The images are maximum intensity projections of subsets of the optical sections. The two panels present **(A; B)** overviews and (i-iii) details: an overlay of DAPI, α-tubulin and H3S10p, (ii) α-tubulin alone and (iii) an overlay of DAPI and H3S10p. Scale bar = 50 µm (overviews) or 10 µm (details).

4.3.4.1.3.2 Irregular MI/MII spindle orientation and/-or positioning

As described for metaphase I above, irregular spindle positioning and/-or irregular orientation can lead to a failure of second polar body expulsion. Confocal images of examples are presented in Figure 43.

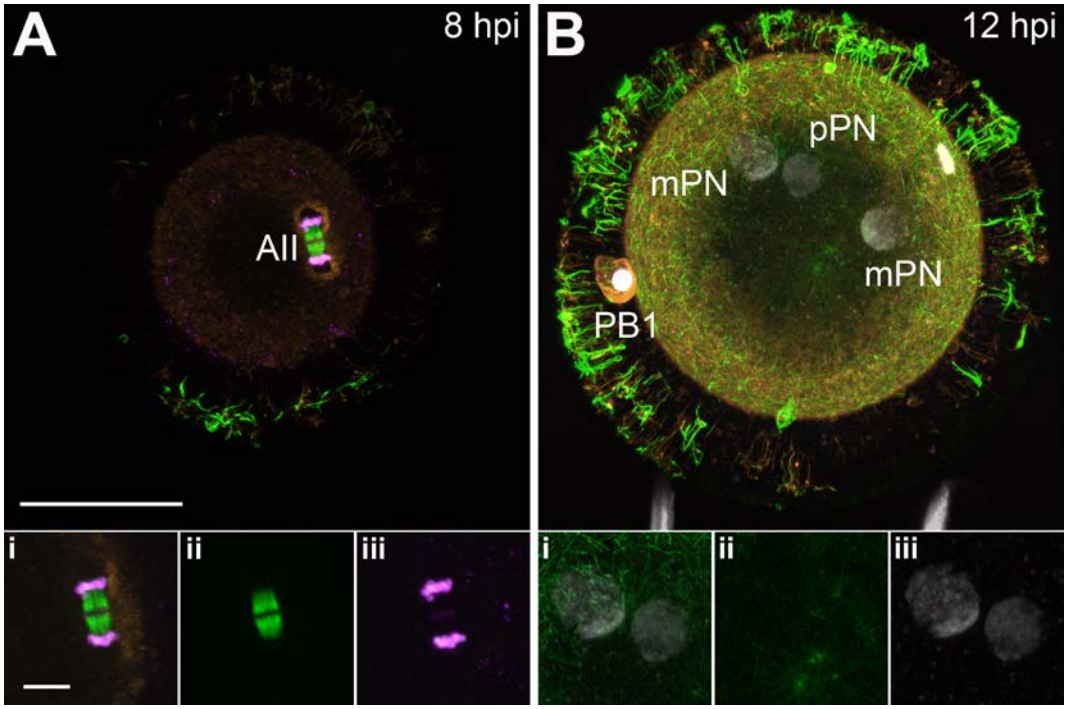

Figure 43: Irregular AII spindle.
A) Oocyte with an irregular orientation of the anaphase II spindle, which leads to a failure of second polar body extrusion. **(B)** Oocyte containing one paternal pronucleus with a diffuse chromatin structure, two maternal pronuclei with granular chromatin and a single first polar body due to a failure of second polar body extrusion. DAPI-stained DNA is depicted in white, α-tubulin in green, f-actin in orange and H3S10p in magenta. The images are maximum intensity projections of subsets of the optical sections.The two panels present (A; B) overviews and (i-iii) details: (i) an overlay of DAPI, α-tubulin and H3S10p, (ii) α-tubulin alone and (iii) an overlay of DAPI and H3S10p. Scale bar = 50 µm (overviews) or 10 µm (details).

4.3.4.1.3.3 Abnormal AII spindle and chromatin segregation disturbances

In this study, a remarkable proportion of the anaphase II aberrations recorded involved both chromosome segregation and MII/AII spindle. Schematic representations of these abnormalities are illustrated in Figure 44. Confocal image stacks of fertilized self-enucleated oocytes and fertilized oocytes exhibiting multipolar anaphase II spindle are shown in Figure 45 and in Figure 46 respectively.

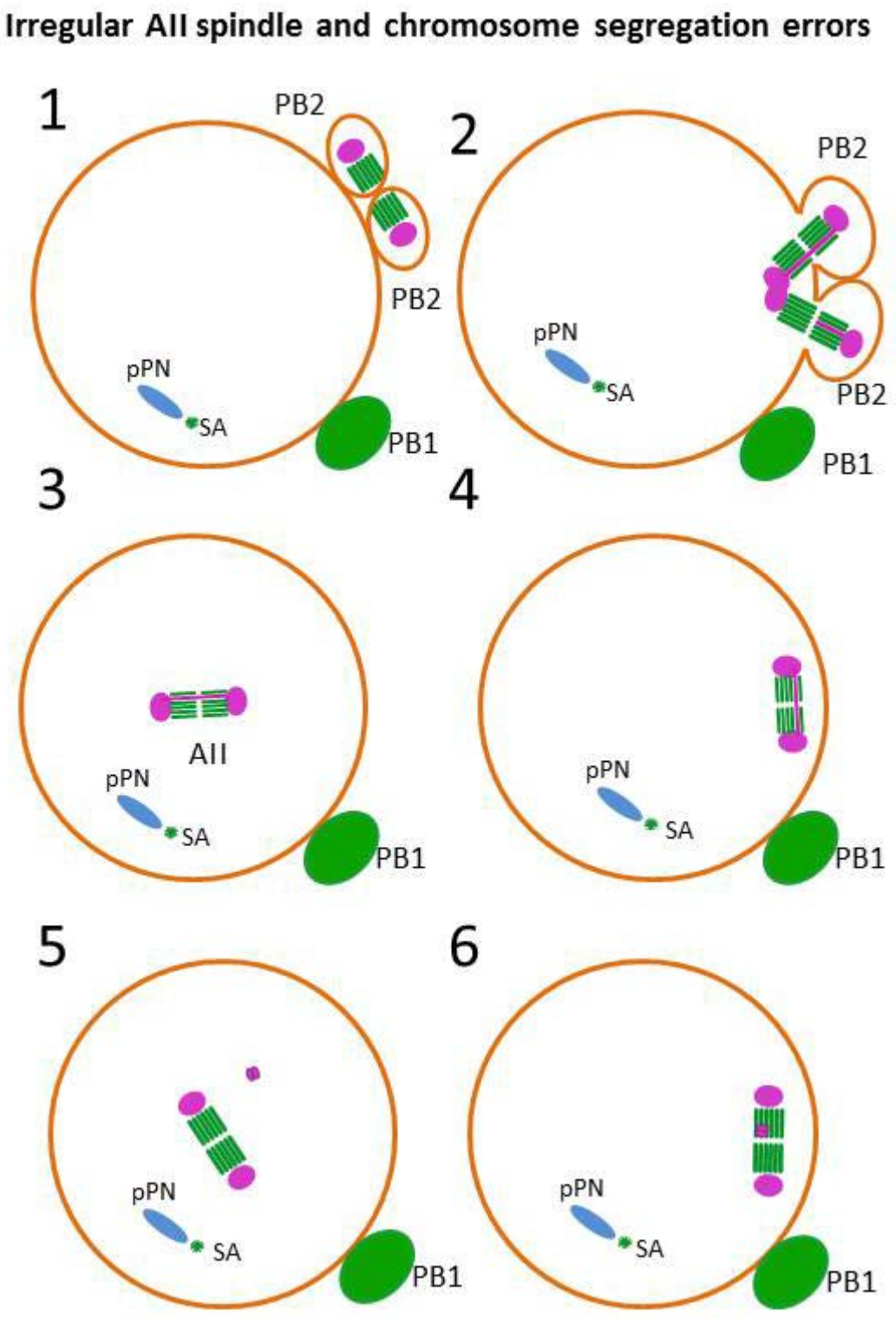

Figure 44: Schematic illustration of anomalies observed in anaphase II.
(**1**) Self-enucleation of the oocyte. (**2**) Multipolar anaphase II with one intact and one broken chromatin bridge. (**3**) Incorrect positioning of the anaphase II spindle and chromatin bridge. (**4**) Chromatin bridge and incorrect orientation of the anaphase II spindle parallel to the oocyte surface. (**5**) Irregular orientation of the anaphase II spindle and an unaligned chromosome. (**6**) Incorrect positioning of the anaphase II spindle and lagging chromosome.

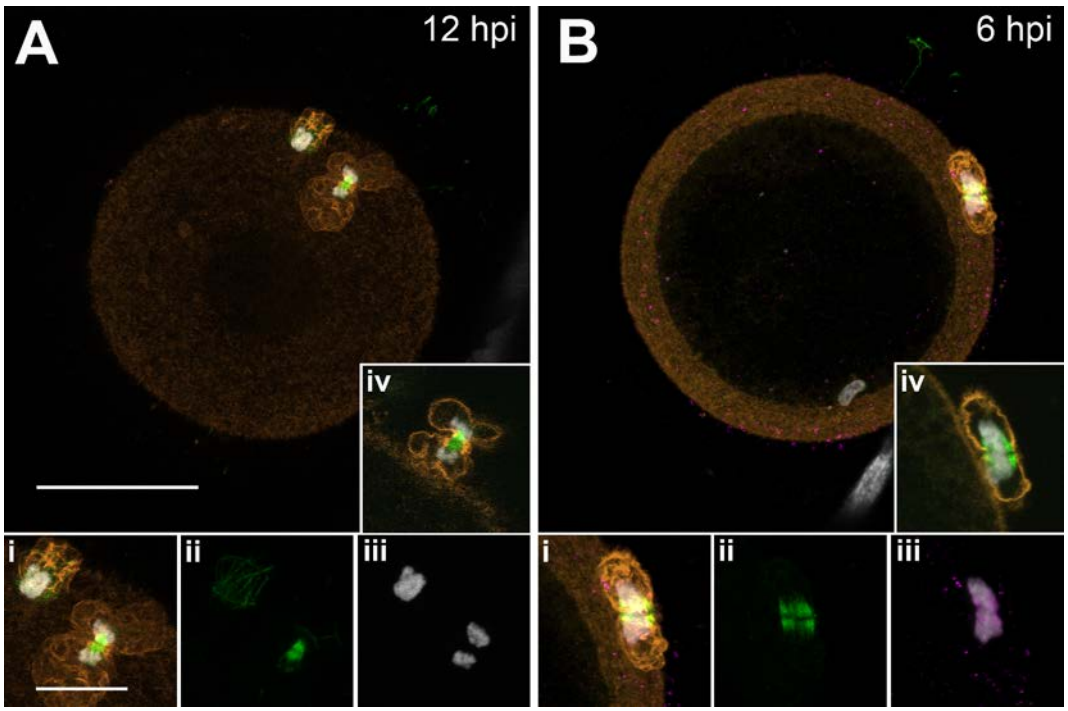

Figure 45: Examples of self-enucleation of the oocytes.
Panels composed by 2 slices of abnormal oocytes (A; B) and (i) detail presented in DAPI-α-tubulin channels, (ii) same detail shown in α-tubulin, (iii) detail on chromatin conformation and (iv) single optical section of anaphase II to highlight the position of the chromosomes and the central spindle outside oocyte cortex. Scale bar = 50 µm (overviews) or 10 µm (details).

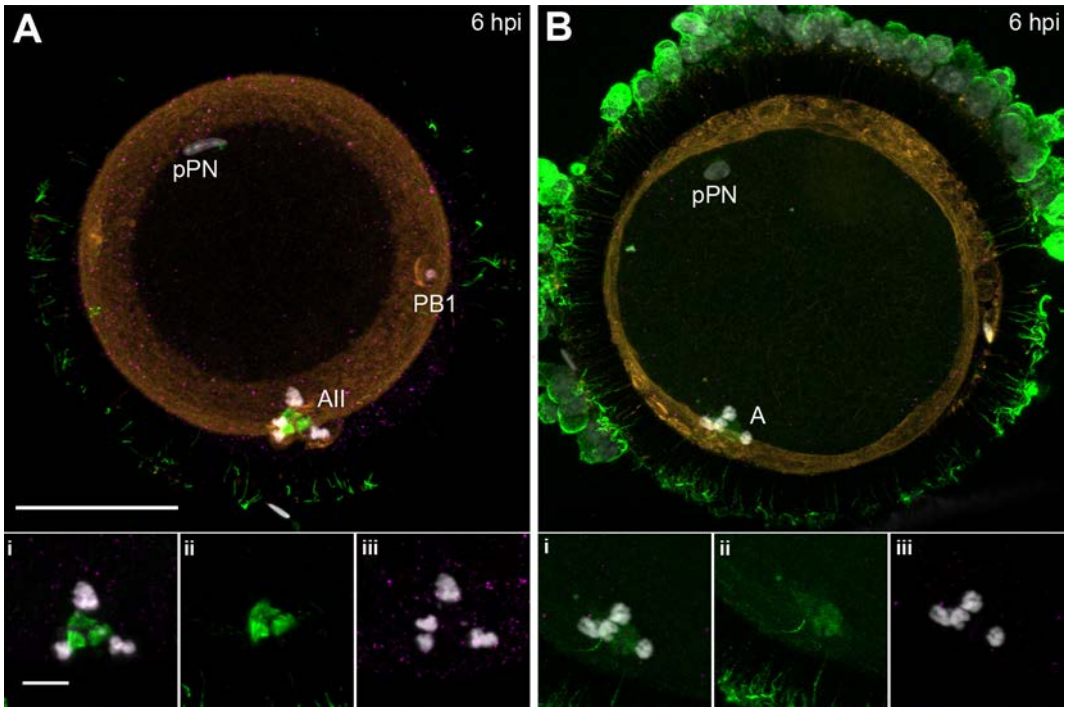

Figure 46: Examples of multipolar anaphase II.
(**A**) Fertilized oocyte displaying a quadripolar anaphase II. A too small first polar body is detectable. The multipolar anaphase II presented four chromatin bridges/ lagging chromosomes. (**B**) Fertilized oocyte presenting a quadripolar anaphase II and also irregular anaphase spindle positioning/ orientation. The multipolar anaphase II presented chromatin bridges. Panels composed by 2 slices of abnormal oocytes (A; B) and (i) detail presented in DAPI-α-tubulin channels, (ii) same detail shown in α-tubulin and (iii) detail on chromatin conformation. Scale bar in oocyte subsets: 50 µm; scale bar in details 10 µm.

In Figure 47 a schematic illustration of the possible development of the maternal DNA after failure of first polar body extrusion is presented. In Figure 48 confocal image stacks of the possible consequences of this failure are shown.

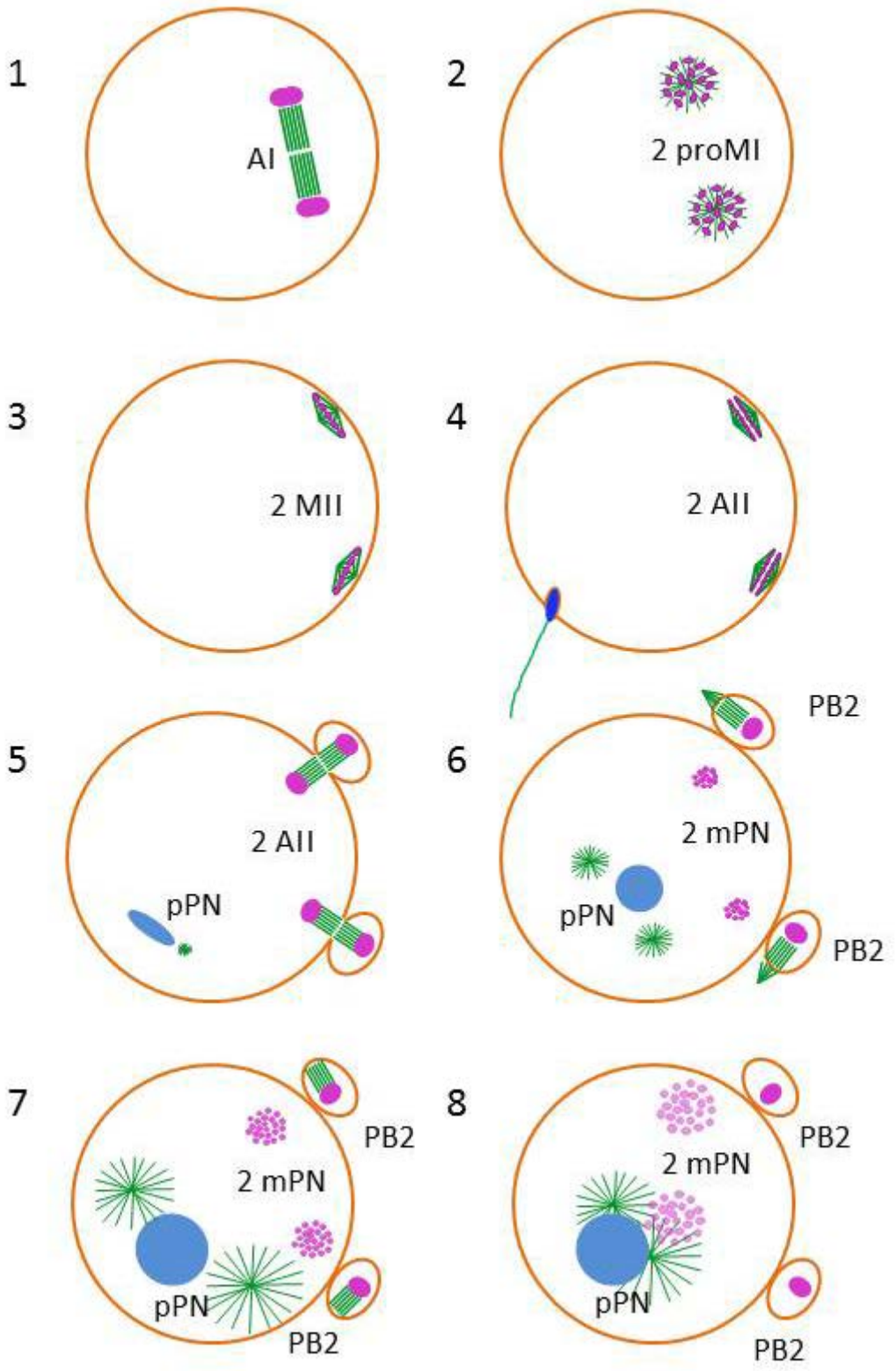

Figure 47: Possible consequences of the failure of the extrusion of the first polar body. Scheme illustrating the formation of two metaphase II spindles and two maternal pronuclei after fertilization.

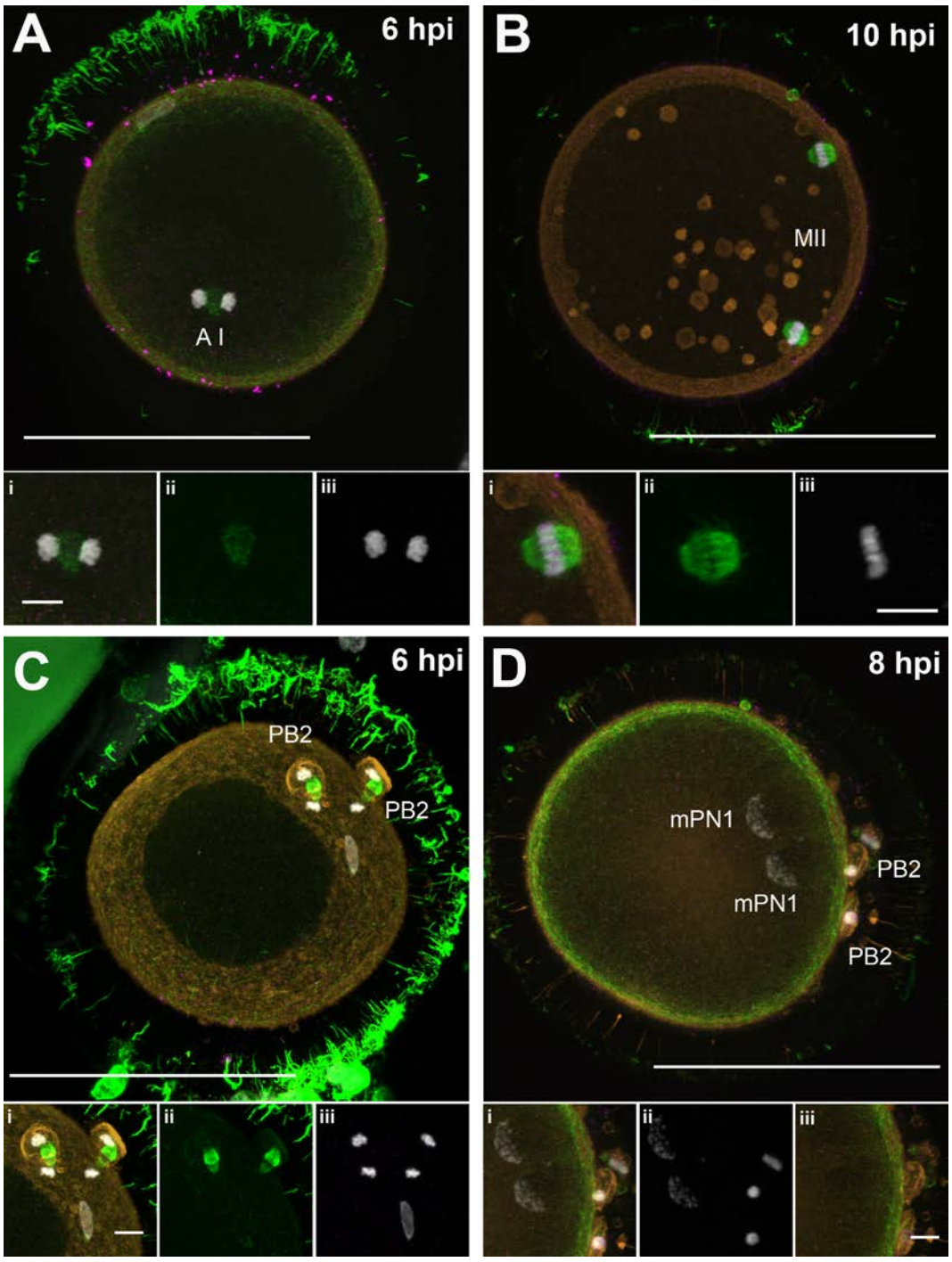

Figure 48: Consequences of failure of first polar body extrusion.
(**A**) Failure of first polar body extrusion due to irregular spindle orientation **(B)** Two metaphase II spindles. **(C)** Two anaphase II spindle and two PB2 as consequence of fertilization **(D)** Two maternal pronuclei after the extrusion of 2 polar bodies in a spontaneously activated oocyte already shown in figure 37. Scale bar in the upper panels = 100 µm; scale bar in detail = 10µm.

In Figure 49 a schematic illustration of the possible outcomes of the failure of second polar body extrusion is presented.

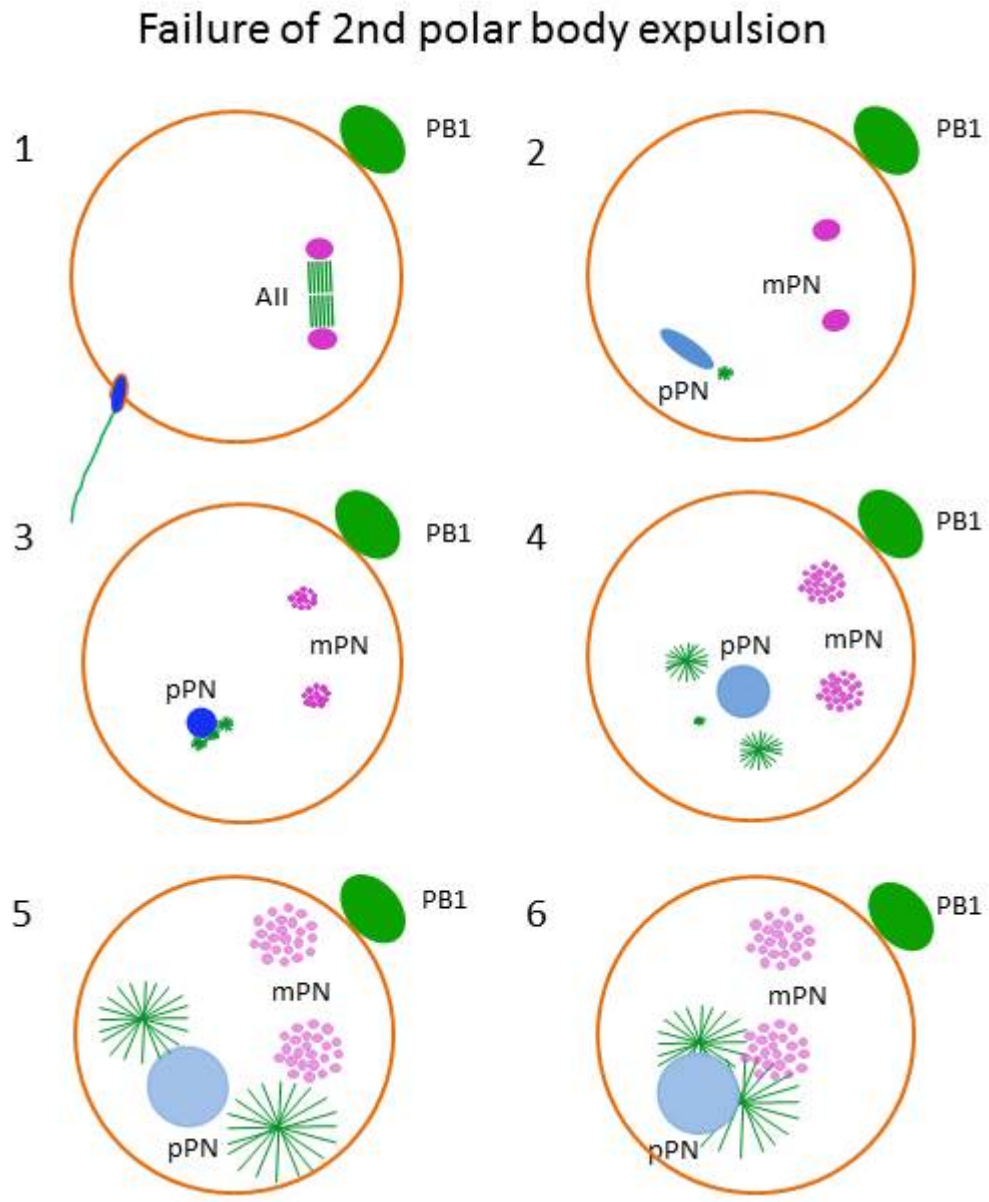

Figure 49: Possible consequences when the extrusion of the second polar body fails. Scheme illustrating the formation two maternal pronuclei after fertilization.

4.3.4.2 Common abnormalities detected between 4 and 12 hpi

The confocal image stacks of the 654 oocytes were used to determine the incidence of the anomalies characterized and classified in this study. For simplicity, oocytes which had been penetrated by one or more sperm and activated i.e. had entered anaphase II, were termed fertilized. 319 oocytes (48.9%) were unfertilized. The data on the occurrence of anomalies in the unfertilized oocytes are presented in Tables 29 and 30. All oocytes analyzed had resumed meiosis, but 163 i.e. 24.9% of all and 51.9% of the unfertilized oocytes were arrested between prometaphase I (proMI) and early prometaphase II (ProMII-A) or had severe anomalies precluding fertilization and/or correct completion of oocyte meiosis (Table 29). 61 i.e. 9.3% of all and 19.1% of the unfertilized oocytes were arrested in prometaphase I. Nearly the same number of oocytes was arrested at an early stage of MII spindle formation. Notably, in 36 (59%) of the 61 oocytes arrested in proMI a failure of chromosome congression to the metaphase plate and formation of a multipolar spindle or a grossly abnormal distribution pattern of the microtubules was seen (Table 30). 19 oocytes, which were arrested in proMI or the meiosis I-II transition or proMII-A, had been penetrated by one or more sperm nuclei. Thereby also early stages of paternal pronucleus formation were observed. Only three oocytes were detected, which were penetrated by sperm but not activated with a presumably normal MII spindle. 20 i.e. 3.1% of all and 6.3 of the unfertilized oocytes had been spontaneously activated and 13 of them showed an irregular ana- or telophase II or one or two irregular maternal pronuclei (Table 30).

As presented in Table 31, 335 (51.2%) of the oocytes were fertilized and 245 (73.3%) of them were monospermic and presumably normal. Notably, in 50 i.e. 14.9% of all fertilized and 20% of the monospermic fertilized oocytes, severe abnormalities of oocyte meiosis II incompatible with normal embryo development were found, including (i) incorrect spindle positioning and/or orientation, (ii) multipolar spindle formation, (iii) lagging chromosomes and chromatin bridges and combinations thereof. In 22 cases, a multipolar ana- or telophase II was observed. 40 (11.9%) of the fertilized oocytes were penetrated by more than on sperm nucleus. Thereby, 33 (9.9%) had no additional anomaly, but in 7 (2.1%) an irregular ana- or telophase II or one or two irregular maternal pronuclei was seen

(Table 30).

Time point (hpi)	**4**	**5**	**6**	**7**	**8**	**10**	**12**	**4-12**	***%***
All oocytes analyzed	33	73	148	53	172	70	105	**654**	***100.0***
Unfertilized oocytes	33	59	86	31	73	22	16	**319**	***48.8***
Abnormal/incompetent oocytes									
Arrest at proMI/MI	10 *30.3*	6 *8.2*	19 *12.8*	7 *13.2*	11 *6.4*	8 *11.4*	0	**61**	***9.3***
Arrest at A/T I	1 *3.0*	0	3 *2.0*	0	4 *2.3*	0	0	**8**	***1.2***
Arrest at meiosis I-II transition	0	2 *2.7*	2 *1.4*	2 *3.8*	1 *0.6*	0	0	**7**	***1.1***
Arrest at proMII-A	2 *6.1*	11 *15.1*	20 *13.5*	8 *15.1*	12 *7.0*	5 *7.1*	1 *1.0*	**59**	***9.0***
proMII-B, penetrated by sperm	0	0	2 *1.4*	0	1 *0.6*	0	0	**3**	***0.5***
Grossly abnormal MII	0	0	0	0	0	1 *1.4*	1 *1.0*	**2**	***0.3***
Failed oocyte activation[a]	0	0	1 *0.7*	1 *1.9*	1 *0.6*	0	0	**3**	***0.5***
Spontaneously activated	0	3 *4.1*	3 *2.0*	2 *3.8*	8 *4.7*	1 *1.4*	3 *2.9*	**20**	***3.1***
total	**13**	**22**	**50**	**20**	**38**	**15**	**5**	**163**	***24.9***

Table 29: Incidence of oocyte maturation arrest and anomalies preventing fertilization.
Shown are the oocytes number and the percentages (in italic). [a] Normal MII, penetrated by sperm.

Time point (hpi)	**4**	**5**	**6**	**7**	**8**	**10**	**12**	**4-12**	***%***
Oocytes arrested at proMI/MI									
Without anomalies	9	3	7	3	1	2	0	**25**	*41.0*
Multipolar ProMI/MI	1	3	10	2	10	4	0	**30**	*49.2*
Abnormal MT organization	0	0	2	2	0	2	0	**6**	*9.8*
total	**10**	**6**	**19**	**7**	**11**	**8**	**0**	**61**	***100.0***
Spontaneosly activated oocytes									
Without additional anomalies	0	2	1	1	1	0	2	**7**	*35.0*
Abnormal A/T II	0	0	1	1	4	1	0	**7**	*35.0*
Two haploid or 1 diploid mPM	0	1	1	0	3	0	1	**6**	*30.0*
total	**0**	**3**	**3**	**2**	**8**	**1**	**3**	**20**	***100.0***

Table 30: Occurrence of abnormalities observed at proMI/MI arrest and spontaneous oocyte activation.

Time point (hpi)	**5**	**6**	**7**	**8**	**10**	**12**	**4-12**	**%**
Fertilized oocytes	14	62	22	99	48	89	**334**	***100.0***
Monospermy without anomalies	13 *92.9*	41 *66.1*	17 *77.3*	69 *69.7*	36 *75.0*	69 *77.5*	**245**	***73.1***
Monospermy with abnormal oocyte meiosis								
Self-enucleation at meiosis II	0	1 *1.6*	0	1 *1.0*	0	0	**2**	***0.6***
Abnormal A/T II spindle position and/or orientation	0	2 *3.2*	0	1 *1.0*	1 *2.1*	3 *3.4*	**7**	***2.1***
Multipolar A/T II	0	5 *8.1*	0	12 *12.1*	1 *2.1*	4 *4,5*	**22**	***6.6***
Missegregated chromosomes at A/T II without spindle anomalies	1 *7.1*	2 *3.2*	0	1 *1.0*	0	0	**4**	***1.2***
Chromatin bridges without A II spindle anomalies	0	1 *1.6*	3 *13.6*	0	0	2 *2.2*	**6**	***1.8***
Chromatin bridges with abnormal A II spindle position/orientation	0	2 *3.2*	0	1 *1.0*	1 *2.1*	1 *1.1*	**5**	***1.5***
Two haploid or 1 diploid mPM	0	0	0	2 *2.0*	1 *2.1*	1 *1.1*	**4**	***1.2***
total	**1**	**13**	**3**	**18**	**4**	**10**	**50**	***14.9***
Polyspermy								
Without anomalies of oocyte meiosis	0	6 *9.7*	2 *9.1*	10 *10.1*	7 *14.6*	8 *9.0*	**33**	***9.9***
With abnormal oocyte meiosis	0	2 *3.2*	0	2 *2.0*	1 *2.1*	2 *2.2*	**7**	***2.1***
total	**0**	**8**	**2**	**12**	**8**	**10**	**40**	***11.9***

Table 31: Incidence of abnormalities in fertilized oocytes per time point.
Shown are oocytes number and percentages (in italic)

5 DISCUSSION

In this study, for the first time, 3D confocal microscopy was used to systematically investigate bovine oocyte maturation and the first stages of the fertilization *in vitro*. Our 4-channel staining enabled us to highlight DNA (DAPI), chromatin condensation (H3S10p), spindle apparatus and cytoplasmic microtubule (α-tubulin), and cortical as well as cytoplasmic f-actin filaments (phalloidin). Confocal microscopy allowed us to reconstruct three-dimensional images of the oocytes which can be viewed from different angles and facilitate proper classification and interpretation of the meiotic maturation stages. Only few studies analysed the *in vitro* maturation of bovine oocytes by CLSM, (KIM et al., 2000; LI et al., 2005) but – in contrast to the present study – no systematic evaluation of different stages, kinetics and abnormalities were performed.

Characterization and classification of substages of oocyte maturation

The series of three-dimensional "snapshots" of oocytes at numerous time points from 0 to 28 hours of IVM was used to reconstruct the course of events of spindle formation, chromosome alignment and segregation, the first polar body expulsion as well as the proceeding through metaphase II.

We identified three types of germinal vesicle chromatin configuration based on the chromatin condensation degree, on the positioning of the chromatin in the GV, and on the contact between the chromatin and the membrane of the germinal vesicle. Similar classification schemes were proposed by other studies (LIU et al., 2006; LODDE et al., 2007; LODDE et al., 2008; LUCIANO et al., 2014),. The authors reported centripetal chromatin condensation in germinal vesicle oocytes proceeding toward GVBD.

In our study, 9.7% of the oocytes fixed between 0 and 6 h IVM appeared to undergo degeneration and all of them were in GV stage. However, in contrast to other authors, we also observed degenerating oocytes in GV1, GV2 and GV3 configurations.

Role of the microtubular network and spindle assembly

In contrast to the findings of (LI et al., 2005) that did not observe any microtubules (MT) at GV stage or at GVBD, we could clearly detect a fine

microtubular network spreading through the entire cytoplasm.

Upon the time of GVBD, we observed a dissolution of the cytoplasmic microtubular network and a thickening of the cortical f-actin meshwork. Subsequently, the chromatin clustered into a single highly condensed aggregate. At this point, few foci of microtubule asters appeared close to the chromatin aggregates, as previously described by (LI et al., 2005). We defined this point as onset of metaphase I spindle formation.

Our CLSM recordings enabled us to identify three different stages of prometaphase I.

- The first stage was defined as appearance of multiple small microtubule asters close to condensed chromatin aggregate after GVBD.
- The second stage started with the individualization of the chromosomes. The microtubular asters span from a single or few strictly related MTOC in the centre of the chromatin aggregate probably outwards. With our staining we were not able to determine the direction of the tubulin nucleation. Further studies are thus needed to understand the dynamics of the MT aster formation.
- The third stage was characterized by microtubules organized between and around the homologous chromosomes, resulting in a disk-shaped MT array.

Many intermediate stages between these three phenotypes were also seen. In accordance with the report by (LI et al., 2005), we observed large metaphase I plates between flat spindle poles. Thus, the formation of two microtubule nucleation plates was revealed. The same structure was observed at metaphase II stage.

As described by (LI et al., 2005) we noticed that many microtubules composing the typical bipolar MI or MII appeared to be linked to chromosomes, although we did not stain kinetochores. Other microtubules seemed to pass thorough the metaphase I or II plate and connect to the other side (interpolar MT).

In accordance with (LI et al., 2005), we were not able to detect any MTOC during anaphase except the anaphase spindles and the midbody between the two chromatin aggregates. Initially we observed an equal surface of attachment

between the two rows of chromosomes and their attached microtubules, giving the anaphase plate a cylindrical/barrel shape.

In more advanced anaphase stages and telophase, the connecting area between the chromosome row remaining in the oocyte and the microtubuli decreased gradually, and the central spindle formed a cone of microtubules with the basis towards the midbody. Finally the microtubules detached from the chromosomes remaining in the oocyte and were – together with the midbody and the cylindrically-shaped outer part of the central spindle attached to the other set of chromosomes - extruded together with the polar body.

No differences in shape of spindles were observed between anaphase I and anaphase II. The diameter of the metaphase II plate was smaller than that of the metaphase I plate.

Time course of oocyte maturation

In our study oocytes were fixed at 2-hour intervals from 0 to 28 h IVM covering the time normally necessary for bovine egg maturation *in vitro*. In our laboratory the standard time of insemination was 23 hours after start incubation, therefore we investigated groups of oocytes fixed also at this time point. We reported the presence of GV oocytes from 0 to 6 h IVM followed by a dramatic decrease at 8 h. Similar data were also described by authors using different methods (SIRARD et al., 1989; KASTROP et al., 1990; KIM et al., 2000).

In our study, GVBD occurred between 6 and 8 h IVM. A similar timing for GVBD was reported by (SIRARD et al., 1989) whereas (LI et al., 2005) reported a slightly later timing of this event. Prometaphase I took place between 6 and 16 hours, with a peak at 10 hours, similar as in the study of (SIRARD et al., 1989). However, the latter study used phase-contrast microscopy and was therefore not able to resolve different prometaphase stages as was done in our study. The peak of metaphase I was at 16 hours IVM, with a range from 12 to 22 hours.

In our study the first morphologically normal oocytes in anaphase I were detected at 12 h IVM and the last at 20 h IVM. Similar data were reported by other authors (KASTROP et al., 1990; DOMINKO & FIRST, 1997; KIM et al., 2000; LI et al., 2005).

Interestingly, a similar timing of progression through meiosis I and II as well as

similar changes in chromatin configuration and spindle organization after resumption of meiosis were observed by CLSM analysis in human oocytes (COMBELLES et al., 2002), supporting the role of the bovine as a model system.

Abnormalities of oocyte maturation

The systematic investigation of oocytes from 0 to 28 h IVM enabled us to detect the most common abnormalities occurring during maturation, to characterize them and to correlate the types of anomalies with the time of appearance. The most relevant abnormality detected was irregular anaphase I. Errors in this phase were first recorded at 10 h and could be observed till 23 h IVM. In particular the most frequent disturbances were chromatin bridges and irregular anaphase I spindle in addition to chromatin bridges. The errors occurring at anaphase I appeared to be caused by failure of chromosome congression, proper alignment or homologous chromosome segregation. An irregular spindle was mainly combined with chromosome alignment or segregation errors with the exception of irregular spindle orientation/or positioning. These findings strongly suggested an involvement of the chromosomes in irregular spindle formation whereas irregular orientation or positioning alone might be related to abnormalities in the cooperation between microtubules and microfilaments (KIM et al., 2000). All disturbances including both chromosome segregation and sole spindle abnormalities severely impair the chance of further development. Our observations of irregular anaphase I could be possible explanation of the findings of (DOMINKO & FIRST, 1997) that reported a correlation between the time required for first polar body extrusion and low developmental capacity.

During our investigation of GV oocytes, we noted that many oocytes (28/43) at GV3 exhibited a particular chromatin compaction phenotype. They displayed separate chromatin particles or chromosome aggregates far from the main chromosome cluster. Separate chromosome aggregates were also observed in prometaphase I, especially in the first stage (proMI-A) but also further during metaphase I. We were also able to detect unaligned chromosomes in the later prometaphase I (proMI-B) and also in the metaphase I. These findings strongly suggest that the irregular chromatin aggregation into a single aggregate during early stages of meiosis resumption might be associated with chromosome segregation errors.

In our study the time ranges of prometaphase I and II were remarkably longer than the other maturation stages. At 23 to 28 h IVM, 10/167 oocytes did not reach meiosis II. The major proportion of them appeared to be arrested/strongly delayed at prometaphase I-A stage or displaying an irregular metaphase I organization as for example exhibiting multipolar metaphase I spindle. These findings strongly suggest the activation of a check-point in this prometaphase I stage. The potential role of DNA damage response and checkpoints in mammalian oocytes were reviewed by (CARROLL & MARANGOS, 2013) They illustrated how permissive the checkpoints in fully grown mammalian oocytes are. Future studies need to address mechanisms involved in the surveillance of the DNA integrity at this particular stage. One possibility is staining for γ-H2A.X. This particular histone is called “guardian of the genome” (FERNANDEZ-CAPETILLO et al., 2004) because of its role in recruiting repair factors to the site of DNA damage after phosphorylation on COOH terminus. Staining of γH2A.X foci through antibodies was demonstrated to be a sensitive quantitative method for the detection of double strand breaks (SEDELNIKOVA et al., 2002).

Timing of Fertilization and Associated Structural Changes

The series of three dimensional CLSM images was used to reconstruct the time course of events of the first steps of *in vitro* fertilization. Compared to the observation reported by (LONG et al., 1993), systematic analysis at 4, 5, 6, 7, 8, 10 and 12 hpi enabled us to precisely follow the asynchronous chromatin remodelling essential for pronuclear formation and to determine the timing of structural changes of the maternal and paternal chromatin. We observed five condensation degrees of maternal pronucleus as well as five stages for the paternal one. The paternal pronucleus appeared to be in a more advanced decondensation stage and had a larger diameter compared to the maternal one. Between 8 and 10 hour post insemination (hpi), we observed that the paternal chromatin was re-condensed in a round, slightly H3S10p positive cluster, whereas at the same time point the maternal pronucleus was still undecondensed after telophase II. From 10 to 12 hpi, both pronuclei reached the same decondensation state and had a similar size. Nevertheless, the maternal pronucleus could be distinguished from the paternal one because of its granular chromatin pattern. This maternal chromatin configuration developed in a more homogeneous pattern after 12 hpi and became no longer recognizable at 28 hpi (data not shown). The paternal pronucleus could

also be identified by the presence of the sperm aster. It appeared already close to the undecondensed sperm nucleus (6 hpi) and followed the paternal de- and recondensing, spreading radially into the cytoplasm interlacing with the cytosplamic network. We identified four stages in sperm aster formation and correlated them to the timing of paternal pronuclear formation. Classification of the sperm aster was also performed by other authors (NAVARA et al., 1995a; NAVARA et al., 1995b). In (LONG et al., 1993) they considered sperm aster formation in bovine zygotes as a process independent of pronuclear formation, we were able to observed a clear correlation between the sperm aster stage and the paternal pronucleus stage. The first detectable signs of sperm aster formation coincided with the first decondensation stage of the paternal pronucleus (pPN0) and was located close to the previous position of the posterior end of the sperm nucleus. (DOMINKO & FIRST, 1997) reported the first penetrated sperm nucleus at 5 hpi regardless to the time of insemination or to maturation stage.

Characterization of anomalies and notable interesting findings

In our study, 48.9% of the analysed oocytes were unfertilized. This group includes i) spontaneously activated oocytes, ii) oocytes that were arrested at prometaphase I/ metaphase I, and iii) oocytes at prometaphase II.

We recorded a total quote of 3.1% spontaneously activated oocytes. This low rate was in line with our previous findings in IVM. Among the spontaneously activated oocytes, we distinguished three groups: i) morphologically normal oocytes at least in anaphase II stage; ii) oocytes displaying anomalies at anaphase II; and iii) oocytes presenting two small haploid or one presumably diploid maternal pronucleus. Whether this phenotype is caused by failure in the anaphase II is not clear yet. In our study a large proportion of oocytes did not reach the meiosis I (9.3%) and most of them appeared to be arrested at prometaphase I stage (proMI-B). 41% of prometaphase I - metaphase I arrested oocytes were morphologically normal, while 59% displayed clearly detectable morphological anomalies. Notably, both groups of arrested oocytes were penetrated by sperm, but not activated. Nevertheless, sperm nuclei underwent decondensation.

Interestingly, quite the same number of oocytes arrested at proMI-MI appeared to be arrested at early stage of prometaphase II. As described for oocytes arrested at proMI-MI, also early proMII oocytes were detected displaying both

morphologically normal as well as morphologically abnormal phenotypes. Further studies, including kinetochore and centrosome staining, are needed for better understanding the reasons for the delay/arrest at this stage.

In our study, oocytes arrested at proMII-A were more prone to polyspermic penetration and further development of paternal pronuclei compared to the more advanced proMII-B. A possible explanation might be incomplete acquisition of capacity to activate the polyspermy block that is fully reached at metaphase II (DUCIBELLA et al., 1993).

Of the monospermic activated oocytes (representing the 73.35% of fertilized oocytes), 14.97% exhibited severe anomalies at anaphase I, making normal embryo development impossible. These anomalies appeared to be comparable to those recorded during the first meiosis. In addition, failure of polar body extrusion could lead to different anomalies after fertilization. If the failure of expulsion involved the first polar body, two metaphase II plates could form and followed by two anaphase II figures after sperm penetration. This phenotype might lead to different outcomes (see Figure 40). The supernumerary maternal pronucleus could be confined and no longer involved in the embryo formation or could develop as single haploid nucleus over cleavages and contribute to the formation of a mixoploid embryo. Similar outcomes can result, when the oocyte fails to extrude the second polar body. In this case two separate pronuclei could form (see Figure 40).

The proportion of oocytes fertilized by two or more sperm represented 11.9% of the fertilized oocytes. Polyspermy appeared either as an isolated event or combined with irregular anaphase II. Interestingly, in presence of failure of polar body extrusion and fertilization of two sperm, we observed also the formation of two maternal and two paternal pronuclei (see Figure 40). Two syngamies of these two pronuclei pairs could provide an explanation to a clinical case of true hermaphroditism reported by (SOUTER et al., 2007).

We noted self-enucleated oocytes after anaphase II as reported in by (LONG et al., 1993) as well as in parthenogenetically activated bovine oocytes (POWELL & BARNES, 1992).

Conclusion and Perspectives

This systematic investigation of bovine oocyte maturation and fertilization by 3D confocal microscopy provided for the first time a detailed time course of structural changes during these processes and an overview of potential errors at the various steps. The results of this thesis might have a number of implications in animal reproductive biotechnologies and also in assisted reproduction techniques in humans.

One practical application of the immunostaining and subsequent observation by CLSM is the analysis of oocytes inseminated with semen from bulls affected by the so-called “Bovine Male Subfertility”. This pathology is characterized by exceptionally poor outcomes and low blastocyst rates after IVF in presence of normal semen parameters as progressive motility and morphology. (PAUSCH et al., 2014) described as cause a non-sense mutation of the transmembrane protein 95 encoding by the *TMEM95* gene leading to a premature stop-codon of this protein. Due to the poor reproductive performance characterizing these bulls, (PAUSCH et al., 2014) suggested an involvement of the TMEM95 protein in fertilization mechanisms. Therefore, bovine oocytes were fixed at 12 and 28 hpi after insemination with semen of affected bulls and analysed by CLSM as done in this study (data not shown). First results revealed that the sperm of the affected bulls could pass the zona pellucida but failed to penetrate into the oocyte (data not shown). Thereby a considerable proportion of spontaneously activated oocytes were found, most of them with a single maternal pronucleus.

CLSM analysis might be also a useful tool for the investigation of the effects of agents or environmental conditions on oocyte quality. As an example, several studies have been already undertaken to identify the potential deleterious effects of bisphenol A on oocyte maturation in mice (EICHENLAUB-RITTER et al., 2008; TRAPPHOFF et al., 2013) and in bovine (FERRIS et al., 2015) by immunostaining and subsequent CLSM visualization of chromatin and microtubules.

The observations of this study in the bovine model could help to unravel mechanisms responsible for implantation failures in humans as well as mosaicism formation in the early embryo development (before differentiation in ICM and trophectoderm) reported in literature (see Figure 39, Figure 40, Figure 47 and Figure 49). Many mechanisms are proposed in are summarized in (TAYLOR et al., 2014). This kind of analysis might help to explain also mechanisms

underlying the formation of monozygotic twins, and semi-identical twins (SOUTER et al., 2007).

6 ZUSAMMENFASSUNG

Zeitlicher Ablauf und Fehler bei der in vitro Reifung und Befruchtung boviner Eizellen

In dieser Arbeit wurden systematisch die Reifung und die ersten Stadien der Befruchtung von Rinder-Eizellen mittels confocaler Laser-Scanning-Mikroskopie (CLSM) und nachfolgender 3-D-Rekonstruktion untersucht. Die Eizellen wurden aus Ovarien vom Schlachthof aus 2-8 mm Follikeln isoliert und zu unterschiedlichen Zeitpunkten der In-vitro-Maturation (IVM) und In-vitro Fertilisation (IVF) fixiert. Nach Anfärbung der DNA, Serin-10-phosphoryliertem Histon H3 (H3S10p), der Mikrotubuli und F-Actin-Filamente mit vier verschiedenen Fluoreszenzfarbstoffen wurden die Eizellen im Ganzen in optischen Serienschnitten aufgenommen. In der Auswertung wurden Stadien der Meiose vom Germinalvesikel bis zur Metaphase II morphologisch charakterisiert und der ungefähre Zeitablauf bestimmt. Mit dem gleichen methodischen Ansatz wurden die ersten Schritte der Befruchtung untersucht: das Eindringen des Spermiums und die Aktivierung der Eizelle, die Bildung des maternalen und paternalen Vorkerns, die Ausbildung des „Sperm Aster“ und der ungefähre Zeitablauf dieser Vorgänge. Parallel dazu wurden die bei der Eizellreifung und Befruchtung *in vitro* entdeckten Anomalien charakterisiert und klassifiziert, um anschließend ihre Häufigkeit zu bestimmen. Im Rahmen dieser Untersuchung entstand eine große Sammlung dreidimensionaler mikroskopischer Bilder, die Rinder-Eizellen in unterschiedlichen Stadien der mutmaßlich normalen Reifung und Befruchtung sowie ein Spektrum ganz unterschiedlicher schwerwiegender Anomalien erfasst.

Insgesamt wurden 1078 Eizellen in 2-Stundenintervallen von 0 bis 28 Stunden IVM fixiert und analysiert. Nach unseren Beobachtungen waren nahezu alle Eizellen vor der *in vitro* Maturation im Germinalvesikel (GV) Stadium, nach 10 h hatten praktisch alle Eizellen die Meiose wieder aufgenommen und den GV aufgelöst. Aus der großen Zahl dreidimensionaler Momentaufnahmen wurden die mutmaßlich normale Ausbildung des Spindelapparates und die Anordnung der Chromosomen in der Meiose I und II rekonstruiert. Gleichzeitig wurde ein Spektrum von Anomalien der Meiose I dokumentiert, von der Bildung einer

multipolaren Spindel, der falschen Positionierung der Spindel bis zu Fehlern bei der Chromosomensegregation und dem Auftreten von Chromatinbrücken in der Anaphase I. Zur Untersuchung des Befruchtungsvorgangs wurden insgesamt 654 Eizellen zu den Zeitpunkten 4, 5, 6, 7, 8, 10 und 12 Stunden nach der Besamung (hpi) im Ganzen aufgenommen und analysiert. Bei der Auswertung wurden der Zeitrahmen des Eindringens der Spermien und der Zeitablauf der Bildung des väterlichen und mütterlichen Vorkerns sowie des „Sperm Aster“ bestimmt. Die Entwicklung der beiden Vorkerne und des „Sperm Aster“ wurde jeweils in fünf Phasen unterteilt. So konnte dargestellt werden, wie der Kern des Spermiums kurz nach dem Eindringen dekondensiert, um vorübergehend wieder zu rekondensieren und einen zunächst kleinen dichten paternalen Vorkern zu bilden, der erneut expandiert. 24,9 % der Eizellen waren in der Meiose vor der Metaphase II arretiert oder waren bereits spontan aktiviert, und konnten so nicht mehr befruchtet werden. Bei 26,9 % der penetrierten und aktivierten Eizellen wurden schwerwiegende Anomalien gefunden: 11,9 % wiesen eine Polyspermie auf, 17 % Aberrationen der Meiose der Eizelle.

Diese Ergebnisse dieser Untersuchungen tragen dazu bei, die komplexen Vorgänge der Eizellreifung und Befruchtung beim Rind und bei anderen Säugern einschließlich des Menschen weiter aufzuklären und die Diagnostik und Therapie von Fertilitätsstörungen zu verbessern.

7 SUMMARY

In this study, bovine oocyte maturation and early fertilization stages were systematically investigated by confocal laser scanning microscopy (CLSM) and subsequent 3-D-reconstruction. Grade I and II oocytes were isolated from 2–8 mm follicles from slaughterhouse ovaries and fixed at different time points of *in vitro* maturation (IVM) and *in vitro* fertilization (IVF). After staining the DNA, Serine 10 phosphorylated histone H3 (H3S10p), microtubules and f-actin microfilaments with four different fluorescence dyes, the oocytes were imaged *in toto* by serial optical sections. In the subsequent analysis, meiotic stages from the germinal vesicle to the metaphase II were morphologically characterized, and the approximate time course was determined. Using the same methodological approach, the first stages of fertilization were investigated: sperm penetration into the oocyte, completion of oocyte meiosis, the development of the maternal and paternal pronucleus, the formation of the sperm aster and the approximate time course. In parallel, the anomalies detected during *in vitro* oocyte maturation and fertilization were characterized and classified to subsequently determine their incidence. This study provided a large collection of three-dimensional microscopic images of bovine oocytes at different stages of presumably normal maturation and fertilization. Moreover, a spectrum of different severe anomalies was documented.

In total, 1078 oocytes were fixed at 2-hour intervals from 0 to 28 hours of IVM and analyzed. Nearly all oocytes fixed before IVM were still in the germinal vesicle (GV) stage, at 10 hours virtually all oocytes had resumed meiosis and the GV had been broken down. The large number of three-dimensional snapshots of oocytes was used to reconstruct the presumably normal formation of the spindle apparatus and the chromosome alignment in meiosis I and II. Moreover, a spectrum of anomalies of meiosis I was documented: from the formation of a multipolar spindle, incorrect positioning of the spindle to chromosome segregation errors and the occurrence of chromatin bridges in anaphase I.

To investigate the early steps of fertilization, in total 654 oocytes were fixed at 4, 5, 6, 7, 8, 10 and 12 hours post insemination (hpi), imaged in toto and morphologically analyzed. Thereby, we determined the time frame of sperm

penetration and oocyte activation, and the approximate time course of the development of the maternal and paternal pronucleus and the sperm aster. The formation of the two pronuclei and of the sperm aster was divided into 5 stages. Thus, we could show how the sperm nucleus shortly after penetrating into the oocyte decondenses and transiently recondenses to a small dense paternal pronucleus which decondenses again.

24.9 % of the oocytes were arrested in meiosis before metaphase II or had been already spontaneously activated and could not be fertilized. 26.9% of the penetrated and activated oocytes had severe anomalies: 11.9 % were polyspermic, 17% showed meiotic aberrations of the oocyte.

The results of this study contribute to further elucidate the complex processes of oocyte maturation and fertilization in cattle and other mammals including humans and to improve the diagnostics and therapies of fertility problems.

8 REFERENCES

Abbott AL, Fissore RA, Ducibella T. Identification of a Translocation Deficiency in Cortical Granule Secretion in Preovulatory Mouse Oocytes. Biology of Reproduction 2001; 65: 1640-7.

Allworth AE, Albertini DF. Meiotic Maturation in Cultured Bovine Oocytes Is Accompanied by Remodeling of the Cumulus Cell Cytoskeleton. Developmental Biology 1993; 158: 101-12.

Anifandis G, Messini C, Dafopoulos K, Sotiriou S, Messinis I. Molecular and Cellular Mechanisms of Sperm-Oocyte Interactions Opinions Relative to in Vitro Fertilization (IVF). International Journal of Molecular Sciences 2014; 15: 12972.

Arlotto T, Schwartz JL, First NL, Leibfried-Rutledge ML. Aspects of follicle and oocyte stage that affect in vitro maturation and development of bovine oocytes. Theriogenology 1996; 45: 943-56.

Bachvarova R, De Leon V, Johnson A, Kaplan G, Paynton BV. Changes in total RNA, polyadenylated RNA, and actin mRNA during meiotic maturation of mouse oocytes. Developmental Biology 1985; 108: 325-31.

Barros C, Yanagimachi R. Induction of Zona Reaction in Golden Hamster Eggs by Cortical Granule Material. Nature 1971; 233: 268-9.

Berg U, Brem G. In vitro Production of Bovine Blastocysts by in vitro Maturation and Fertilization of Oocytes and Subsequent in vitro Culture. Reproduction in Domestic Animals 1989; 24: 134-9.

Bianchi E, Doe B, Goulding D, Wright GJ. Juno is the egg Izumo receptor and is essential for mammalian fertilization. Nature 2014; 508: 483-7.

Bianchi E, Wright GJ. Cross-species fertilization: the hamster egg receptor, Juno, binds the human sperm ligand, Izumo1. Philosophical Transactions of the Royal

Society B: Biological Sciences 2015; 370

Buckett WM, Chian R-C, Dean NL, Sylvestre C, Holzer HEG, Tan SL. Pregnancy loss in pregnancies conceived after in vitro oocyte maturation, conventional in vitro fertilization, and intracytoplasmic sperm injection. Fertility and Sterility 2008; 90: 546-50.

Campbell KHS, Fisher P, Chen WC, Choi I, Kelly RDW, Lee JH, Xhu J. Somatic cell nuclear transfer: Past, present and future perspectives. Theriogenology 2007; 68, Supplement 1: S214-S31.

Carroll J, Marangos P. The DNA damage response in mammalian oocytes. Frontiers in Genetics 2013; 4

Chalbi M, Barraud-Lange V, Ravaux B, Howan K, Rodriguez N, Soule P, Ndzoudi A, Boucheix C, Rubinstein E, Wolf JP, Ziyyat A, Perez E, Pincet F, Gourier C. Binding of sperm protein Izumo1 and its egg receptor Juno drives Cd9 accumulation in the intercellular contact area prior to fusion during mammalian fertilization. Development 2014; 141: 3732-9.

Chohan KR, Hunter AG. Meiotic competence of bovine fetal oocytes following in vitro maturation. Animal Reproduction Science 2003; 76: 43-51.

Chohan KR, Hunter AG. In vitro maturation, fertilization and early cleavage rates of bovine fetal oocytes. Theriogenology 2004; 61: 373-80.

Combelles CMH, Cekleniak NA, Racowsky C, Albertini DF. Assessment of nuclear and cytoplasmic maturation in in-vitro matured human oocytes. Human Reproduction 2002; 17: 1006-16.

De La Fuente R, Eppig JJ. Transcriptional Activity of the Mouse Oocyte Genome: Companion Granulosa Cells Modulate Transcription and Chromatin Remodeling. Developmental Biology 2001; 229: 224-36.

De La Fuente R. Chromatin modifications in the germinal vesicle (GV) of mammalian oocytes. Developmental Biology 2006; 292: 1-12.

Dieci C, Lodde V, Franciosi F, Lagutina I, Tessaro I, Modina SC, Albertini DF, Lazzari G, Galli C, Luciano AM. The Effect of Cilostamide on Gap Junction Communication Dynamics, Chromatin Remodeling, and Competence Acquisition in Pig Oocytes Following Parthenogenetic Activation and Nuclear Transfer. Biology of Reproduction 2013; 89: Article 68, 1-11.

Dominko T, First NL. Timing of meiotic progression in bovine oocytes and its effect on early embryo development. Molecular reproduction and development 1997; 47: 456-67.

Ducibella T, Kurasawa S, Duffy P, Kopf GS, Schultz RM. Regulation of the polyspermy block in the mouse egg: maturation-dependent differences in cortical granule exocytosis and zona pellucida modifications induced by inositol 1,4,5-trisphosphate and an activator of protein kinase C. Biol Reprod 1993; 48: 1251-7.

Eichenlaub-Ritter U, Vogt E, Cukurcam S, Sun F, Pacchierotti F, Parry J. Exposure of mouse oocytes to bisphenol A causes meiotic arrest but not aneuploidy. Mutation Research/Genetic Toxicology and Environmental Mutagenesis 2008; 651: 82-92.

Erickson BH. Development and Senescence of the Postnatal Bovine Ovary1. Journal of Animal Science 1966; 25: 800-5.

Fair T, Hyttel P, Greve T. Bovine oocyte diameter in relation to maturational competence and transcriptional activity. Molecular reproduction and development 1995; 42: 437-42.

Fair T, Hyttel P, Greve T, Boland M. Nucleus structure and transcriptional activity in relation to oocyte diameter in cattle. Molecular reproduction and development 1996; 43: 503-12.

Fair T, Hulshof SCJ, Hyttel P, Greve T, Boland M. Nucleus ultrastructure and transcriptional activity of bovine oocytes in preantral and early antral follicles. Molecular reproduction and development 1997; 46: 208-15.

Fernandez-Capetillo O, Lee A, Nussenzweig M, Nussenzweig A. H2AX: the histone guardian of the genome. DNA Repair 2004; 3: 959-67.

Ferreira EM, Vireque AA, Adona PR, Meirelles FV, Ferriani RA, Navarro PAAS. Cytoplasmic maturation of bovine oocytes: Structural and biochemical modifications and acquisition of developmental competence. Theriogenology 2009; 71: 836-48.

Ferris J, Favetta LA, King WA. Bisphenol A Exposure during Oocyte Maturation in vitro Results in Spindle Abnormalities and Chromosome Misalignment in Bos taurus. Cytogenetic and Genome Research 2015; 145: 50-8.

Florman HM, Bechtol KB, Wassarman PM. Enzymatic dissection of the functions of the mouse egg's receptor for sperm. Developmental Biology 1984; 106: 243-55.

Hassold T, Hunt P. To err (meiotically) is human: the genesis of human aneuploidy. Nat Rev Genet 2001; 2: 280-91.

Herman B, Langevin MA, Albertini DF. The effects of taxol on the organization of the cytoskeleton in cultured ovarian granulosa cells. Eur J Cell Biol 1983; 31: 34-45.

Hewitson L, Simerly C, Schatten G. Inheritance defects of the sperm centrosome in humans and its possible role in male infertility. International journal of andrology 1997; 20 Suppl 3: 35-43.

Hewitson L, Haavisto A, Simerly C, Jones J, Schatten G. Microtubule Organization and Chromatin Configurations in Hamster Oocytes During Fertilization and Parthenogenetic Activation, and After Insemination With Human

Sperm. The Journal of Urology 1998; 159: 1772.

Hinrichs K, Choi YH, Love LB, Varner DD, Love CC, Walckenaer BE. Chromatin Configuration Within the Germinal Vesicle of Horse Oocytes: Changes Post Mortem and Relationship to Meiotic and Developmental Competence. Biology of Reproduction 2005; 72: 1142-50.

Hyttel P, Fair T, Callesen H, Greve T. Oocyte growth, capacitation and final maturation in cattle. Theriogenology 1997; 47: 23-32.

Inoue N, Ikawa M, Isotani A, Okabe M. The immunoglobulin superfamily protein Izumo is required for sperm to fuse with eggs. Nature 2005; 434: 234-8.

Jin M, Fujiwara E, Kakiuchi Y, Okabe M, Satouh Y, Baba SA, Chiba K, Hirohashi N. Most fertilizing mouse spermatozoa begin their acrosome reaction before contact with the zona pellucida during in vitro fertilization. Proceedings of the National Academy of Sciences 2011; 108: 4892-6.

Kaji K, Oda S, Shikano T, Ohnuki T, Uematsu Y, Sakagami J, Tada N, Miyazaki S, Kudo A. The gamete fusion process is defective in eggs of Cd9-deficient mice. Nat Genet 2000; 24: 279-82.

Kastrop PMM, Bevers MM, Destrée OHJ, Kruip TAM. Changes in protein synthesis and phosphorylation patterns during bovine oocyte maturation in vitro. Journal of Reproduction and Fertility 1990; 90: 305-10.

Kim N, Cho S, Choi S, Kim E, Park S, Lim J. The distribution and requirements of microtubules and microfilaments in bovine oocytes during in vitro maturation. Zygote 2000; 8: 25-32.

Klinovska K, Sebkova N, Dvorakova-Hortova K. Sperm-Egg Fusion: A Molecular Enigma of Mammalian Reproduction. International Journal of Molecular Sciences 2014; 15: 10652.

Le Naour F, Rubinstein E, Jasmin C, Prenant M, Boucheix C. Severely Reduced Female Fertility in CD9-Deficient Mice. Science 2000; 287: 319-21.

Lefèvre B, Gougeon A, Nomé F, Testart J. In vivo changes in oocyte germinal vesicle related to follicular quality and size at mid-follicular phase during stimulated cycles in the cynomolgus monkey. Reproduction, nutrition, development 1989; 29: 523-31.

Li G-P, Liu Y, Bunch TD, White KL, Aston KI. Asymmetric division of spindle microtubules and microfilaments during bovine meiosis from metaphase I to metaphase III. Molecular Reproduction and Development 2005; 71: 220-6.

Liu Y, Sui H-S, Wang H-L, Yuan J-H, Luo M-J, Xia P, Tan J-H. Germinal vesicle chromatin configurations of bovine oocytes. Microscopy Research and Technique 2006; 69: 799-807.

Lodde V, Modina S, Galbusera C, Franciosi F, Luciano AM. Large-scale chromatin remodeling in germinal vesicle bovine oocytes: Interplay with gap junction functionality and developmental competence. Molecular Reproduction and Development 2007; 74: 740-9.

Lodde V, Modina S, Maddox-Hyttel P, Franciosi F, Lauria A, Luciano AM. Oocyte morphology and transcriptional silencing in relation to chromatin remodeling during the final phases of bovine oocyte growth. Molecular Reproduction and Development 2008; 75: 915-24.

Lonergan P, Monaghan P, Rizos D, Boland MP, Gordon I. Effect of follicle size on bovine oocyte quality and developmental competence following maturation, fertilization, and culture in vitro. Molecular Reproduction and Development 1994; 37: 48-53.

Long CR, Pinto-Correia C, Duby RT, De Leon FAP, Boland MP, Roche JF, Robl JM. Chromatin and microtubule morphology during the first cell cycle in bovine zygotes. Molecular Reproduction and Development 1993; 36: 23-32.

Louvet-Vallée S, Vinot S, Maro B. Mitotic Spindles and Cleavage Planes Are Oriented Randomly in the Two-Cell Mouse Embryo. Current Biology 2005; 15: 464-9.

Luciano AM, Modina S, Vassena R, Milanesi E, Lauria A, Gandolfi F. Role of Intracellular Cyclic Adenosine 3′,5′-Monophosphate Concentration and Oocyte-Cumulus Cells Communications on the Acquisition of the Developmental Competence During In Vitro Maturation of Bovine Oocyte. Biol Reprod 2004; 70: 465-72.

Luciano AM, Franciosi F, Modina SC, Lodde V. Gap Junction-Mediated Communications Regulate Chromatin Remodeling During Bovine Oocyte Growth and Differentiation Through cAMP-Dependent Mechanism(s). Biol Reprod 2011; 85: 1252-9.

Luciano AM, Franciosi F, Dieci C, Lodde V. Changes in large-scale chromatin structure and function during oogenesis: A journey in company with follicular cells. Animal Reproduction Science 2014; 149: 3-10.

Mattson BA, Albertini DF. Oogenesis: Chromatin and microtubule dynamics during meiotic prophase. Molecular reproduction and development 1990; 25: 374-83.

Messinger SM, Albertini DF. Centrosome and microtubule dynamics during meiotic progression in the mouse oocyte. Journal of Cell Science 1991; 100: 289-98.

Minhas BS, Capehart JS, Bowen MJ, Womack JE, McCrady JD, Harms PG, Wagner TE, Kraemer DC. Visualization of pronuclei in living bovine zygotes. Biol Reprod 1984; 30: 687-91.

Miyado K, Yamada G, Yamada S, Hasuwa H, Nakamura Y, Ryu F, Suzuki K, Kosai K, Inoue K, Ogura A, Okabe M, Mekada E. Requirement of CD9 on the Egg Plasma Membrane for Fertilization. Science 2000; 287: 321-4.

Miyara F, Migne C, Dumont-Hassan M, Meur AL, Cohen-Bacrie P, Aubriot F-X, Glissant A, Nathan C, Douard S, Stanovici A, Debey P. Chromatin configuration and transcriptional control in human and mouse oocytes. Molecular Reproduction and Development 2003; 64: 458-70.

Moller CC, Wassarman PM. Characterization of a proteinase that cleaves zona pellucida glycoprotein ZP2 following activation of mouse eggs. Developmental Biology 1989; 132: 103-12.

Muro Y, Okabe M. Mechanisms of Fertilization—A View From the Study of Gene-Manipulated Mice. Journal of Andrology 2011; 32: 218-25.

Navara C, Simerly C, Zoran S, Schatten G. The sperm centrosome during fertilization in mammals: implications for fertility and reproduction. Reproduction, Fertility and Development 1995a; 7: 747-54.

Navara CS, First NL, Schatten G. Microtubule Organization in the Cow during Fertilization, Polyspermy, Parthenogenesis, and Nuclear Transfer: The Role of the Sperm Aster. Developmental Biology 1994; 162: 29-40.

Navara CS, Simerly C, Schatten G. Imaging motility during fertilization. Theriogenology 1995b; 44: 1099-114.

Navara CS, First NL, Schatten G. Phenotypic variations among paternal centrosomes expressed within the zygote as disparate microtubule lengths and sperm aster organization: correlations between centrosome activity and developmental success. Proceedings of the National Academy of Sciences 1996; 93: 5384-8.

Okabe M, Adachi T, Takada K, Oda H, Yagasaki M, Kohama Y, Mimura T. Capacitation-related changes in antigen distribution on mouse sperm heads and its relation to fertilization rate in vitro. Journal of Reproductive Immunology 1987; 11: 91-100.

Okabe M. The cell biology of mammalian fertilization. Development 2013; 140: 4471-9.

Palermo G, Munné S, Cohen J. The human zygote inherits its mitotic potential from the male gamete. Human Reproduction 1994; 9: 1220-5.

Palermo G, Colombero L, Rosenwaks Z. The human sperm centrosome is responsible for normal syngamy and early embryonic development. Reviews of Reproduction 1997; 2: 19-27.

Parfenov V, Potchukalina G, Dudina L, Kostyuchek D, Gruzova M. Human antral follicles: Oocyte nucleus and the karyosphere formation (electron microscopic and autoradiographic data). Gamete Research 1989; 22: 219-31.

Pausch H, Kölle S, Wurmser C, Schwarzenbacher H, Emmerling R, Jansen S, Trottmann M, Fuerst C, Götz K-U, Fries R. A Nonsense Mutation in TMEM95 Encoding a Nondescript Transmembrane Protein Causes Idiopathic Male Subfertility in Cattle. PLOS Genetics 2014; 10: e1004044.

Pincus G, Enzmann EV. THE COMPARATIVE BEHAVIOR OF MAMMALIAN EGGS IN VIVO AND IN VITRO : I. THE ACTIVATION OF OVARIAN EGGS. The Journal of Experimental Medicine 1935; 62: 665-75.

Pinto-Correia C, Poccia DL, Chang T, Robl JM. Dephosphorylation of sperm midpiece antigens initiates aster formation in rabbit oocytes. Proceedings of the National Academy of Sciences 1994; 91: 7894-8.

Powell R, Barnes FL. The kinetics of oocyte activation and polar body formation in bovine embryo clones. Molecular reproduction and development 1992; 33: 53-8.

Rawe VY, Terada Y, Nakamura S, Chillik CF, Olmedo SB, Chemes HE. A pathology of the sperm centriole responsible for defective sperm aster formation,

syngamy and cleavage. Human Reproduction 2002; 17: 2344-9.

Raz T, Ben-Yosef D, Shalgi R. Segregation of the pathways leading to cortical reaction and cell cycle activation in the rat egg. Biol Reprod 1998; 58: 94-102.

Rubinstein E, Ziyyat A, Wolf J-P, Le Naour F, Boucheix C. The molecular players of sperm–egg fusion in mammals. Seminars in Cell & Developmental Biology 2006; 17: 254-63.

Russo V, Martelli A, Berardinelli P, Di Giacinto O, Bernabò N, Fantasia D, Mattioli M, Barboni B. Modifications in chromatin morphology and organization during sheep oogenesis. Microscopy Research and Technique 2007; 70: 733-44.

Sanders JR, Swann K. Molecular triggers of egg activation at fertilization in mammals. Reproduction 2016; 152: R41-R50.

Sathananthan AH, Kola I, Osborne J, Trounson A, Ng SC, Bongso A, Ratnam SS. Centrioles in the beginning of human development. Proceedings of the National Academy of Sciences 1991; 88: 4806-10.

Sathananthan AH, Ratnam SS, Ng SC, Tarín JJ, Gianaroli L, Trounson A. The sperm centriole: its inheritance, replication and perpetuation in early human embryos. Human Reproduction 1996; 11: 345-56.

Sathananthan AH. Paternal Centrosomal Dynamics in Early Human Development and Infertility. Journal of Assisted Reproduction and Genetics 1998; 15: 129-39.

Satouh Y, Inoue N, Ikawa M, Okabe M. Visualization of the moment of mouse sperm–egg fusion and dynamic localization of IZUMO1. Journal of Cell Science 2012; 125: 4985-90.

Schatten G, Simerly C, Schatten H. Microtubule configurations during fertilization, mitosis, and early development in the mouse and the requirement for

egg microtubule-mediated motility during mammalian fertilization. Proceedings of the National Academy of Sciences 1985; 82: 4152-6.

Schatten G. The Centrosome and Its Mode of Inheritance: The Reduction of the Centrosome during Gametogenesis and Its Restoration during Fertilization. Developmental Biology 1994; 165: 299-335.

Sedelnikova OA, Rogakou EP, Panyutin IG, Bonner WM. Quantitative Detection of 125IdU-Induced DNA Double-Strand Breaks with γ-H2AX Antibody. Radiation Research 2002; 158: 486-92.

Simerly C, Wu G-J, Zoran S, Ord T, Rawlins R, Jones J, Navara C, Gerrity M, Rinehart J, Binor Z, Asch R, Schatten G. The paternal inheritance of the centrosome, the cell's microtubule-organizing center, in humans, and the implications for infertility. Nat Med 1995; 1: 47-52.

Sirard M-A, Richard F, Blondin P, Robert C. Contribution of the oocyte to embryo quality. Theriogenology 2006; 65: 126-36.

Sirard MA, Florman HM, Leibfried-Rutledge ML, Barnes FL, Sims ML, First NL. Timing of nuclear progression and protein synthesis necessary for meiotic maturation of bovine oocytes. Biol Reprod 1989; 40: 1257-63.

Sirard MA, Coenen K, Bilodeau S. Effect of fresh or cultured follicular fractions on meiotic resumption in bovine oocytes. Theriogenology 1992; 37: 39-57.

Sirard MA. Resumption of meiosis: mechanism involved in meiotic progression and its relation with developmental competence. Theriogenology 2001; 55: 1241-54.

Souter V, Parisi M, Nyholt D, Kapur R, Henders A, Opheim K, Gunther D, Mitchell M, Glass I, Montgomery G. A case of true hermaphroditism reveals an unusual mechanism of twinning. Human Genetics 2007; 121: 179-85.

Sui H-S, Liu Y, Miao D-Q, Yuan J-H, Qiao T-W, Luo M-J, Tan J-H. Configurations of germinal vesicle (GV) chromatin in the goat differ from those of other species. Molecular reproduction and development 2005; 71: 227-36.

Sun Q-Y. Cellular and molecular mechanisms leading to cortical reaction and polyspermy block in mammalian eggs. Microscopy Research and Technique 2003; 61: 342-8.

Sun X-S, Liu Y, Yue K-Z, Ma S-F, Tan J-H. Changes in germinal vesicle (GV) chromatin configurations during growth and maturation of porcine oocytes. Molecular reproduction and development 2004; 69: 228-34.

Taylor TH, Gitlin SA, Patrick JL, Crain JL, Wilson JM, Griffin DK. The origin, mechanisms, incidence and clinical consequences of chromosomal mosaicism in humans. Human Reproduction Update 2014; 20: 571-81.

Terada Y, Simerly CR, Hewitson L, Schatten G. Sperm Aster Formation and Pronuclear Decondensation During Rabbit Fertilization and Development of a Functional Assay for Human Sperm. Biol Reprod 2000; 62: 557-63.

Terada Y. Human Sperm Centrosomal Function during Fertilization, a Novel Assessment for Male Sterility. Human Cell 2004; 17: 181-6.

Tesařik J, Pilka L, Drahorád J, Čechová D, Veselský L. The role of cumulus cell-secreted proteins in the development of human sperm fertilizing ability: implication in IVF. Human Reproduction 1988; 3: 129-32.

Thérien I, Manjunath P. Effect of Progesterone on Bovine Sperm Capacitation and Acrosome Reaction. Biology of Reproduction 2003; 69: 1408-15.

Trapphoff T, Heiligentag M, El Hajj N, Haaf T, Eichenlaub-Ritter U. Chronic exposure to a low concentration of bisphenol A during follicle culture affects the epigenetic status of germinal vesicles and metaphase II oocytes. Fertility and

Sterility 2013; 100: 1758-67.e1.

Vajta G, Gjerris M. Science and technology of farm animal cloning: State of the art. Animal Reproduction Science 2006; 92: 211-30.

Wang W, Hosoe M, Li R, Shioya Y. Development of the competence of bovine oocytes to release cortical granules and block polyspermy after meiotic maturation. Development, Growth & Differentiation 1997; 39: 607-15.

Wassarman PM. Gamete interactions during mammalian fertilization. Theriogenology 1994; 41: 31-44.

Wickramasinghe D, Ebert KM, Albertini DF. Meiotic competence acquisition is associated with the appearance of M-phase characteristics in growing mouse oocytes. Developmental Biology 1991; 143: 162-72.

Yamagata K, Yamazaki T, Yamashita M, Hara Y, Ogonuki N, Ogura A. Noninvasive visualization of molecular events in the mammalian zygote. genesis 2005; 43: 71-9.

Zernicka-Goetz M, Pines J. Use of Green Fluorescent Protein in Mouse Embryos. Methods 2001; 24: 55-60.

9 INDEX OF FIGURES

10 INDEX OF TABLES

11 ACKNOWLEDGEMENTS

First of all I would like to express my gratitude to Univ.- Prof. Dr. Eckhard Wolf for providing me the opportunity to do my doctoral thesis at the Chair for Molecular Animal Breeding and Biotechnology of the LMU Munich.

I am particularly grateful to Dr. Felix Andreas Habermann for his guidance, endless patience and constant support.

I would also like to thank Dr. Myriam Reichenbach and Tuna Güngör for the precious expertise and for the help in the laboratory. Thanks also to Elisabeth Kemter for her valuable suggestions and her help.

Special thanks to all my colleagues at Moorversuchsgut, in particular Mayuko Kurome, Prof. Valeri Zakhartchenko and my fellow graduate students Sofia, Michaela, Arne, Janet, Anna and Ingrid for the wonderful working atmosphere and reciprocal support . Particular thanks to Kilian Simmet for his patience.

Finally, I am grateful to my wonderful family for the inestimable and never-ending support.